AEDC-TR-79-11

c.6

Aircraft Motion Sensitivity to Dynamic Stability Derivatives

T. F. Langham
ARO, Inc.

January 1980

Final Report for Period October 1, 1977 – September 30, 1978

Approved for public release; distribution unlimited.

ARNOLD ENGINEERING DEVELOPMENT CENTER
ARNOLD AIR FORCE STATION, TENNESSEE
AIR FORCE SYSTEMS COMMAND
UNITED STATES AIR FORCE

This report has been reviewed by the Office of Public Affairs (PA) and is releasable to the National Technical Information Service (NTIS). At NTIS, it will be available to the general public, including foreign nations.

APPROVAL STATEMENT

This report has been reviewed and approved.

ALEXANDER F. MONEY
Project Manager
Directorate of Technology

Approved for publication:

FOR THE COMMANDER

MARION L. LASTER
Director of Technology
Deputy for Operations

UNCLASSIFIED

REPORT DOCUMENTATION PAGE		READ INSTRUCTIONS BEFORE COMPLETING FORM
1. REPORT NUMBER AEDC-TR-79-11	2. GOVT ACCESSION NO.	3. RECIPIENT'S CATALOG NUMBER
4. TITLE (and Subtitle) AIRCRAFT MOTION SENSITIVITY TO DYNAMIC STABILITY DERIVATIVES		5. TYPE OF REPORT & PERIOD COVERED Final Report, Oct 1, 1977 - Sept 30, 1978 6. PERFORMING ORG. REPORT NUMBER
7. AUTHOR(s) T. F. Langham, ARO, Inc., a Sverdrup Corporation Company		8. CONTRACT OR GRANT NUMBER(s)
9. PERFORMING ORGANIZATION NAME AND ADDRESS Arnold Engineering Development Center/DOT Air Force Systems Command Arnold Air Force Station, Tennessee 37389		10. PROGRAM ELEMENT, PROJECT, TASK AREA & WORK UNIT NUMBERS Program Elements 62201F 921E07
11. CONTROLLING OFFICE NAME AND ADDRESS Arnold Engineering Development Center/DOS Air Force Systems Command Arnold Air Force Station, Tennessee 37389		12. REPORT DATE January 1980 13. NUMBER OF PAGES 139
14. MONITORING AGENCY NAME & ADDRESS(if different from Controlling Office)		15. SECURITY CLASS. (of this report) UNCLASSIFIED 15a. DECLASSIFICATION/DOWNGRADING SCHEDULE N/A

16. DISTRIBUTION STATEMENT (of this Report)

Approved for public release; distribution unlimited.

17. DISTRIBUTION STATEMENT (of the abstract entered in Block 20, if different from Report)

18. SUPPLEMENTARY NOTES

Available in Defense Technical Information Center (DTIC)

19. KEY WORDS (Continue on reverse side if necessary and identify by block number)

dynamics	attack aircraft	mathematical models
stability	fighter bombers	angle of attack
aircraft	simulation	maneuverability
motion	mathematical analysis	damping

20. ABSTRACT (Continue on reverse side if necessary and identify by block number)

A six-degree-of-freedom, nonlinear dynamic derivative sensitivity study has been conducted on a fighter/bomber and an attack-type aircraft. The dynamic derivatives investigated in the study were C_{ℓ_q}, C_{n_q}, C_{m_p}, C_{m_r}, $C_{\ell_{\dot\beta}}$, and $C_{n_{\dot\beta}}$. For the cross-coupling derivatives, C_{ℓ_q} was shown to have the most significant effect on the level and 3-g turning flight motion, followed by C_{n_q} and C_{m_p} with

DD FORM 1 JAN 73 1473 EDITION OF 1 NOV 65 IS OBSOLETE

UNCLASSIFIED

20. ABSTRACT (Continued)

the derivative C_{m_r} showing little to negligible effect in the same regime. For the acceleration derivatives, $C_{\ell_{\dot{\beta}}}$ was shown to have a significant influence on the aircraft motion. The $C_{n_{\dot{\beta}}}$ derivative had little effect on the simulated motion. The analysis also documents the configuration dependency of the cross-coupling derivatives and investigates the effects of nonlinear variations in the derivatives on the aircraft motion.

ERRATA

AEDC-TR-79-11, January 1980
(UNCLASSIFIED REPORT)

AIRCRAFT MOTION SENSITIVITY TO
DYNAMIC STABILITY DERIVATIVES

T. F. Langham, ARO, Inc.

Arnold Engineering Development Center
Air Force Systems Command
Arnold Air Force Station, Tennessee 37389

The following changes should be made in subject report:

Page 1 Last sentence should read:

Analysis of the data was completed on September 30, 1978, and the manuscript was submitted for publication on January 2, 1979.

Page 7 Paragraph 2, 4th sentence should read:

This degradation in correlation is not due to an inadequacy in the aircraft equations of motion at high angle of attack but results from improper or inadequate modeling of the aircraft aerodynamics in this regime.

Page 8 Paragraph 4, last sentence should read:

The results of the study were incomplete because each cross-coupling derivative was varied with all other cross-coupling derivatives kept at zero; therefore, any effects that might have occurred from the interaction of the derivatives were not considered.

Page 17 Paragraph 2, third sentence should read:

The effect of C_{m_r} variation on the motion for the attack aircraft (Fig. 26) appeared to be insignificant, even with the expanded scales on roll rate p.

Page 73 The legend for Figure 20. Continued should be as follows:

FIGHTER/BOMBER

○ BASELINE - NOMINAL CC AND $\dot{\beta}$ DERIVATIVES

△ $C_{n_q} = 0.0$

□ $C_{n_q} = -2.0$

Page 134 The last equation on the page should read as follows:

$$(S - L_p)(S - M_q)(S - N_r) - (S - L_p) N_q M_r - (S - N_r)(M_p - A) L_q$$
$$- (S - M_q)(N_p - B) L_r - (N_p - B) M_r L_q - (M_p - A) N_q L_r = 0$$

PREFACE

The work reported herein was conducted by the Arnold Engineering Development Center (AEDC), Air Force Systems Command (AFSC) for the NASA Langley Research Center, the NASA Ames Research Center, and the Air Force Flight Dynamics Laboratory/FGC. Project monitors were Mr. William Gilbert for the Langley Research Center, Mr. Gerald Malcolm for the Ames Research Center, and 1st Lt Rob Crombie for the Air Force Flight Dynamics Laboratory. The results of this research were obtained by ARO, Inc., AEDC Division (a Sverdrup Corporation Company), operating contractor for the AEDC, AFSC, Arnold Air Force Station, Tennessee, under ARO Project No. P34A-T3A. Analysis of the data was completed on September 30, 1978, and the manuscript was submitted for publication on January 2, 1978.

CONTENTS

ILLUSTRATIONS

Figure | Page

TABLES

APPENDIXES

1.0 INTRODUCTION

The simulation of aircraft motion through analytical techniques has become an important tool in the development, testing, and operational phases of fighter aircraft. Pilot-in-the-loop simulators, which in the past have been used primarily for pilot proficiency and training, are presently being applied to the development and testing phases of new fighter aircraft. Aircraft subsystems, such as automatic departure prevention systems, stall inhibitors, spin-prevention concepts, etc. (Refs. 1 through 4), are continually being evaluated in motion simulators such as the NASA Langley Differential Maneuvering Simulator (Ref. 5).

In general, correlation of flight and simulated aircraft motion is good in the low angle-of-attack unstalled flight regime. As the angle of attack increases to the extremes of the aircraft operating envelope, the level of correlation diminishes correspondingly. This is unfortunate since most of the aircraft handling problems of greatest interest for simulator evaluation occur at high angles of attack. This degradation in correlation, resulting from poor "before-the-fact" simulation, is not due to an inadequacy in the aircraft equations of motion at high angle of attack but results from improper or inadequate modeling of the aircraft aerodynamics in this regime. The poor definition of the aircraft dynamic characteristics at high angles of attack is believed to be a major factor in this deficiency.

The classical method of modeling the aircraft dynamic characteristics in motion simulation uses the direct damping derivatives (C_{m_q}, C_{n_r}, C_{ℓ_p}, etc.) and cross derivatives (C_{n_p}, C_{ℓ_r}). This method has proved to be accurate in low-angle-of-attack flight where aircraft aerodynamics are linear and cross-coupling and acceleration derivatives are small. As angle of attack increases and associated nonlinear flow resulting from separation and asymmetric vortex shedding occurs, the secondary cross-coupling (C_{n_q}, C_{ℓ_q}, C_{m_r}, C_{m_p}) and acceleration ($C_{n_{\dot\beta}}$, $C_{\ell_{\dot\beta}}$) derivatives may become large. Orlik-Ruckemann, Hanff, and Laberge at NAE (Ref. 6) have shown experimentally, with a nonairplane model (cone wing), that the magnitude of the cross-coupling rate derivatives in combination with acceleration derivatives at high angles of attack approach and/or exceed those of the direct damping derivatives. Likewise NASA Langley through the use of a curved flow tunnel (Ref. 7) has shown the $\dot\beta$ acceleration derivatives for an airplane model to be the predominant terms at high angles of attack in the classical $C_{n_r} + C_{n_{\dot\beta}}$ and $C_{\ell_r} + C_{\ell_{\dot\beta}}$ combinations measured in forced-oscillation experiments.

Assuming that aircraft do exhibit both cross-coupling and acceleration derivatives of the magnitude of those in Refs. 6 and 7, the question arises as to the importance of these derivatives in aircraft flight mechanics.

The Arnold Engineering Development Center is presently conducting research to define what aerodynamic parameters are necessary for achieving good "before-the-fact" aircraft motion simulation in high-angle-of-attack flight. Definition of these parameters is important for the design of future experimental test apparatus in which measurements of these parameters will be made.

The subject analysis defines the importance of cross-coupling and acceleration damping derivatives in the high-angle-of-attack operation of aircraft. Derivatives investigated in the analysis are C_{m_p}, C_{m_r}, C_{ℓ_q}, C_{n_q}, $C_{n_{\dot{\beta}}}$, and $C_{\ell_{\dot{\beta}}}$. Two types of aircraft are used in the analysis, a fighter/bomber and attack aircraft. Changes in the response to control perturbations for each of the aircraft are investigated with both individual and nonlinear simultaneous variations of cross-coupling and acceleration derivatives. Time histories of the aircraft motion are generated using a six-degree-of-freedom, nonlinear, computer program. The analysis addresses only the maneuvering angle-of-attack flight regime ($\alpha < 25$ deg).

2.0 BACKGROUND

Before the 1960's, aircraft dynamic cross-coupling and acceleration derivatives were generally considered insignificant in fighter aircraft motion simulation and dynamic stability analysis. These assumptions were good primarily because aircraft of this era were operating at moderate angles of attack where both cross-coupling and acceleration derivatives possessed small values. In the mid-1960's, it became necessary for the operating envelopes of these same aircraft to be extended to high angles of attack under combat conditions. Analytical simulation of this partly stalled, high-angle-of-attack maneuvering flight was generally unsuccessful. Any successful correlation was generally an "after-the-fact" correlation resulting from many parameter variations to achieve a suitable combination of aerodynamics. It became apparent that better representation of the aerodynamics of an aircraft would be needed to achieve a good before-the-fact analytical simulation of aircraft in high-angle-of-attack maneuvering flight.

An investigation conducted at AEDC in 1976 (Ref. 8) provided some insight into the importance of dynamic cross and cross-coupling derivatives in motion simulation studies of fighter aircraft in the maneuvering flight regime. The aircraft motion sensitivity to the various derivatives in level and turning flight was evaluated by a five-degree-of-freedom, linearized stability program. The results of the study were incomplete because the cross-coupling derivatives were varied with all other derivatives kept at zero; therefore, any effects that might have occurred from the interaction of the derivatives were not considered.

An additional study (Ref. 9) was conducted in 1978 at AEDC to determine the sensitivity of the spinning motion of fighter aircraft to dynamic cross-coupling and acceleration derivatives. Results indicate that the dynamic derivatives can produce significant effects on the aircraft spinning motion and should be considered when conducting a spin analysis. The results also indicate that the spinning motion sensitivity to the dynamic cross-coupling and acceleration derivatives investigated is configuration dependent.

An aircraft sensitivity study evaluating cross-coupling derivatives has been conducted by Curry and Orlik-Ruckemann (Ref. 10). This study addresses both level and turning flight conditions for a fighter/bomber configuration at high angles of attack. Since only one aircraft was used in the study, the configuration dependence of the derivatives was not addressed. Also, the basic aerodynamic data matrix used in the motion simulation did not include nonlinear effects of some static and dynamic derivatives that are predominant at high angles of attack.

From a review of the above investigations, it was concluded that all of the aerodynamic characteristics of the aircraft configurations should be incorporated in the mathematical model for an accurate evaluation of the effects of cross-coupling derivatives in motion simulation. Also, the cross-coupling derivatives should be included (at some nominal values) in the sensitivity study when each derivative is varied individually.

3.0 METHOD OF ANALYSIS

A six-degree-of-freedom, nonlinear, motion program was used in the analysis. The program was formulated by North American Rockwell (Ref. 11) using a fourth-order Runge-Kutta integration algorithm with a fixed integration step size. The program input and aerodynamic modules have since been modified for adaptation to the cross-coupling and acceleration dynamic derivatives. The equations describing the aircraft motion are rigid-body equations referenced to a body-fixed axis system (Fig. 1) at the aircraft center of gravity (cg). The basic equations are as follows:

Forces:

$$\dot{u} = rv - qw - g \sin\theta + \frac{F_X}{m} + \frac{T_X}{m} \tag{1}$$

$$\dot{v} = pw - ru + g \cos\theta \sin\phi + \frac{F_Y}{m} \tag{2}$$

$$\dot{w} = qu - pv + g \cos\theta \cos\phi + \frac{F_Z}{m} + \frac{T_Z}{m} \tag{3}$$

Moments:

$$\dot{p} = \frac{I_Y - I_Z}{I_X} qr + \frac{I_{XZ}}{I_X} (\dot{r} + pq) + \frac{M_X}{I_X} \tag{4}$$

$$\dot{q} = \frac{I_Z - I_X}{I_Y} pr + \frac{I_{XZ}}{I_Y} (r^2 - p^2) + \frac{M_Y}{I_Y} + \frac{M_{YT}}{I_Y} - \frac{I_E \Omega_E}{I_Y} r \tag{5}$$

$$\dot{r} = \frac{I_X - I_Y}{I_Z} pq - \frac{I_{XZ}}{I_Z} (\dot{p} - qr) - \frac{M_Z}{I_Z} + \frac{I_E \Omega_E}{I_Z} q \tag{6}$$

The external forces and moments (F_X, F_Y, F_Z, M_X, M_Y, and M_Z) in the equations are comprised of aerodynamic coefficients representative of the aircraft. The external force and moment contributions attributable to engine thrust (including gyroscopic effect) are represented by T_X, T_Z, M_{YT}, $I_E\Omega_E r$, and $I_E\Omega_E q$. Development of the aerodynamic mathematical model in representing each aircraft is presented in Appendix A.

Auxiliary equations used in this analysis are given as follows:

$$\alpha = \tan^{-1}\left(\frac{w}{u}\right), \qquad \beta = \sin^{-1}\left(\frac{v}{V}\right) \tag{7}$$

$$\dot{\alpha} = \frac{u\dot{w} - w\dot{u}}{u^2 + w^2}, \qquad \dot{\beta} = \dot{v} - \frac{v}{V^2}\left(\frac{u\dot{u} + v\dot{v} + w\dot{w}}{\sqrt{u^2 + w^2}}\right) \tag{8}$$

$$V = \sqrt{u^2 - v^2 + w^2}, \qquad \gamma = \tan^{-1}\left(\frac{h}{\sqrt{\dot{x}^2 + \dot{y}^2}}\right) \tag{9}$$

$$\dot{\theta} = q \cos\phi - r \sin\theta, \qquad \dot{\phi} = p + \tan\theta\,(r\cos\phi - q\sin\phi) \tag{10}$$

$$\dot{\psi} = \frac{r\cos\phi + q\sin\phi}{\cos\theta}, \qquad \Omega = \sqrt{p^2 + q^2 + r^2} \tag{11}$$

The six-degree-of-freedom program was modified to compute the initial trim required for level (1-g) and steady turning (3-g) flight conditions. For the trimmed level flight condition, either a rudder or elevator doublet was executed to excite the appropriate derivative because of the near-zero p, q, and r body axis rates associated with 1-g trimmed flight. The turning flight condition provided larger values of the q and r rates, thereby giving the cross-coupling moments larger values because of the control doublet action. In a coordinated turn, the body axis roll rate, p, is zero; therefore, the derivatives associated with p were deleted from the trim equations.

Initially, all derivatives under investigation were given nominal values; next, individual variations in each derivative were performed with the other derivatives fixed at their nominal values. By maintaining nominal (nonzero) values for all derivatives, the possible derivative interaction effects described in Ref. 12 were included. Angular motion changes about the aircraft cg and changes in the cg path with variations of the derivatives were used in the analysis for ascertaining the significance of each derivative.

4.0 TECHNICAL DATA

4.1 AIRCRAFT CONFIGURATIONS

Two aircraft configurations were selected for this dynamic sensitivity study. Each was selected on the basis of inherent, high-angle-of-attack, lateral/directional flight characteristics. The intent was to select aircraft that would exhibit a range of lateral/directional stability characteristics typical of current high-performance military aircraft. On the basis of these criteria, a typical fighter/bomber and an attack configuration were selected for the analysis.

The fighter/bomber configuration shown in Fig. 2 represents a twin-engine, swept-low-wing-type aircraft. Past performance has shown that this aircraft possesses a "wing rock" or dutch roll oscillation at high angles of attack, followed by a directional divergence as angle of attack exceeds approximately 23 deg. This configuration was considered an extreme case of modern fighter aircraft that experiences "wing rock" in difficult tracking maneuvers.

The attack configuration shown in Fig. 3 represents a single-engine, swept-high-wing-type aircraft. This configuration exhibits some directional instability at angles of attack above 20 deg while still possessing lateral stability. The aircraft departure is characterized by an abrupt "nose slice." The attack aircraft possesses aerodynamics corresponding to a shoulder-wing configuration in contrast to the fighter/bomber low-wing configuration.

4.2 BASIC AERODYNAMIC AND INERTIA DATA

The aerodynamic data matrices used in modeling both aircraft configurations were obtained from low-speed wind tunnel tests. The data for the attack aircraft were obtained from the Navy. The fighter/bomber data matrices were formulated from data presented in Refs. 13 and 14. The basic matrices are a combination of static and dynamic oscillatory aerodynamic data in the body axis system shown in Fig. 1. Data are input to the matrices in table look-up form as functions of the variables shown in the equations of Appendix A.

Mass, inertia, and geometric characteristics of the aircraft configurations are presented in Table 1. Although the magnitudes of the mass and inertia of the two aircraft are considerably different, the mass distributions along the reference axes of the aircraft are similar. Figure 4 presents the mass distributions of several modern fighter aircraft. All of these aircraft with the exception of the F-5 have similar mass distributions along their reference axes.

5.0 RESULTS AND DISCUSSION

5.1 GENERAL

The aircraft motion sensitivity study was conducted in level and 3-g turning flight at an altitude of 30,000 ft (9,144 m). Two types of aircraft were used in the analysis, a fighter/bomber and attack aircraft. The primary analysis centers around the fighter/bomber with the attack aircraft being used to ascertain and confirm configuration dependence. Turning flight conditions simulated the aircraft in the maneuvering flight regime. The trim angle of attack of 20 deg was selected for most flight conditions. The aircraft airspeed was adjusted to achieve the desired load factor at the trimmed angle of attack. It was assumed that the low-speed aerodynamics for both aircraft were valid for the speed ranges encountered. A summary of the initial flight conditions for simulating the aircraft/flight combinations is given in Table 2. It should be noted that the attack aircraft was used only in turning flight simulations. Also shown in Table 2 are trim conditions for an angle of attack of 15 deg; these were used for selected runs discussed in Section 5.3 on nonlinear effects.

The 20-deg trim angle of attack provided a flight condition where the cross-coupling (CC) and $\dot{\beta}$ acceleration derivative variations would have their maximum effectiveness and yet provide a small, positive, static stability margin. Prolonged operation above this angle of attack may result in inadvertent loss of controllability. This is indicated by the characteristics shown in Fig. 5. Above 20 deg, the static lateral/directional stability parameters, C_{n_β} and C_{ℓ_β}, become unstable, resulting in $C_{n_{\beta_{dynamic}}}$ ($C_{n_\beta} \cos\alpha - I_{ZZ}/I_{XX}\, C_{\ell_\beta} \sin\alpha$) becoming negative near 20 deg.

The range over which the dynamic derivatives were varied is presented in Table 3 and corresponds to the approximate maximum and minimum experimental values obtained from recent wind tunnel tests (Refs. 6 and 7). The derivatives $C_{\ell_q} + C_{\ell_{\dot{\alpha}}}$, $C_{n_q} + C_{n_{\dot{\alpha}}}$, and $C_{m_r} - C_{m_{\dot{\beta}}}$ (Fig. 6) were obtained from the program outlined in Ref. 6 using the cone-wing model shown in Fig. 7. It should be noted that the derivatives of Fig. 6 were treated as pure rate terms in the aerodynamic equations of Appendix A. Little is known concerning the magnitude of the CC derivative C_{m_p}. The experimental work performed by Orlik-Ruckemann (Ref. 6) addresses only the CC derivatives associated with pitching and yawing of the model and does not include derivatives resulting from a rolling motion. Since Ref. 6 represents the only known published literature of measured aircraft CC derivatives, the relative magnitude of C_{m_p} continues to remain in question; therefore, maximum and miminum C_{m_p} values identical to those selected for C_{m_r}, -1 to 1 per radian, were used.

The $\dot{\beta}$ acceleration derivatives $C_{\ell_{\dot{\beta}}}$ and $C_{n_{\dot{\beta}}}$ were obtained (Ref. 7) with a fighter/bomber configuration similar to that used in this investigation. The $\dot{\beta}$ derivative variation with angle of attack can be determined from Fig. 8, which presents a comparison of total $C_{n_r} + C_{n_{\dot{\beta}}} \cos \alpha$, $C_{\ell_r} - C_{\ell_{\dot{\beta}}} \cos \alpha$ obtained from a NASA Langley forced-oscillation test and C_{n_r}, C_{ℓ_r} obtained from the Virginia Polytechnic Institute curved-flow tunnel test on a similar model.

The nominal values of the dynamic CC and $\dot{\beta}$ derivatives used in the sensitivity study are presented in Table 4. The nominal values represent extremes of the data obtained in the wind tunnel tests in Refs. 6 and 7. The use of these large values ensures that interactions between derivatives, as described in Section 5.2, are accounted for in the analysis. It should be emphasized that in this analysis the magnitudes of the CC derivatives used are representative of a cone-wing body and not an aircraft configuration. To gain some insight into this potential problem, a comparison of the basic aerodynamic characteristics of the cone-wing model with those for the two aircraft configurations is shown in Figs. 5, 9, and 10. Note that all derivatives are nondimensionalized using standard characteristic references, span, chord, and area. As shown in Fig. 5, the static lateral/directional characteristics of the cone-wing are comparable in magnitude to the aircraft configurations, with a loss in stability occurring near 25-deg angle of attack instead of the 15- to 20-deg angle-of-attack range for the fighter/bomber and attack configurations. The cross derivative, C_{ℓ_r}, for the cone-wing shown in Fig. 9 is quite representative of the attack aircraft. The direct damping derivatives, C_{n_r} and C_{m_q}, for the cone-wing are not as well behaved as the static and cross derivatives, and the trends with angle of attack are not considered representative of the aircraft configurations.

It is interesting to note that in the angle-of-attack range (30 to 40 deg) where C_{m_q} for the cone-wing model acquires large values, the CC derivatives C_{n_q} and C_{ℓ_q} (Fig. 6) also have their extreme values. Indications are that some separated flow mechanism with rotational rate q may be pertubating the derivatives for the cone-wing model. The C_{m_q} derivative of the two aircraft configurations (Fig. 10) is well behaved over the angle-of-attack range presented; how large the C_{n_q} and C_{ℓ_q} derivatives are for these configurations is unknown. It should be recognized that using cone-wing data as representative of the C_{ℓ_q} and C_{n_q} aircraft derivatives is questionable.

5.2 CROSS-COUPLING AND ACCELERATION DERIVATIVE VARIATIONS

5.2.1 Baseline Motion

The approach used for conducting the dynamic sensitivity study was first to establish a baseline motion with which other motions could be compared as derivative variations were made. The baseline maneuvers generated represent unique combinations of aircraft configuration, flight condition, and a nominal set of CC and $\dot{\beta}$ acceleration derivatives. For each baseline maneuver generated, an elevator or rudder doublet was executed at 2 sec into the maneuver to disturb appropriate p, q, and r rotational rates for investigating specific lateral/directional or longitudinal derivatives. Specific baseline maneuvers generated for the fighter/bomber aircraft include: (1) level and 3-g turning flight condition, Figs. 11 and 12, respectively, with nominal values for the CC and $\dot{\beta}$ derivatives and (2) 3-g turning flight (Fig. 13) with nominal values for the CC derivatives, $\dot{\beta}$ derivatives zero. The baseline maneuver for the attack aircraft was generated for the 3-g turning flight condition (Fig. 14) with nominal values for the CC derivatives, $\dot{\beta}$ derivatives zero. Included with each baseline maneuver is an additional maneuver generated for zero aerodynamic CC and acceleration derivatives. This second maneuver is presented as a reference and will be discussed later. It should be noted that in level flight (Fig. 11) the disturbances in p, q, and r rates caused by either elevator or rudder doublets are of a lesser magnitude than corresponding disturbances in the 3-g turning flight (Figs. 12, 13, and 14). As discussed in Section 5.1, airspeed adjustments rather than aerodynamic changes were made to achieve the 3-g load factor for turning flight. This increased airspeed in turning flight (see Table 2) resulted in larger dynamic pressures and therefore greater forces from the control surface deflections. The result was larger p, q, and r rates from control surface doublets in turning flight.

Including large nominal values (Table 4) of the CC and $\dot{\beta}$ derivatives in the baseline maneuver was an attempt to account for the possible interaction effects on the derivatives. The possibility of such an interaction is outlined in Ref. 12 using linearized equations of motion and is included in Appendix B.

For each flight condition/aircraft/derivative variation, a new set of initial trim conditions had to be computed. The variations in the initial Mach number, attitude angles, and angular rates with derivative variations sometimes required large control surface changes because of the ineffectiveness of the surfaces at the high angles of attack. This extensive effort, which was not anticipated, was further complicated because obtaining the multivariable aerodynamic data in the trim program required the use of an iterative solution technique to get a unique set of trim values. Also, the low lateral/directional stability margin for the fighter/bomber imposed strict restraints on the allowable mistrim in the lateral/directional axis.

For each simulation, time histories are presented for the following variables: α, β, $\dot{\beta}$, θ, ϕ, ψ, p, q, r, δ_a, δ_r, and δ_H. Comparison of baseline and reference time histories demonstrates the aerodynamic coupling effect for nominal values of CC and $\dot{\beta}$ derivatives. As shown in Fig. 11 no perturbations in p and r rates occurred from the q motion in the level flight reference case (no CC, $\dot{\beta} = 0$). This was attributable to the lack of aerodynamic coupling terms in the reference case and the minimization of inertia coupling by the near-zero p, q, and r rates associated with trimmed level flight. When the CC and $\dot{\beta}$ derivatives are included (baseline maneuver), the motion no longer remains planar. Both roll and yaw motion of the aircraft are excited by the q rate in combination with the derivatives. For the 3-g turning flight shown in Figs. 12 through 14, a small amount of inertia coupling occurred in the reference maneuver after an elevator doublet. This inertia coupling was overshadowed in the baseline case by the large aerodynamic coupling that ocurred when the nominal CC and $\dot{\beta}$ derivatives were included.

5.2.2 C_{ℓ_q} Derivative Evaluation

The motion sensitivity to the rolling moment caused by the pitch rate derivative, C_{ℓ_q}, is presented in Figs. 15 and 16 for the fighter/bomber in level and 3-g turning flight, respectively. The range over which this derivative was varied was 2.0 (nominal), 0.0, and -2.0 per radian. As expected, the predominant effect was in the p and β motion; the β motions occur as the aircraft rolls about its body axis at high angles of attack. Also expected was the near mirror image in the p and β motion plots for derivative values of 2 and -2 per radian. The divergence from symmetry with increasing time can be attributed to the asymmetry of the static data matrix as a function of β used in the six-degree-of-freedom motion program.

Figures 17 and 18 present the effect of C_{ℓ_q} variations on the motion of the fighter/bomber and attack aircraft, respectively. In each case, only the CC derivatives at nonimal values were included in the baseline motion. The $\dot{\beta}$ derivatives were excluded because of their large damping effect on the aircraft motion, as shown in the baseline comparisons in Figs 12 and 13. There was concern that the heavy damping could overshadow the effectiveness of the CC derivatives. Again, the motion resulting from derivative values of 2 and -2 were near mirror images in p and β motion for both aircraft configurations. The positive value of C_{ℓ_q} produces a divergence in the roll motion of the fighter/bomber but not for attack aircraft. This low roll damping for the fighter/bomber motion is explained by reviewing relative dynamic stability levels of each aircraft shown in Fig. 10. The primary roll damping parameter, C_{ℓ_p}, is significantly lower for the fighter/bomber in the angle-of-attack range from 15 to 20 deg.

Assuming the C_{ℓ_q} derivative to be of the magnitude approaching those used in Figs. 15 through 18, the resulting perturbations in longitudinal and lateral/directional planes for both aircraft configurations are considered to be significant in aircraft motion simulation. For the flight conditions and aircraft configurations used in this sensitivity study, the characteristic effect of C_{ℓ_q} is not considered configuration dependent.

5.2.3 C_{n_q} Derivative Evaluation

The effect of C_{n_q} variation on the motion for the fighter/bomber is shown in Figs. 19 and 20 for level and 3-g turning flight, respectively. As expected for opposite signs of C_{n_q}, the near mirror image was produced in the yaw rate motion. This effect was not noted in sideslip, β as was the case for C_{ℓ_q} because β motion is generated primarily by the aircraft rolling about its axis. Since the roll rate, p, showed negligible effect with C_{n_q} variation, the β variations were likewise small. The amplitudes of the initial r motion observed for the C_{n_q} variation in level flight were about a fourth of the p motion observed for C_{ℓ_q}. The reduced yaw motion can be traced back to more damping in yaw than in roll as shown in the C_{n_r} and C_{ℓ_p} parameters in Fig. 10 at a 20-deg angle of attack.

Figures 21 and 22 present the effect of C_{n_q} variations on the motion of the fighter/bomber and attack aircraft, respectively, with zero $\dot{\beta}$ derivatives. With the loss in damping associated with keeping the $C_{n_{\dot{\beta}}}$ and $C_{\ell_{\dot{\beta}}}$ derivatives at zero, the fighter/bomber aircraft becomes unstable in yaw rate for all values of C_{n_q}. As a result of this instability, any change in the C_{n_q} derivative produces large changes in the yawing motion of the aircraft. These are the same trends as previously shown in the p rate in Fig. 17 for the C_{ℓ_q} derivative variation with $C_{n_{\dot{\beta}}}$ and $C_{\ell_{\dot{\beta}}}$ held at zero. The aircraft has such a low margin of stability that any change in C_{ℓ_q} results in an unstable roll motion (p). Because the attack aircraft has more stability at the conditions examined, the motion resulting from the C_{n_q} variation in Fig. 22 is quickly damped. Similar roll damping was observed in Fig. 18 for the attack aircraft with C_{ℓ_q} variations.

The motion of both the fighter/bomber and attack aircraft is sensitive to the CC derivative C_{n_q}. The level of sensitivity, as discussed above, is dependent upon the stability of the aircraft at the time the derivative variations are performed.

5.2.4 C_{m_r} Derivative Evaluation

The motion sensitivity to the pitching moment attributable to yaw rate derivative, C_{m_r}, is presented in Figs. 23 through 26. An elevator doublet was used to excite the pitch rate, q, but a rudder doublet was used to excite the yaw rate, r. The C_{m_r} derivative was assigned values of 1.0 (nominal), 0.0, and -1.0. The sensitivity of the fighter/bomber in level and 3-g turning flight to C_{m_r} variations is presented in Figs. 23 and 24. For each variation in C_{m_r}, nominal values for the other CC and $\dot{\beta}$ derivatives were included. As documented by Curry in Ref. 10 and in the linearized analysis of Ref. 12, the C_{m_r} derivative variation has a negligible effect on the coupling of the longitudinal and directional aircraft motions.

Figures 25 and 26 present the effect of C_{m_r} variations on the baseline motion of the fighter/bomber and attack aircraft, respectively, with the zero $\dot{\beta}$ derivatives. For the fighter/ bomber configuration, the characteristics of the motion were not significantly effected by C_{m_r} variation, but the aerodynamic coupling did result in a slight phase shift in the longitudinal and lateral motion q and r, respectively. The effect of C_{m_r} variation on the motion for the attack aircraft (Fig. 16) appeared to be insignificant, even with the expanded scales on roll rate p. Overall, the C_{m_r} derivative appears to be of little concern in motion simulation if its magnitude remains within the limits investigated.

5.2.5 C_{m_p} Derivative Evaluation

The motion sensitivity to the pitching moment attributable to roll rate derivative, C_{m_p}, is presented in Figs. 27 through 30. The values over which C_{m_p} was varied were 1.0, 0.0 (nominal), and -1.0 per radian. Figures 27 and 28 present the effect of C_{m_p} variation on the level and 3-g turning flight conditions for the figher/bomber aircraft. For these figures, all CC and $\dot{\beta}$ derivatives with the exception of C_{m_p} were included at their nominal values. Only small effects were noted when the C_{m_p} derivative was included in the fighter/bomber motion in Figs. 27 and 28. Of these effects, angle of attack displayed the largest variation from baseline motion but remained within ± 1 deg of the motion at all times.

Figures 29 and 30 present the effect of C_{m_p} variation in 3-g turning flight for the fighter/bomber and attack aircraft, respectively. For the fighter/bomber aircraft, the influence when the $\dot{\beta}$ derivatives were excluded is quite significant when evaluating the C_{m_p} coupling. Depending on the sign of C_{m_p}, the resulting motion in the longitudinal and lateral planes may be cyclic or divergent. As noted in previous derivative evaluations using the fighter/bomber aircraft, the loss in stability associated with keeping the $\dot{\beta}$ derivatives zero results in an increase in sensitivity of the aircraft to CC derivative variations. Shown in Fig. 30 is the negligible effect of C_{m_p} variation of ± 1 on the attack aircraft motion with all other

CC derivatives at the nominal values. The relative effects of excluding the $\dot{\beta}$ derivatives on the fighter/bomber and attack aircraft motion indicate that several levels of configuration dependency may exist for a particular derivative when conducting a sensitivity study. Aircraft stability must be investigated to achieve a true evaluation of derivative importance.

5.2.6 $C_{\ell_{\dot{\beta}}}$ Derivative Evaluation

The motion sensitivity to the $C_{\ell_{\dot{\beta}}}$ derivative is presented in Figs. 31 and 32. The derivative was varied over the range of 0.2 to -1.0 per radian for the fighter/bomber aircraft in level and 3-g turning flight conditions. Positive values greater than 0.2 resulted in a rapid oscillatory divergence in the roll motion for both level and 3-g turning flight. As shown in Figs. 31 and 32 for $C_{\ell_{\dot{\beta}}} = 0.2$, the characteristic rolling motion was cyclic for the level flight condition, whereas the motion was oscillatory and divergent for 3-g turning flight. The increased dynamic pressure associated with turning flight results in a more effective rudder doublet with correspondingly larger pertubations. For this reason, motion resulting from $C_{\ell_{\dot{\beta}}}$ variations in turning flight is more pronounced. The nominal value of $C_{\ell_{\dot{\beta}}}$ (-1.0) had a strong damping effect on the lateral/directional motion when compared to motion for $C_{\ell_{\dot{\beta}}} = 0.0$ and 0.2. The magnitude of the effectiveness of $C_{\ell_{\dot{\beta}}}$ in damping indicates that gross error may be occurring in motion simulation when the rate and acceleration derivatives are not separated for nonzero values of $C_{\ell_{\dot{\beta}}}$.

5.2.7 $C_{n_{\dot{\beta}}}$ Derivative Evaluation

The motion sensitivity to the $C_{n_{\dot{\beta}}}$ derivative is presented in Figs. 33 and 34 for level and 3-g turning flight, respectively. The sensitivity of the fighter/bomber lateral/directional motion to variations of $C_{n_{\dot{\beta}}}$ was not as significant as that in the $C_{\ell_{\dot{\beta}}}$ variation shown in Figs. 31 and 32, but was still of a magnitude that may be considered necessary for correct motion simulation. As previously noted for the CC derivatives, the importance of the $\dot{\beta}$ derivatives in motion simulation may be strongly dependent on the stability level of the aircraft. As noted in Fig. 5, the lateral/directional stability level of the fighter/bomber aircraft at a 20-deg angle of attack is low.

5.3 NONLINEAR EFFECTS OF CROSS-COUPLING DERIVATIVES

In a stability analysis where derivatives are varied individually and held at constant values, the question of realistic simulation always exists. For the analysis discussed in this section, the CC derivatives C_{ℓ_q}, C_{n_q}, and C_{m_r} were varied in a nonlinear fashion as a function of angle of attack for two aircraft tracking maneuvers. The maneuvers were generated to simulate realistic excursions in the aircraft motion that might occur in a combat situation, i.e., rapid excursions in the longitudinal and lateral/directional planes of motion. Both maneuvers were initiated from a 3-g turning flight condition. The first maneuver (Fig. 35) generated a rapid increase in pitch rate, q, by using elevator control. The second maneuver (Fig. 36) was a rapid bank-to-bank motion using aileron control. The initial trim angle of attack was changed to 15 deg. The angle was reduced to 15 deg because at a 20-deg trim any significant control movement resulted in aircraft motion into and beyond the stalled flight regime. The CC derivatives C_{ℓ_q}, C_{n_q}, and C_{m_r} were implemented as a function of angle of attack as shown in Fig. 6. The new trim conditions for the baseline maneuvers are included in Table 2. For each maneuver, the motion resulting from the inclusion of the nonlinear CC derivatives is compared to the baseline maneuver with no CC derivatives.

Figure 35 presents the effect of the CC derivatives on the baseline motion when disturbed by an elevator step for the fighter/bomber and attack aircraft. The inclusion of the CC derivatives in the baseline motion for the fighter/bomber degraded the lateral/directional damping and resulted in changing the final trim attitudes of ϕ, ψ, and θ. For the attack aircraft, the CC derivatives resulted in driving the aircraft out of the stabilized turn.

Figure 36 presents the effect of the CC derivatives on the baseline motion when disturbed by aileron control movement. The only noticeable effect on the baseline motion for both the fighter/bomber and attack aircraft was in the final pitch and roll attitudes, θ and ϕ. It is significant to note that the lateral/directional damping was not noticeably affected for the excursions in angle of attack and the angular rates encountered. A closer look at the CC derivatives (Fig. 6) and corresponding angular rates as a function of angle of attack revealed that when the derivative magnitudes were of a significant value the corresponding rate was small and vice versa. The effect of the CC derivatives was not noticeable in the transient phase of the maneuver so far as damping was concerned, but resulted in an untrimmed condition because of changes in α, p, q, and r.

The effect of the CC derivatives C_{ℓ_q}, C_{n_q}, and C_{m_r} when combined in a nonlinear fashion is dependent upon flight condition, nature of derivatives, and maneuver.

6.0 CONCLUDING REMARKS

The importance of including aerodynamic cross-coupling terms in the equations of motion of fighter aircraft flying at high angles of attack was examined in a six-degree-of-freedom sensitivity study for level and 3-g turning flight. If the cross-coupling derivatives approach the magnitudes of those used in this study, the following observations and conclusions for the conditions and aircraft configurations investigated are offered:

1. The cross-coupling derivatives C_{ℓ_q} and C_{n_q} are considered important in aircraft motion.

2. The derivatives of pitching moment attributable to rolling and yawing, C_{m_p} and C_{m_r}, are of less importance than C_{ℓ_q} and C_{n_q}. The C_{m_p} derivative produces some coupling effect in the longitudinal and lateral/directional motion for the fighter/bomber, whereas the C_{m_r} derivative appears to be insignificant in aircraft motion.

3. The acceleration derivative $C_{\ell_{\dot\beta}}$ has a strong effect on the damping characteristics of the fighter/bomber lateral/directional motion, whereas $C_{n_{\dot\beta}}$ does not have as strong an effect on the lateral/directional motion. For motion simulation in the high-angle-of-attack flight regime, $\dot\beta$ derivatives should be separated from their rate counterparts, C_{ℓ_r} and C_{n_r}, if other than zero.

4. The effect of nonlinear variations in the cross-coupling derivatives is dependent upon flight condition, nature of derivatives, and type of maneuver.

5. General conclusions resulting from the sensitivity study are not configuration dependent for the two aircraft considered but are stability dependent. The less the stability margin of an aircraft the more sensitive its motions are to derivative variations.

REFERENCES

1. Chen, Robert T. N., Newell, Fred D., and Schelhorn, Arno E. "Development and Evaluation of an Automatic Departure Prevention System and Stall Inhibitor for Fighter Aircraft." AFFDL-TR-73-29, April 1973.

2. Gilbert, William P., Nguyen, Luat T., and Van Gunst, Roger W. "Simulator Study of Applications of Automatic Departure- and Spin-Prevention Concepts to a Variable-Sweep Fighter Aircraft." NASA TM X-2928, 1973.

3. Moore, Frederick L., Anglin, Ernie L., Adams, Mary S., Deal, Perry L., and Person, Lee H. "Utilization of a Fixed-Base Simulator to Study the Stall and Spin Characteristics of Fighter Airplanes." NASA TN D-6117, March 1971.

4. Gilbert, William P., Nguyen, Luat T., Van Gunst, Roger W. "Simulator Study of the Effectiveness of an Automatic Control System Designed to Improve the High-Angle-of-Attack Characteristics of a Fighter Airplane." NASA TN D-8176, 1976.

5. Ashworth, B. R. and Kahlbaum, William M., Jr. "Description and Performance of the Langley Differential Maneuvering Simulator." NASA TN D-7304, June 1973.

6. Orlik-Ruckemann, K. J., Hanff, E. S., Laberge, J. G. "Direct and Cross-Coupling Subsonic Moment Derivatives Due to Oscillatory Pitching and Yawing of an Aircraft-Like Model of Angles of Attack up to 40° in Ames 6 x 6 Wind Tunnel." NAE LTR-UA-38, 1976.

7. Coe, Paul L., Graham, Bruce, H., Chambers, Joseph R. "Summary of Information on Low-Speed Lateral-Directional Derivatives Due to Rate of Change of Sideslip $\dot{\beta}$." NASA TN D-7972, September 1975.

8. Butler, R. W. "Aircraft Motion Sensitivity to Cross and Cross-Coupling Damping Derivatives." AEDC-TR-76-138, (AD-A032654), November 1976.

9. Butler, R. W. and Langham, T. F. "Sensitivity of Aircraft Spinning Motion to Dynamic Cross-Coupling and Acceleration Derivatives." AEDC-TR-78-12, October 1978.

10. Curry, W. H. and Orlik-Ruckemann, K. J. "Sensitivity of Aircraft Motion to Aerodynamic Cross-Coupling at High Angles of Attack." AGARD-CPP-235, May 1978.

11. North American Rockwell. "Digital Simulation User's Manual." NR70H-232-2, June 1970.

12. Butler, R. W. and Langham, T. F. "Aircraft Motion Sensitivity to Variations in Dynamic Stability Parameters." AGARD-CPP-235, May 1978.

13. Anglin, Ernie L. "Static Force Test of a Model of a Twin-Jet Fighter Airplane for Angles of Attack from -10 Degrees to 110 Degrees and Sideslip Angles from -40 Degrees to 40 Degrees." NASA TN D-6425, August 1971.

14. Grafton, Sue B. and Libbey, Charles E. "Dynamic Stability Derivatives of a Twin-Jet Fighter Model for Angles of Attack from -10 Degrees to 110 Degrees." NASA TN D-6091, 1971.

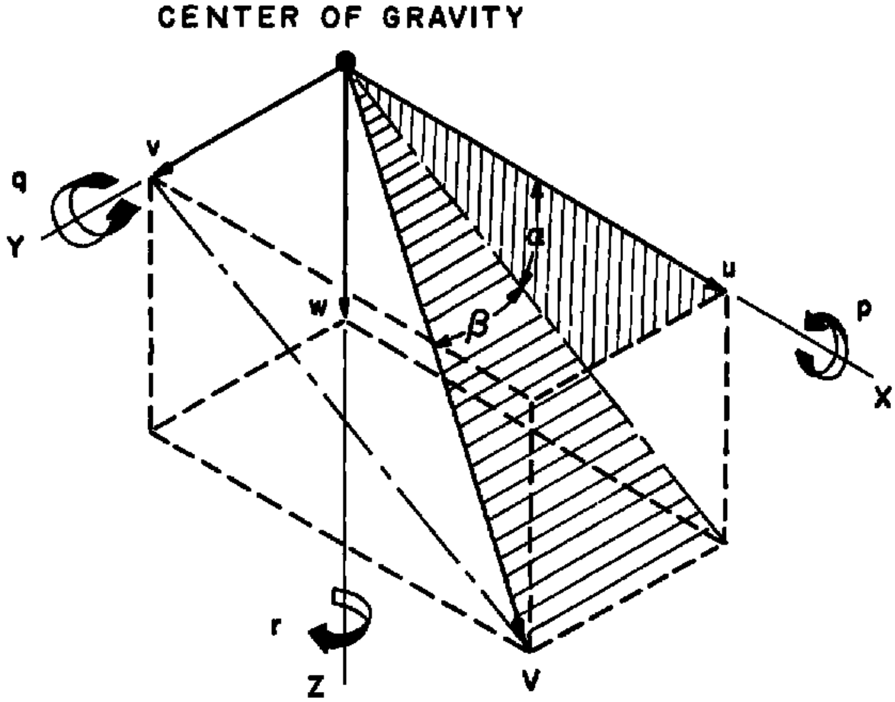

Figure 1. Body axis system.

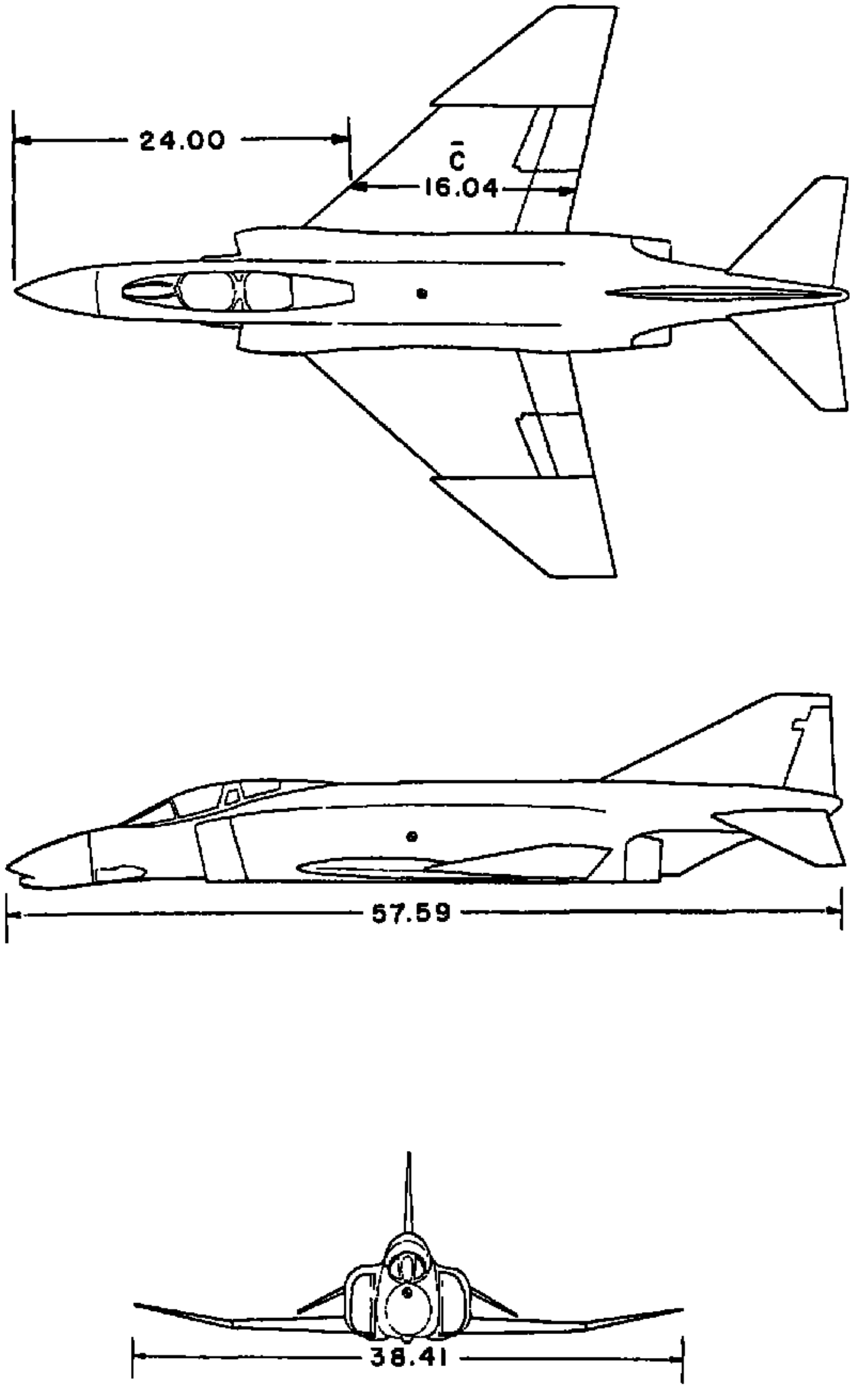

DIMENSIONS IN FEET

Figure 2. Fighter/bomber aircraft configuration.

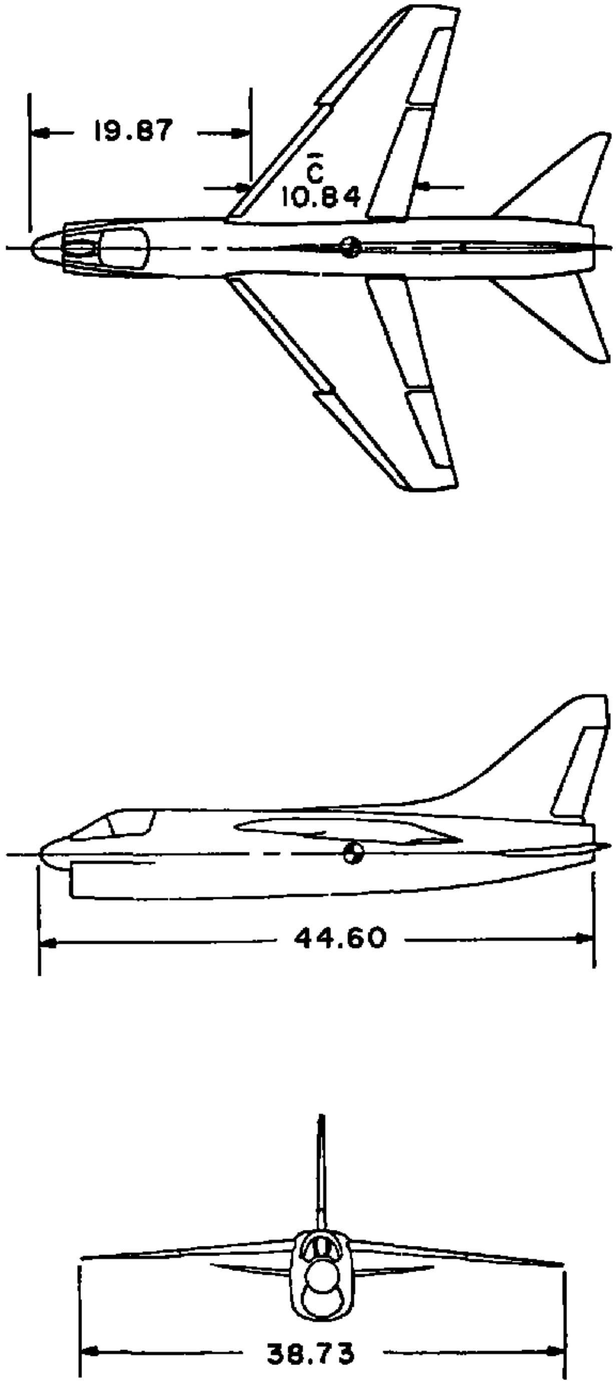

DIMENSIONS IN FEET

Figure 3. Attack aircraft configuration.

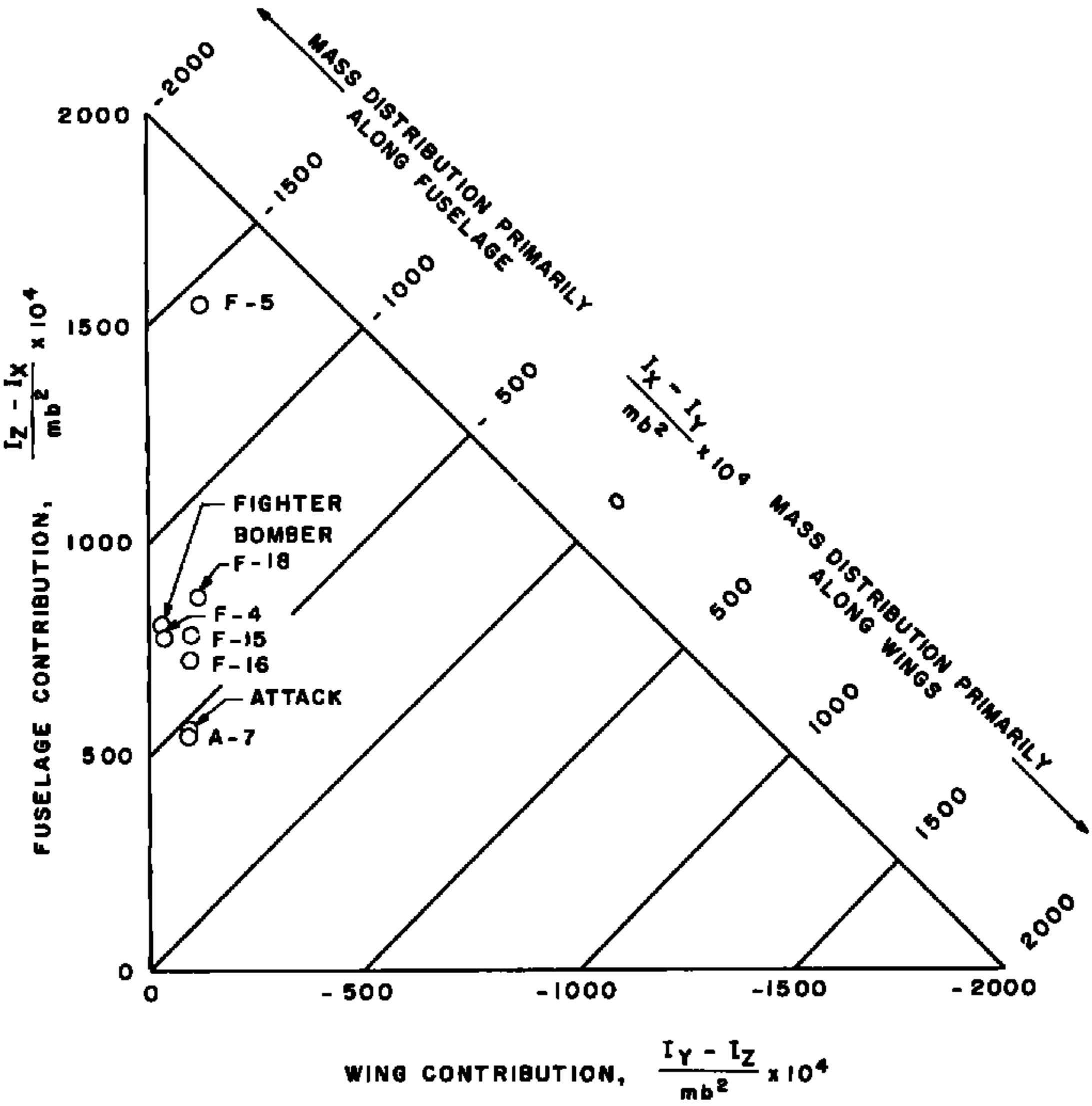

Figure 4. Aircraft mass distribution.

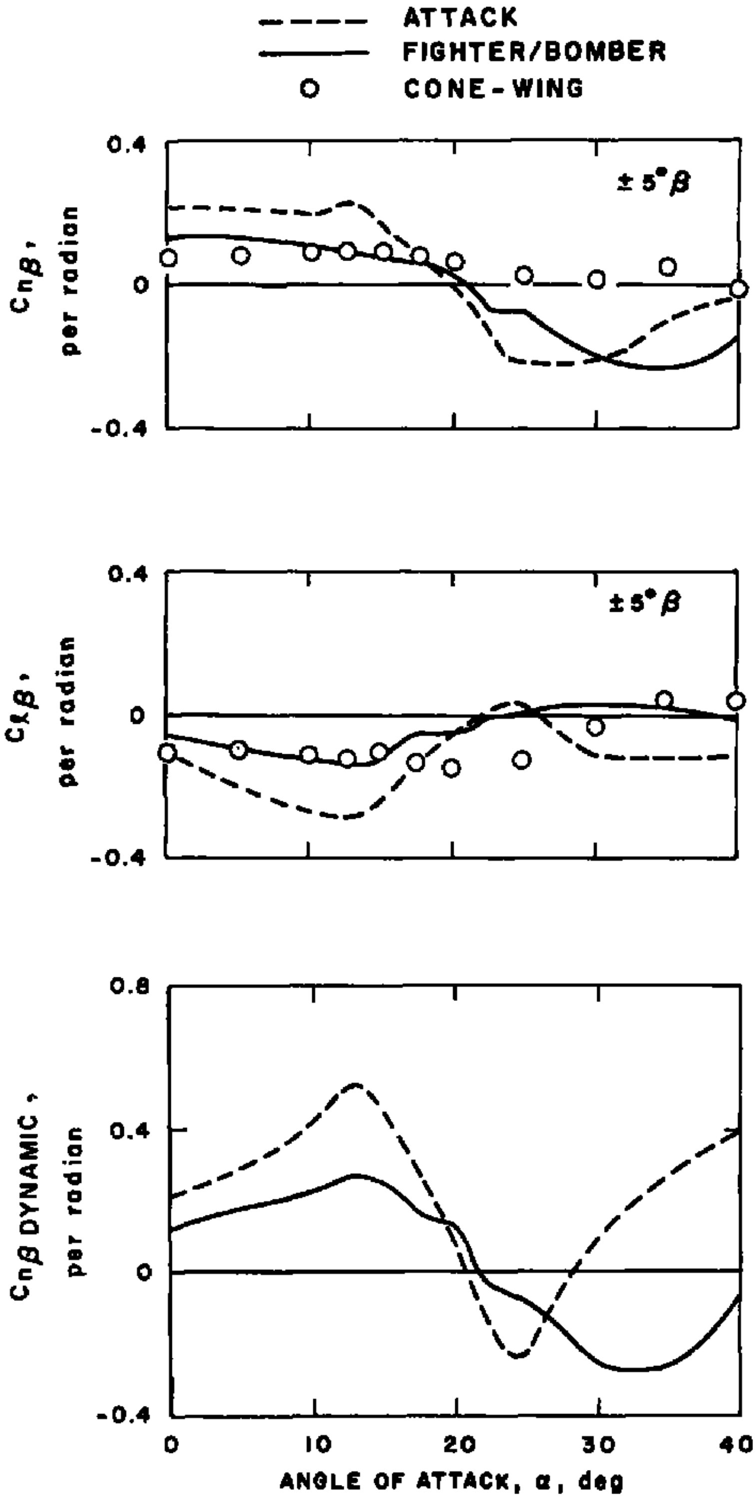

Figure 5. Static stability parameters.

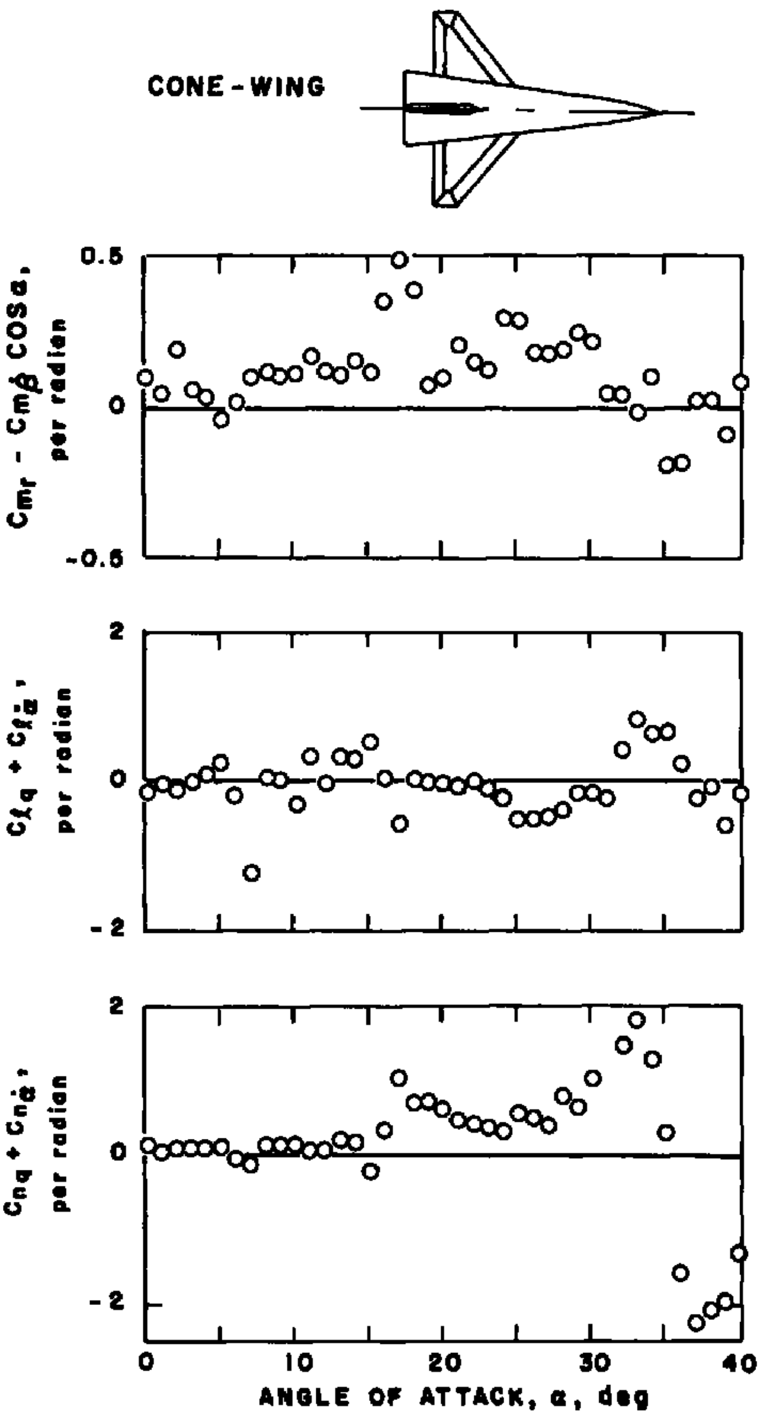

Figure 6. Cross-coupling derivatives, $M_\infty = 0.7$, $\beta = 0$ deg.

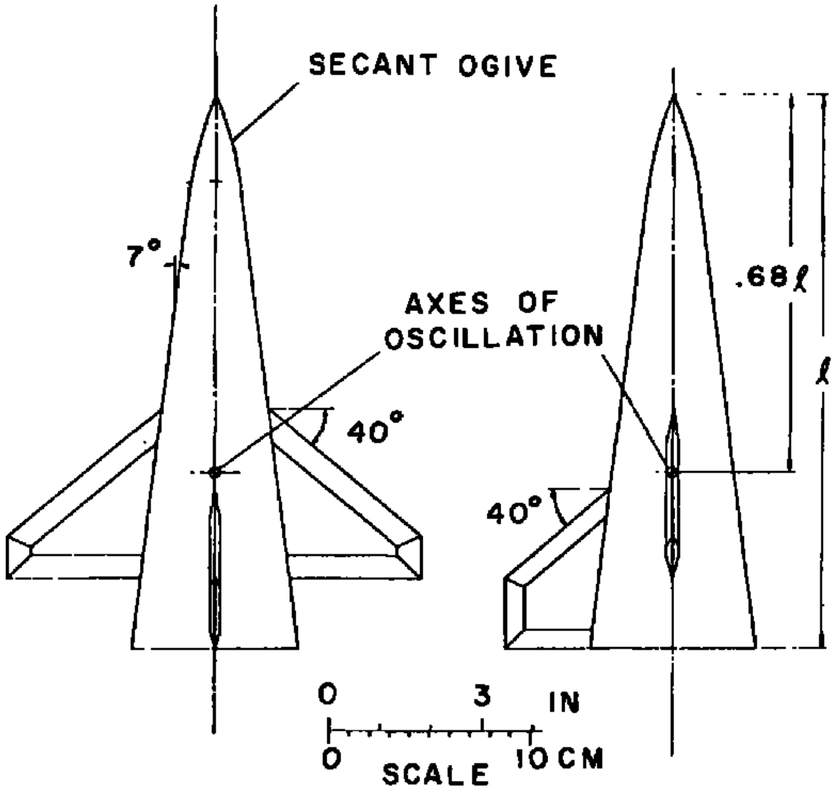

Figure 7. Cone-wing model.

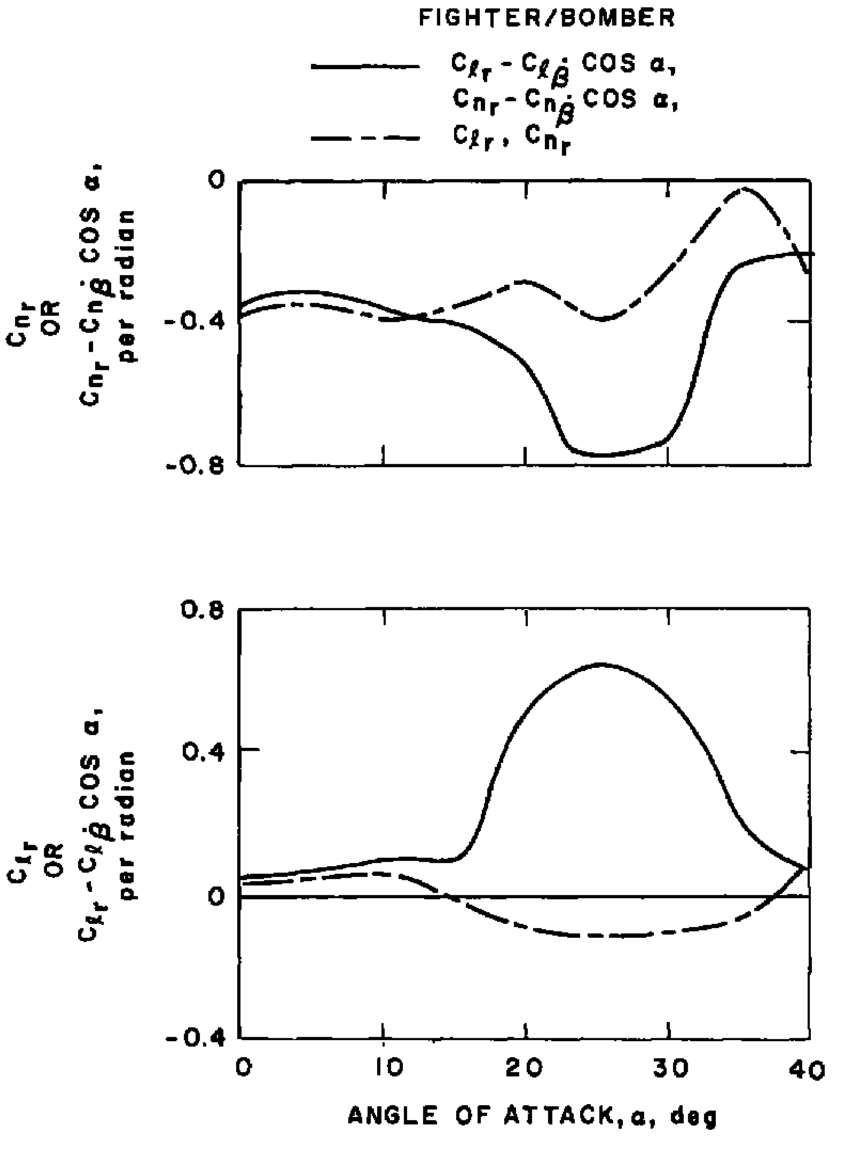

Figure 8. Roll and yaw damping derivatives.

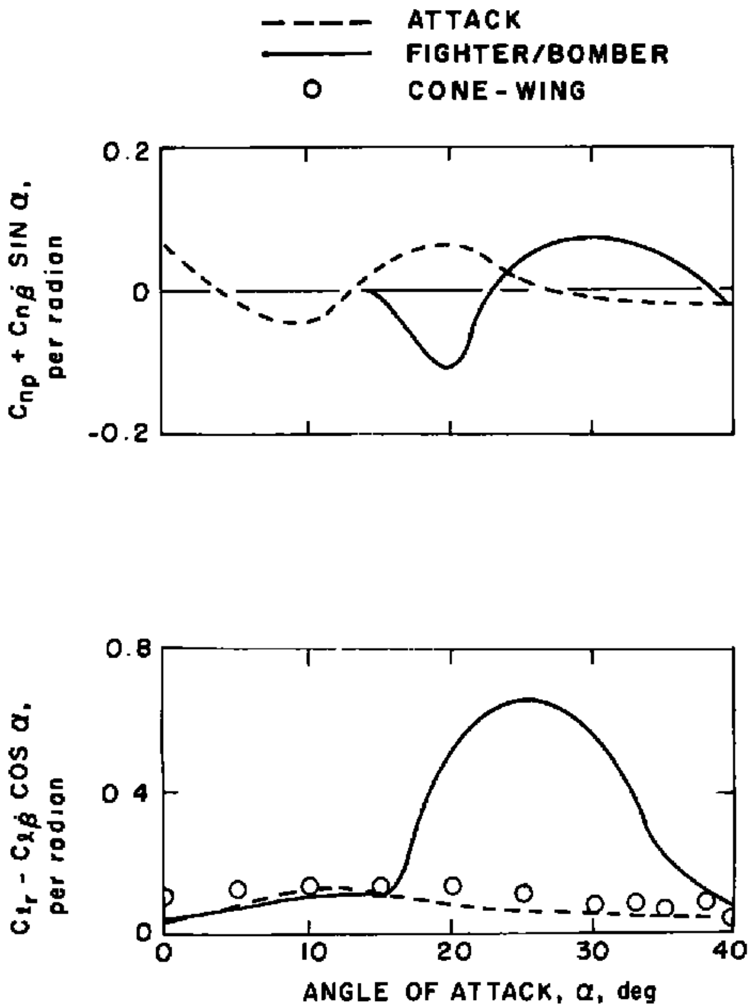

Figure 9. Dynamic cross derivatives.

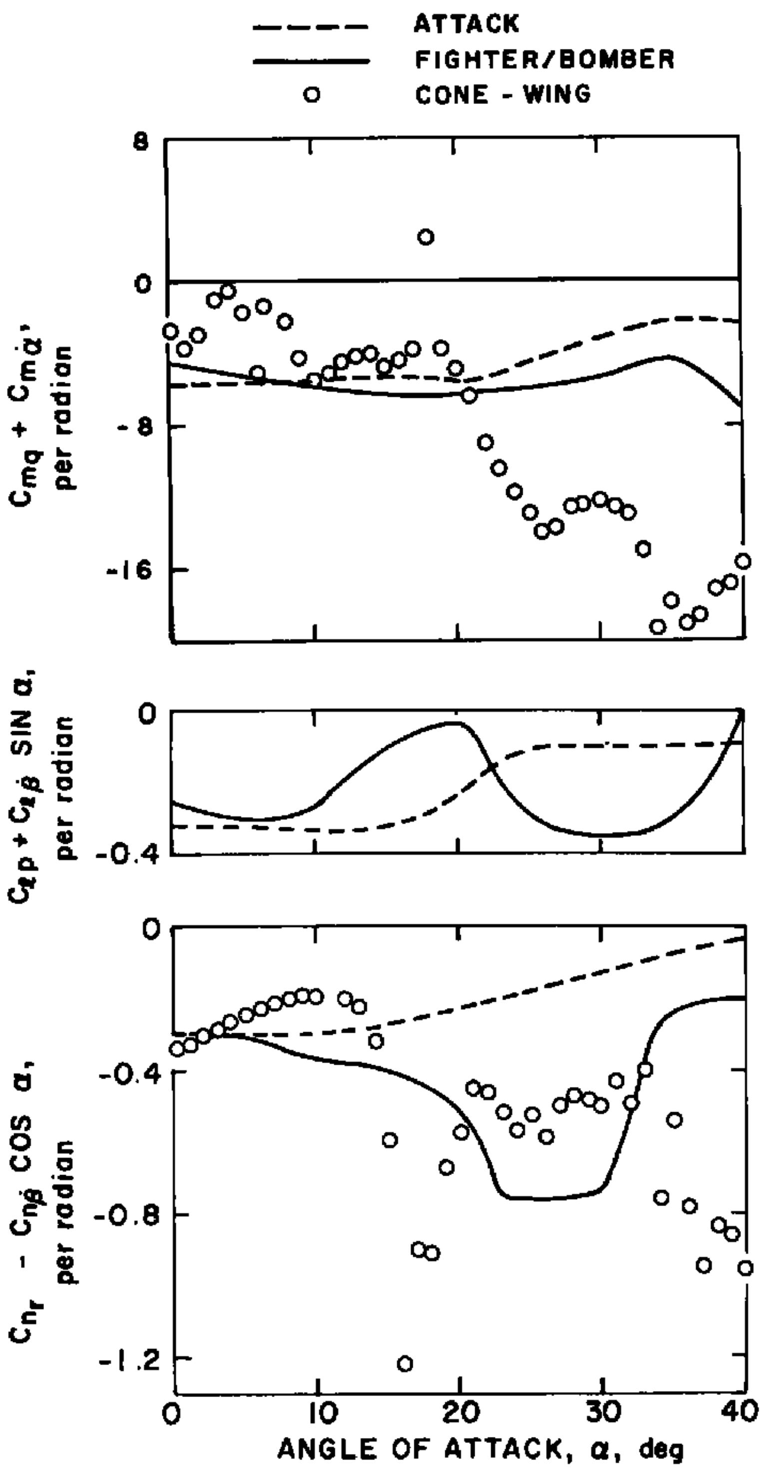

Figure 10. Dynamic direct derivatives.

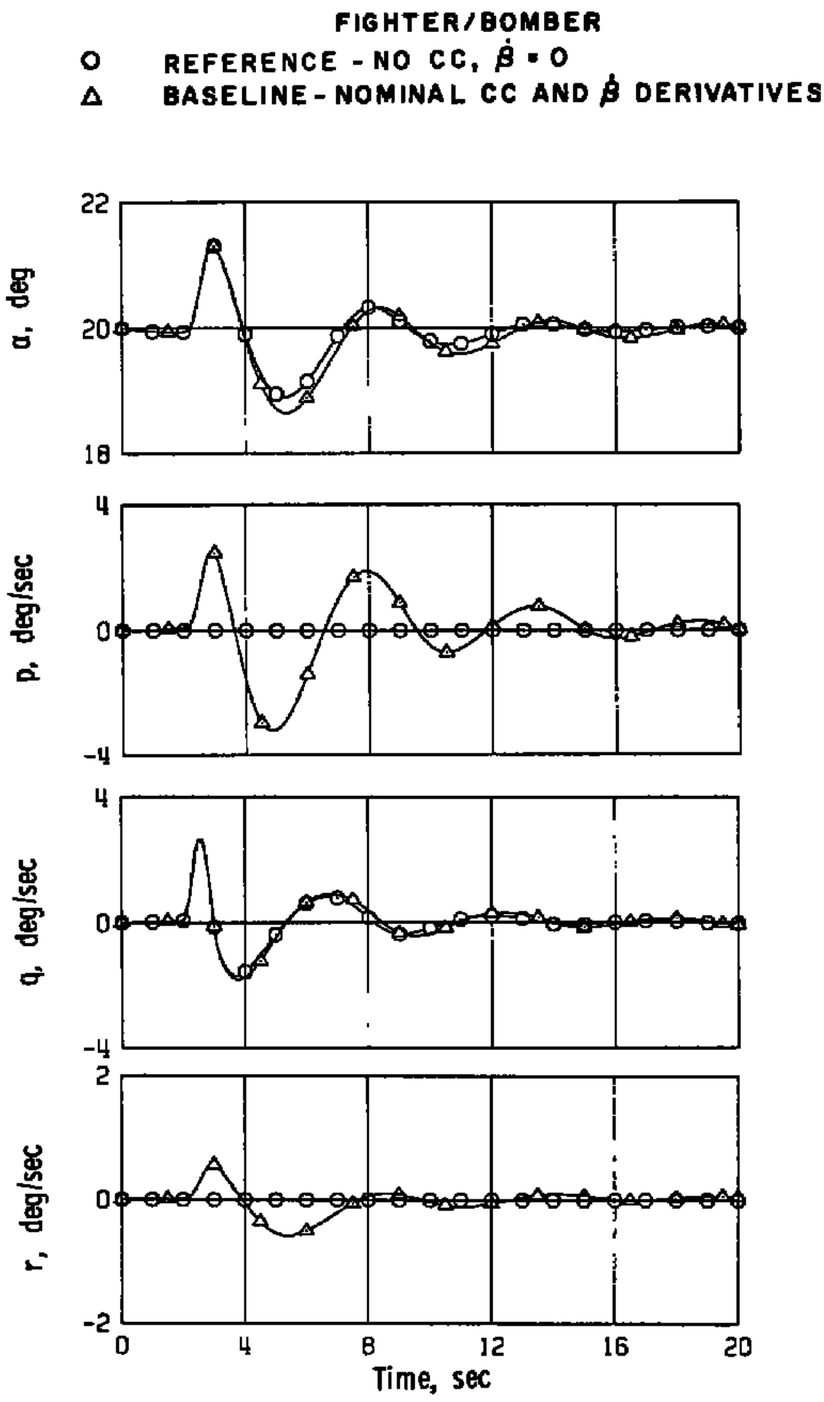

a. Elevator doublet

Figure 11. Fighter/bomber baseline motion, level flight, nominal cross-coupling and $\dot{\beta}$ derivatives.

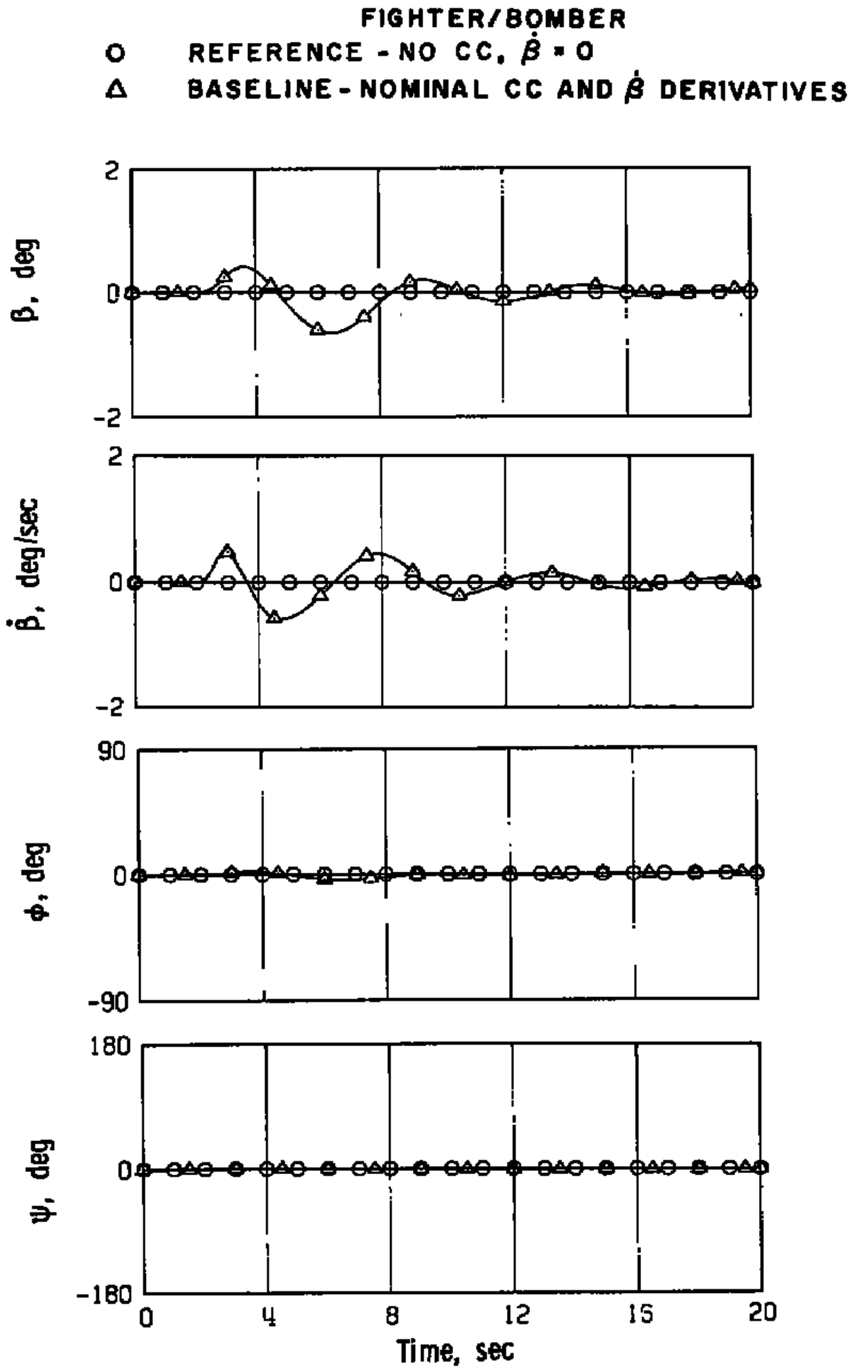

a. Continued
Figure 11. Continued.

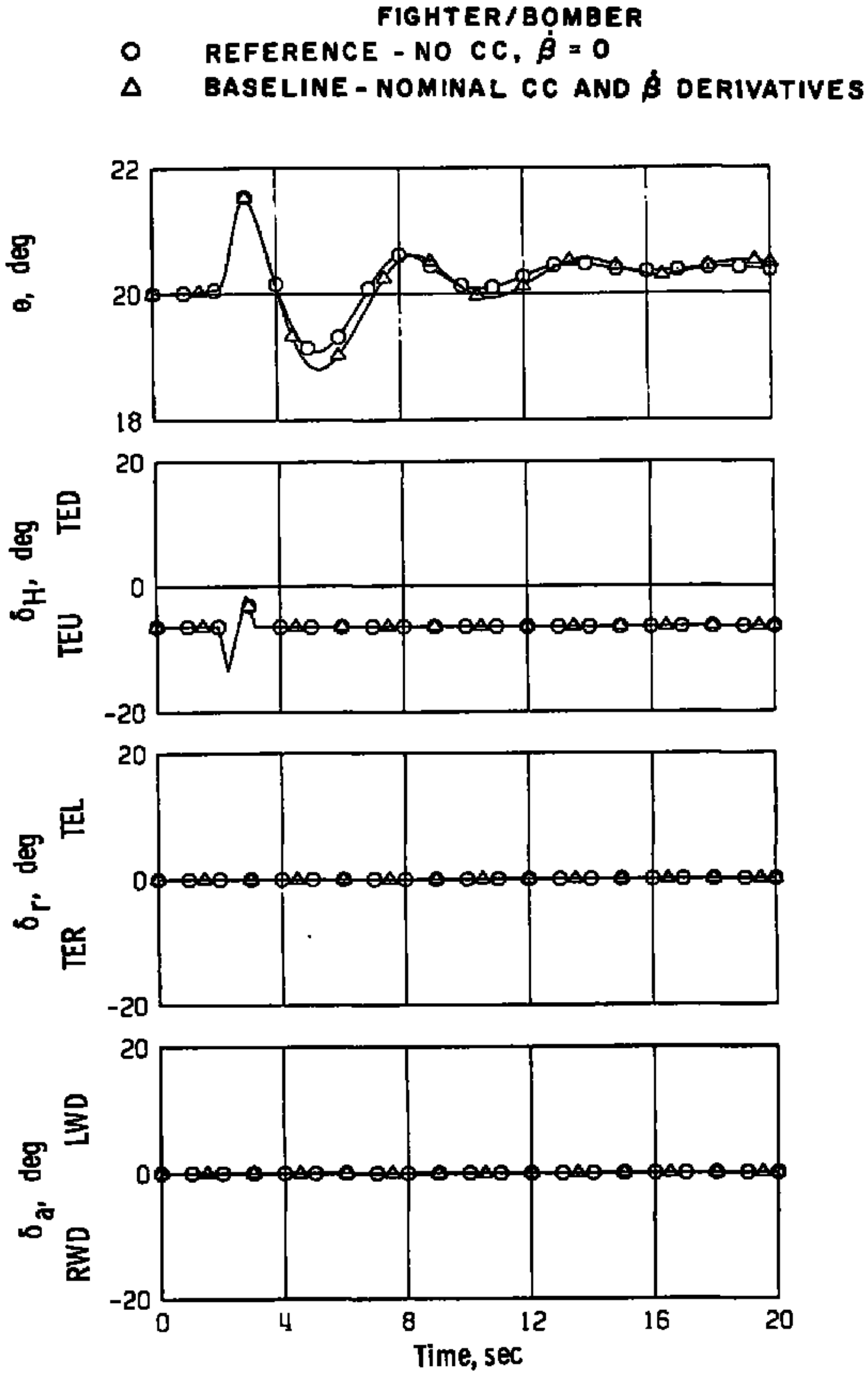

a. Concluded
Figure 11. Continued.

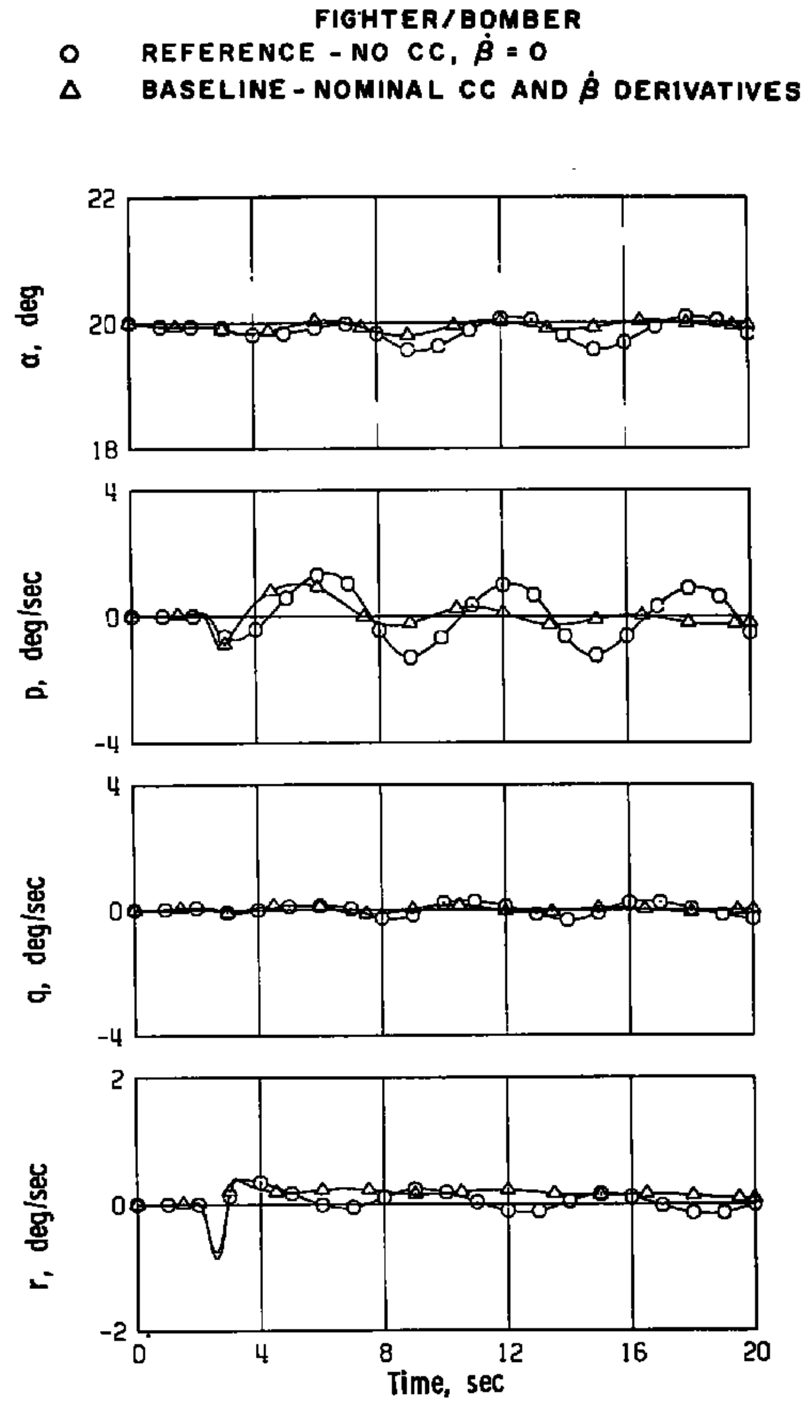

b. Rudder doublet
Figure 11. Continued.

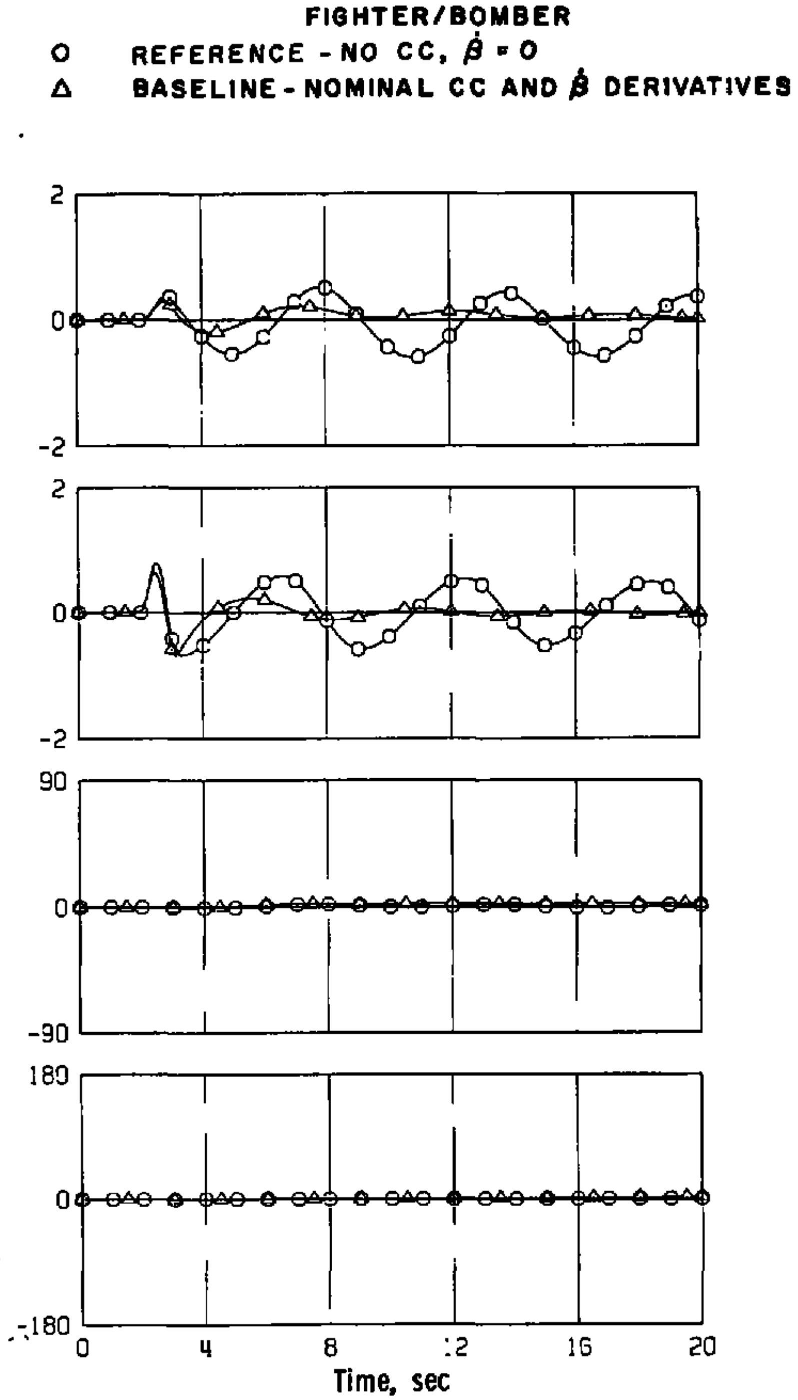

b. Continued
Figure 11. Continued.

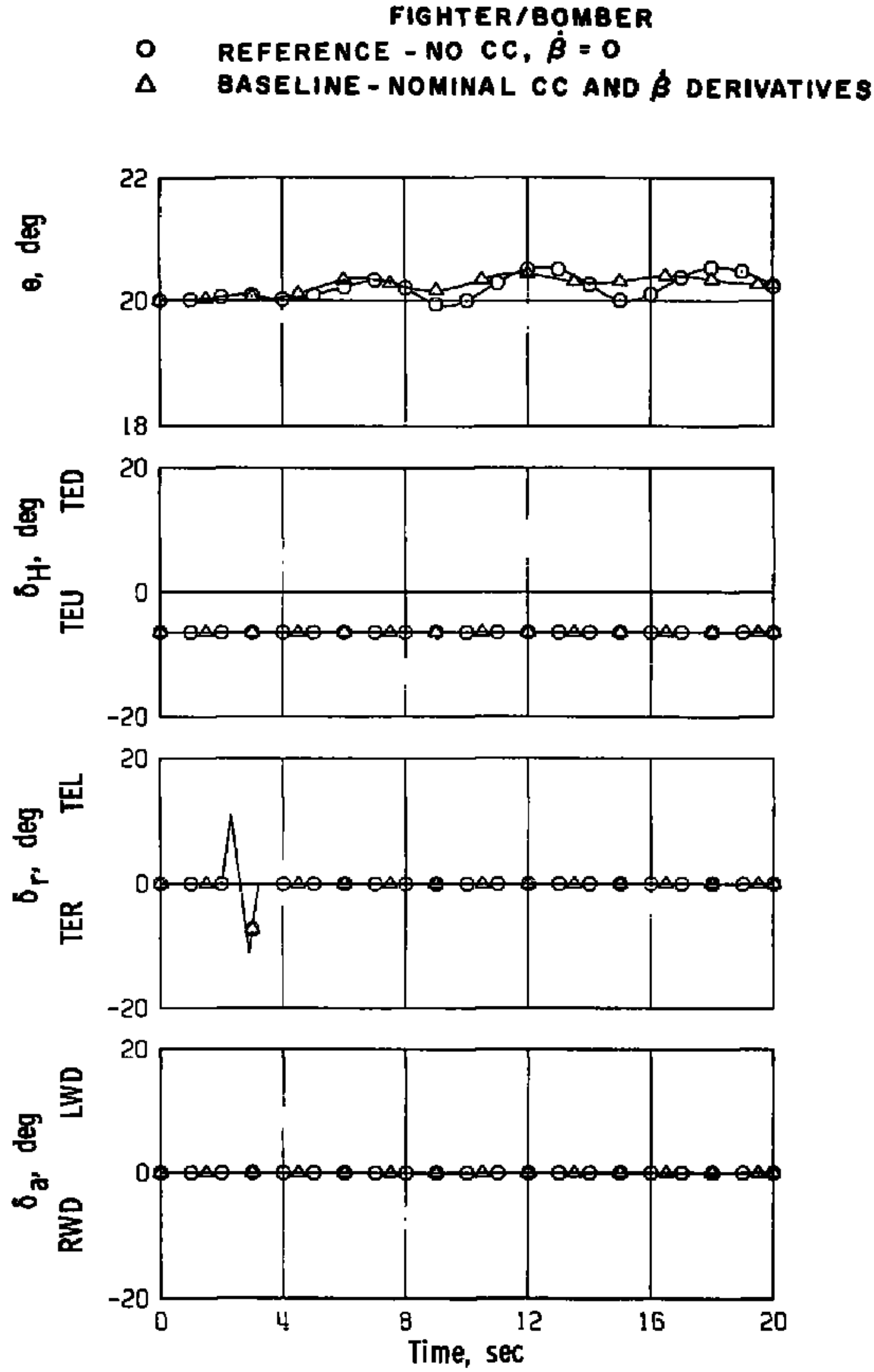

b. Concluded
Figure 11. Concluded.

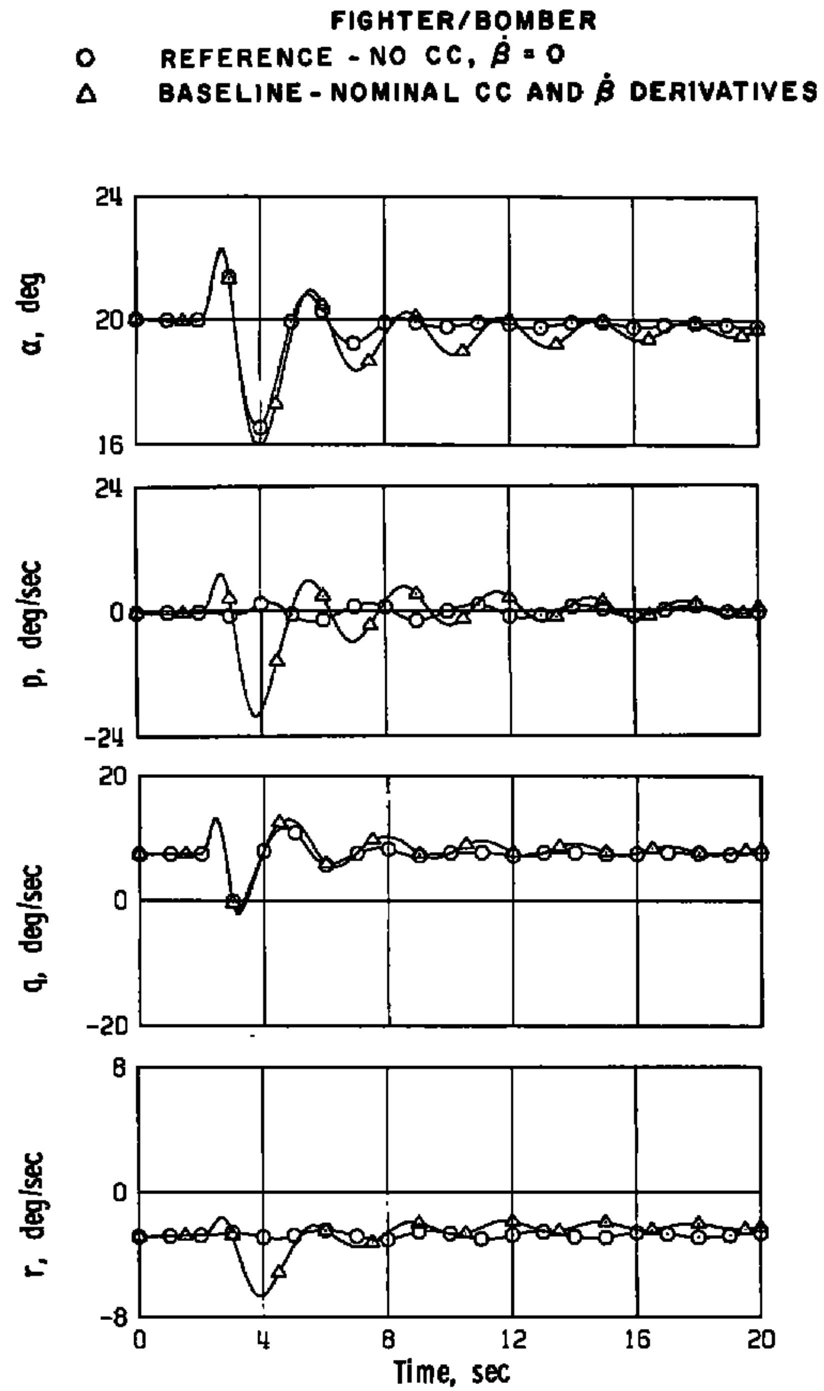

a. Elevator doublet

Figure 12. Fighter/bomber baseline motion, 3-g turning flight, nominal cross-coupling and $\dot{\beta}$ derivatives.

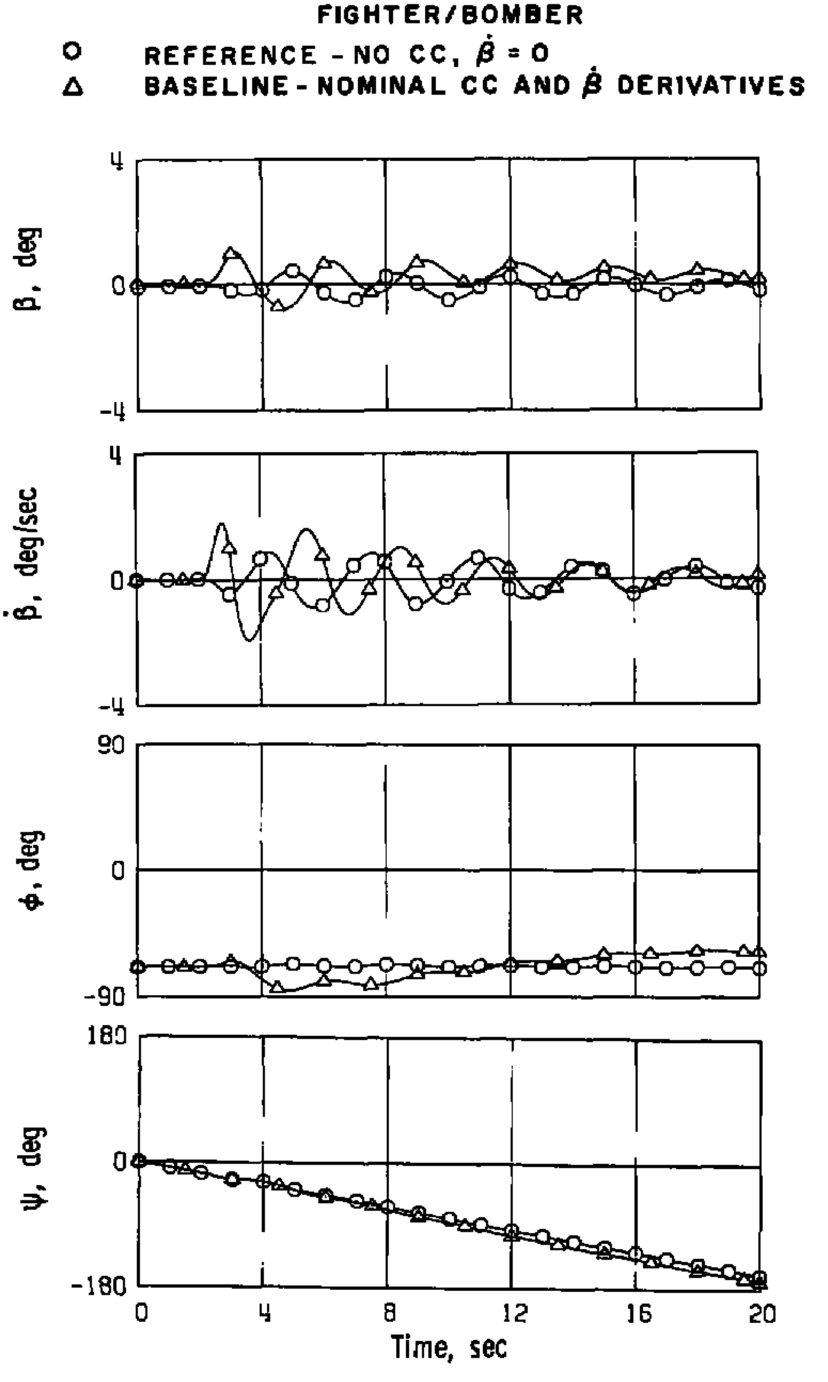

a. Continued
Figure 12. Continued.

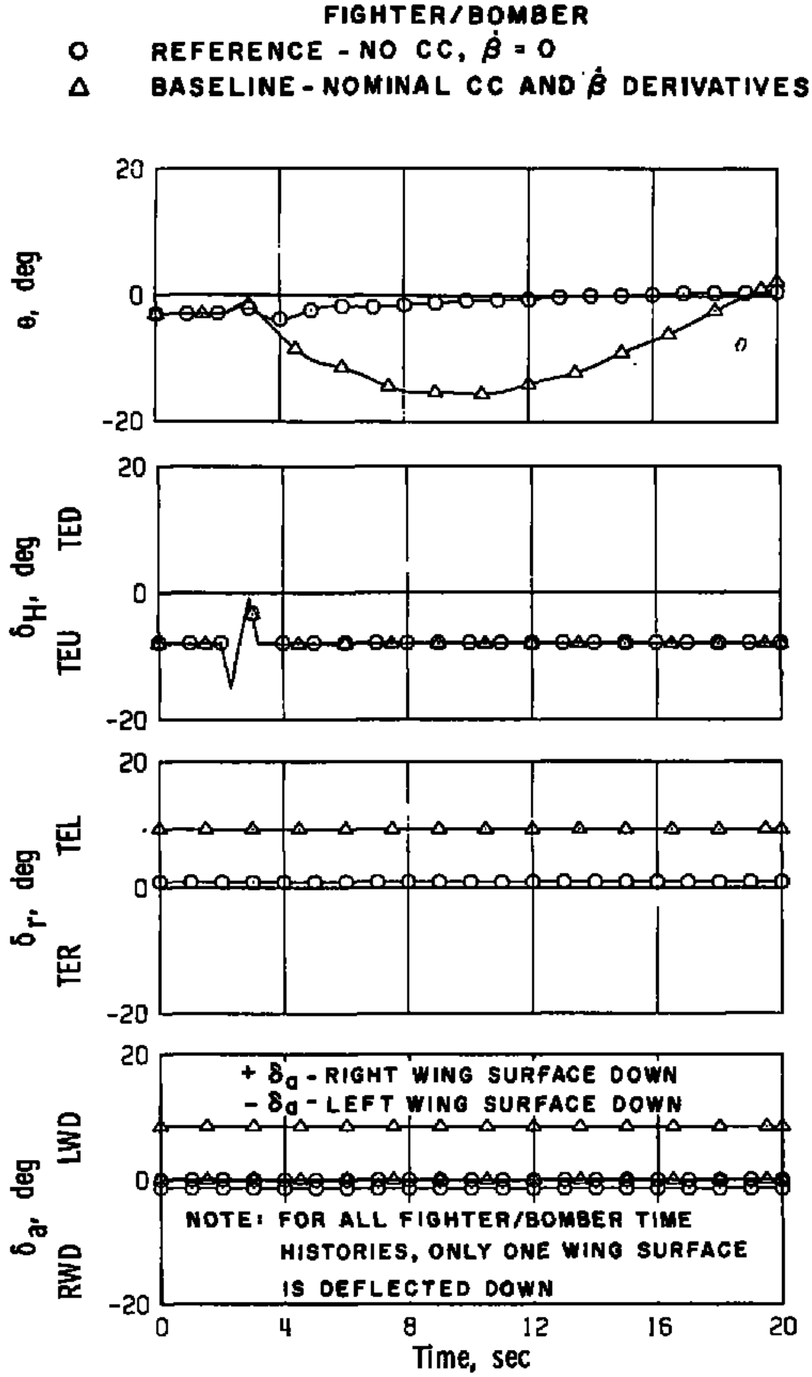

a. Concluded
Figure 12. Continued.

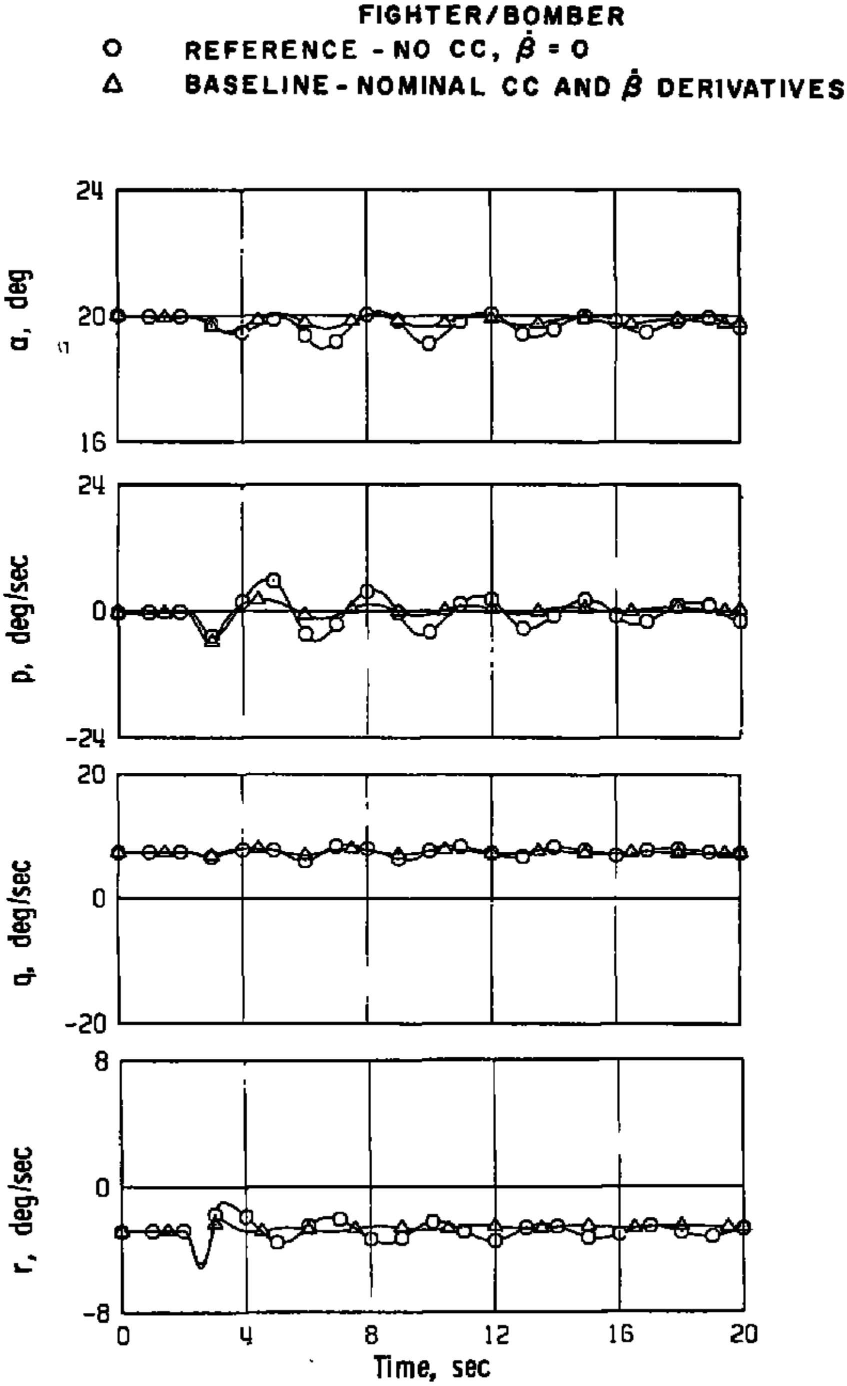

b. Rudder doublet
Figure 12. Continued.

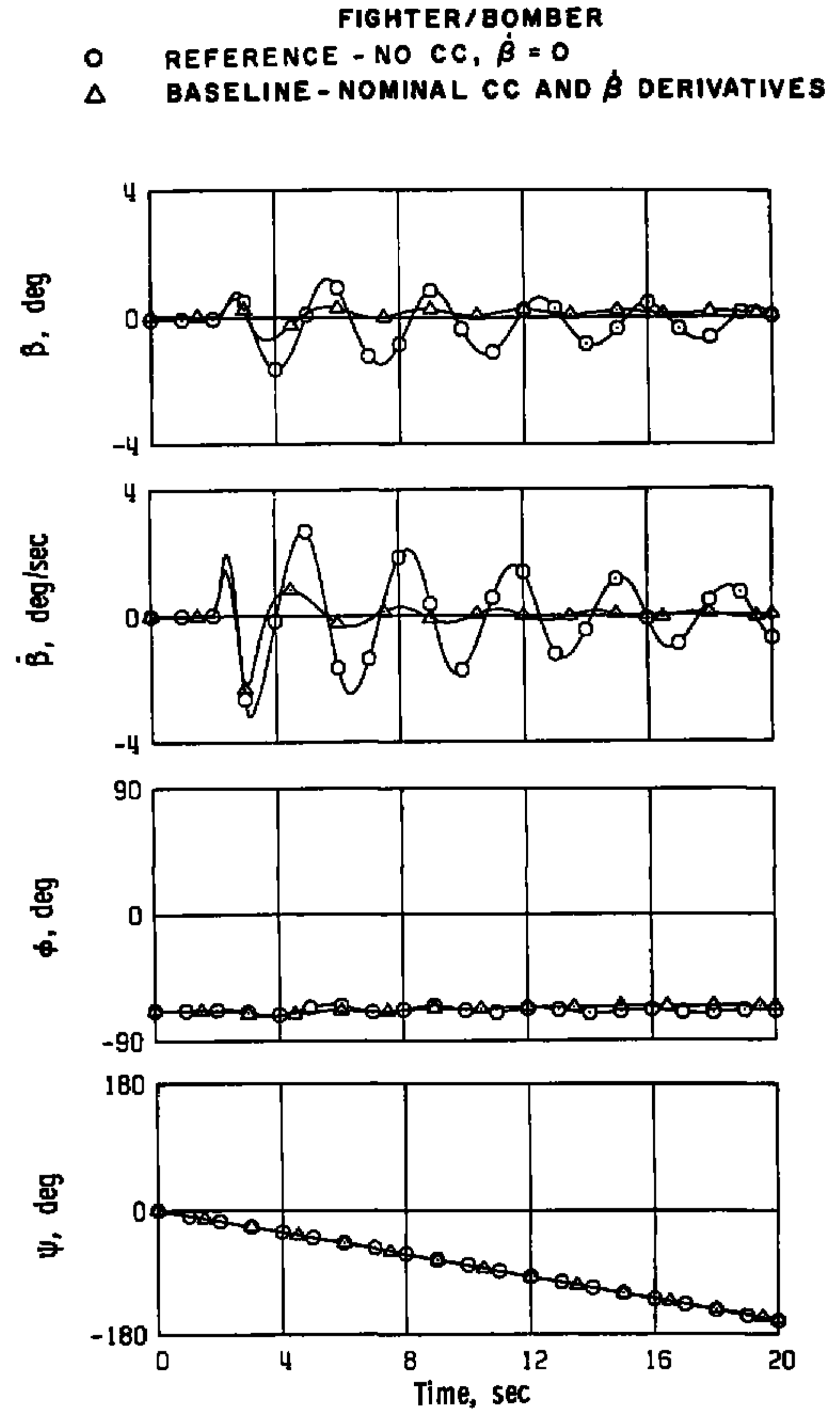

b. Continued
Figure 12. Continued.

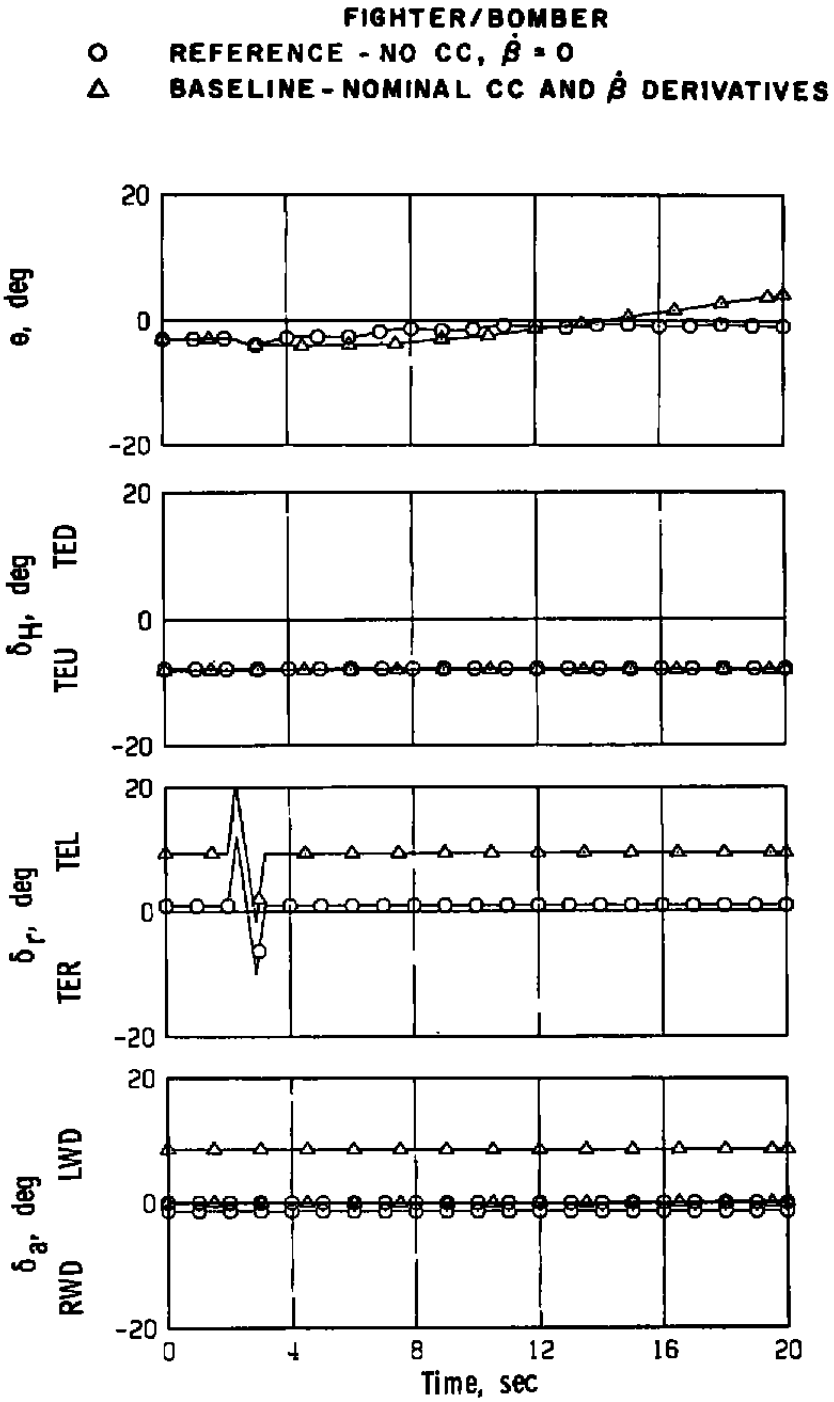

b. Concluded
Figure 12. Concluded.

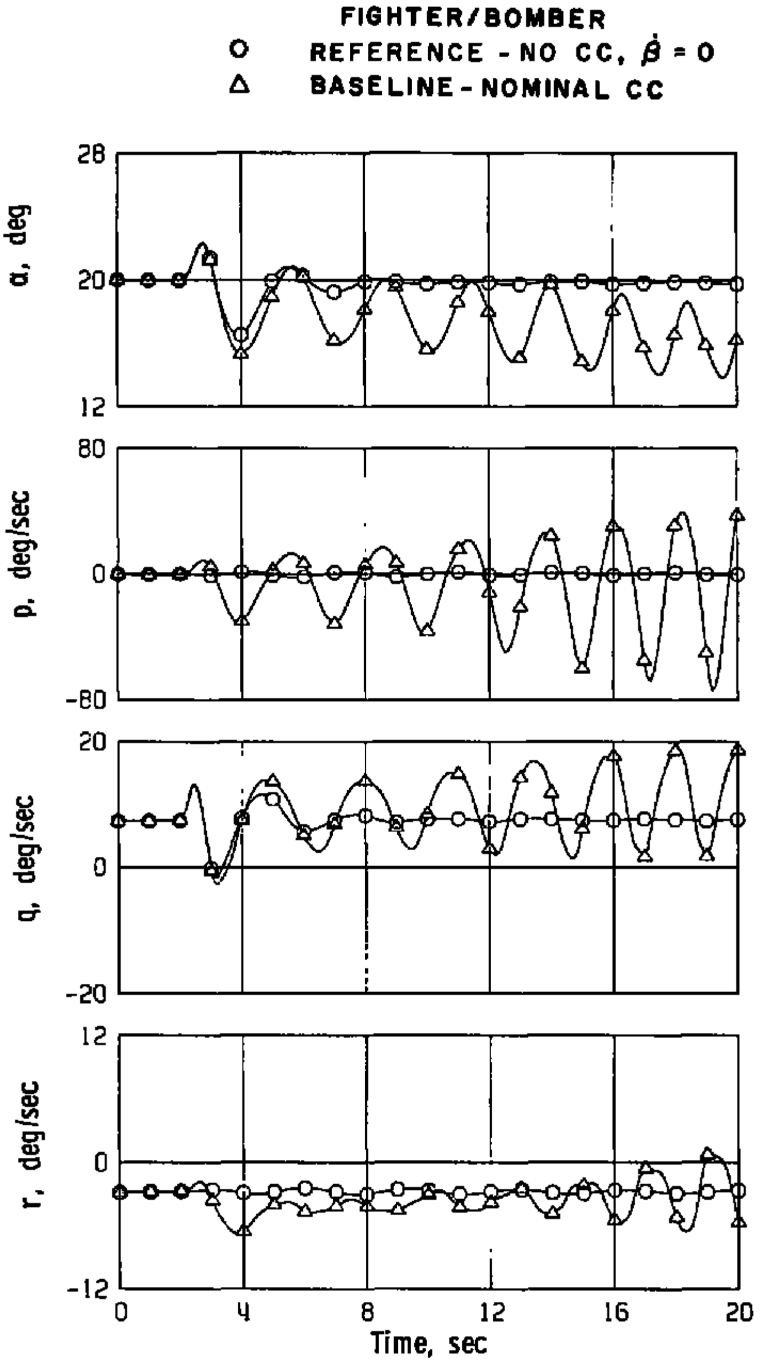

a. Elevator doublet

Figure 13. Fighter/bomber baseline motion, 3-g turning flight, nominal cross-coupling derivatives, $\dot{\beta}$ derivatives zero.

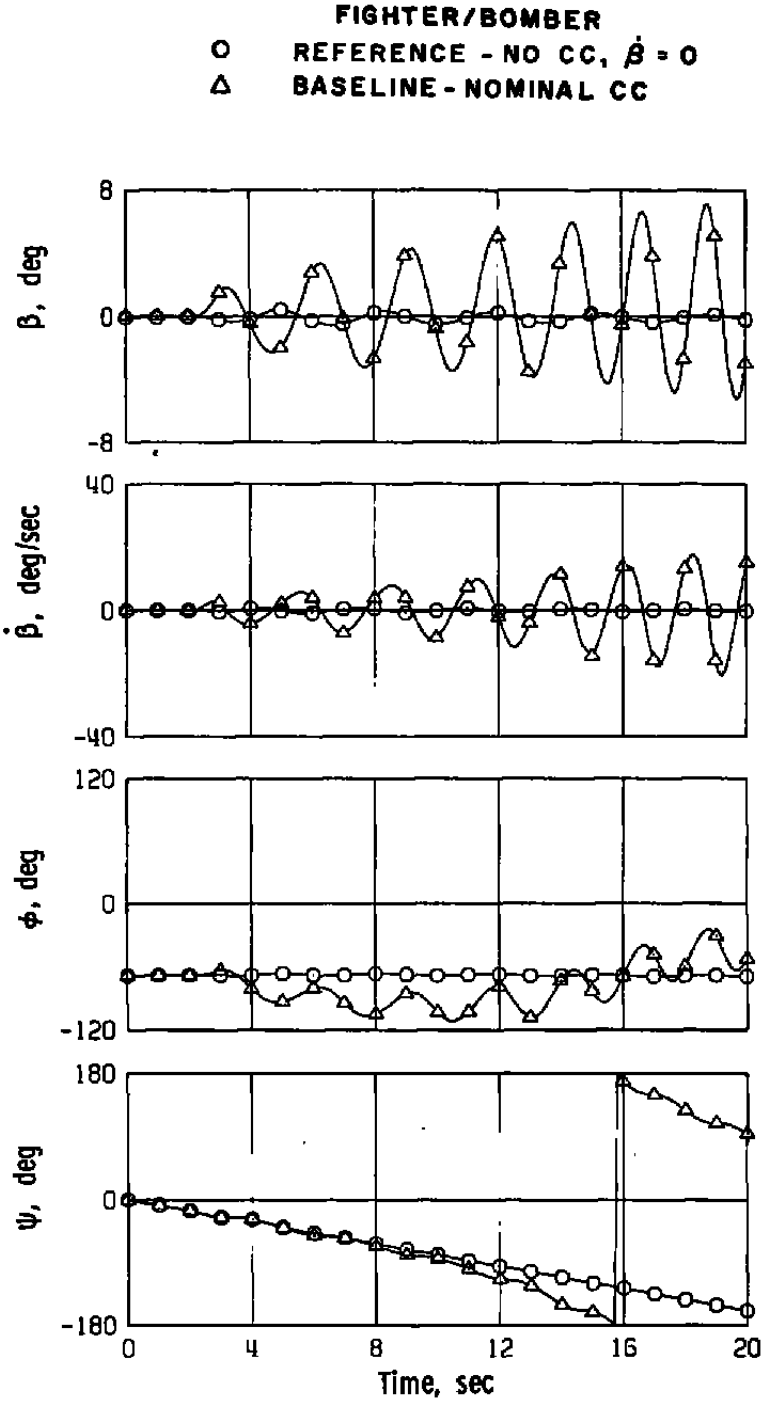

a. Continued
Figure 13. Continued.

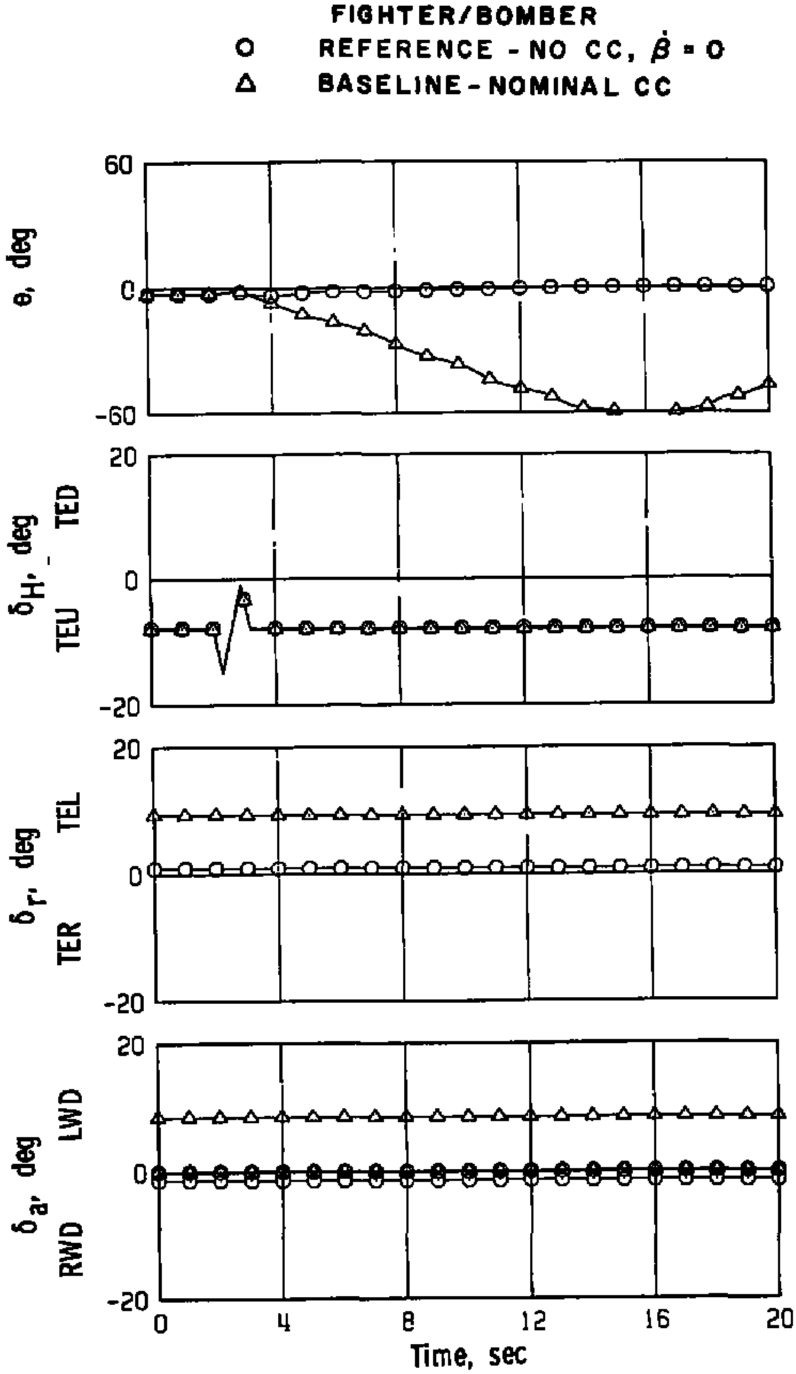

a. Concluded
Figure 13. Continued.

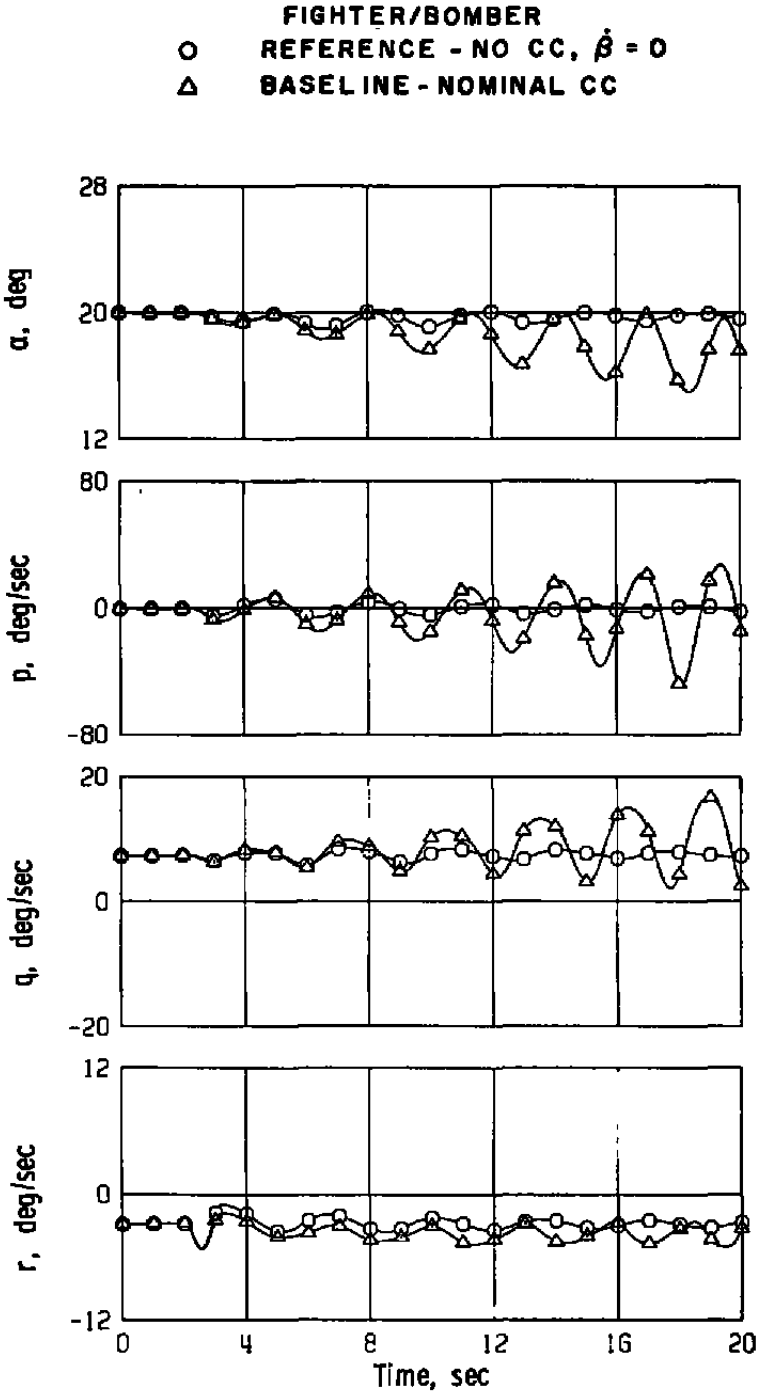

b. Rudder doublet
Figure 13. Continued.

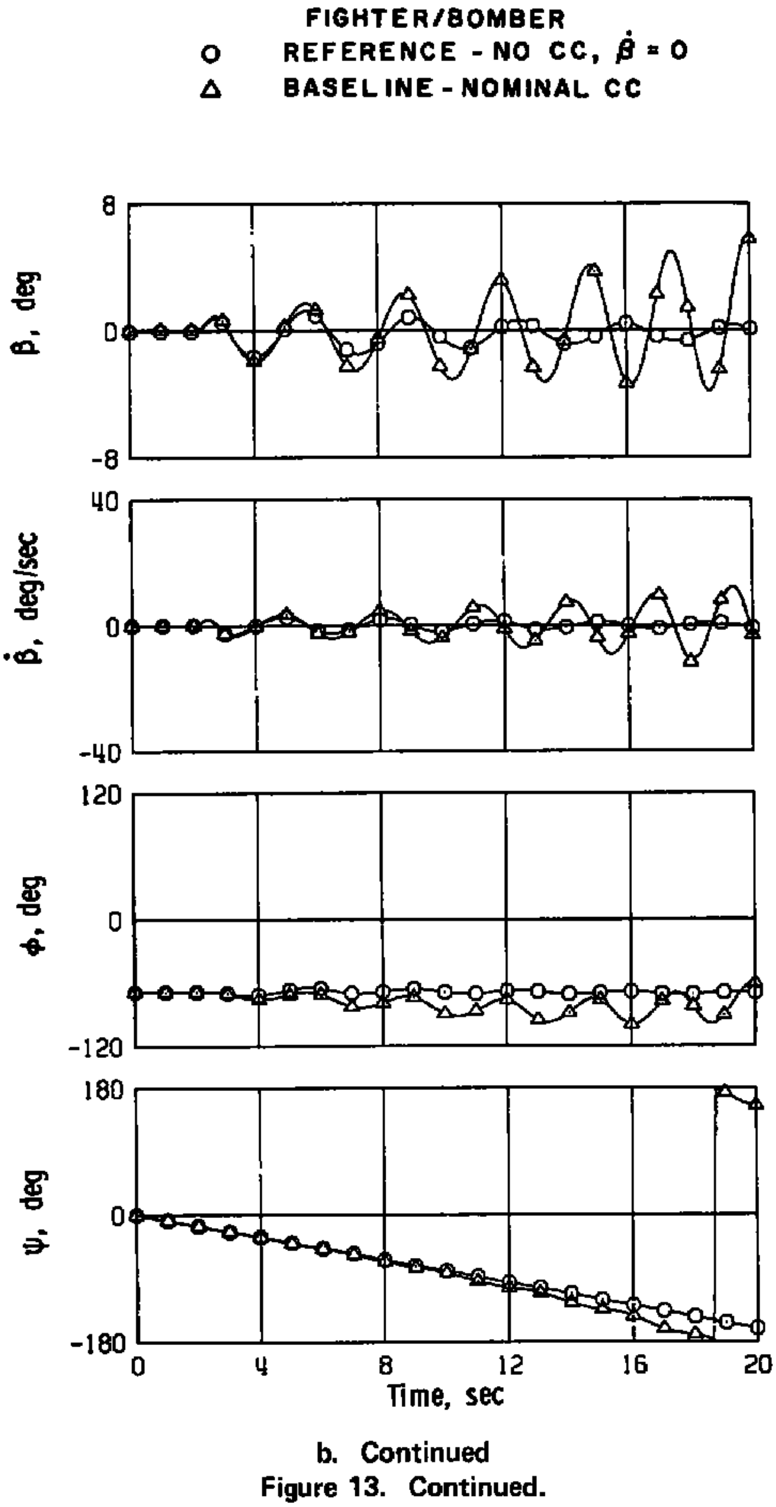

b. Continued
Figure 13. Continued.

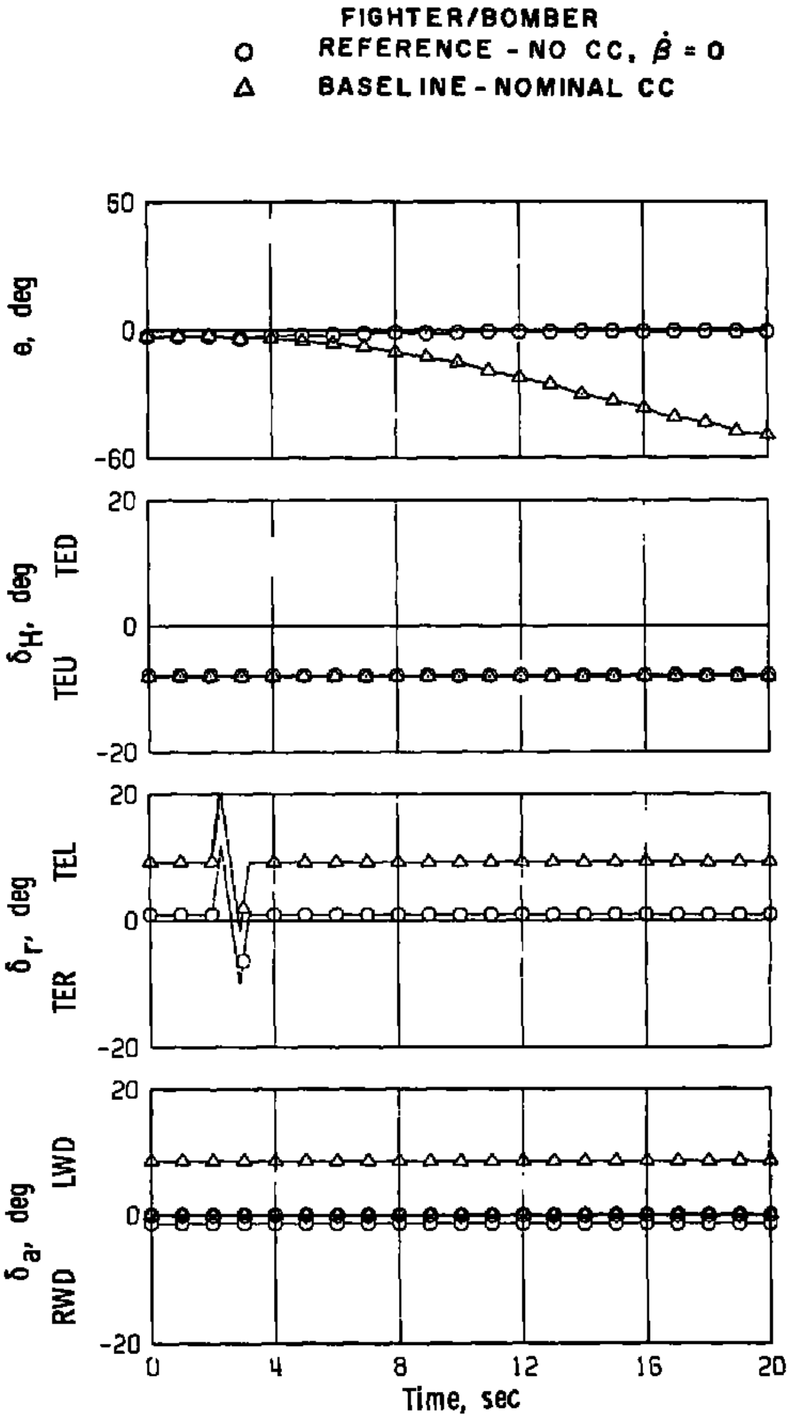

b. Concluded
Figure 13. Concluded.

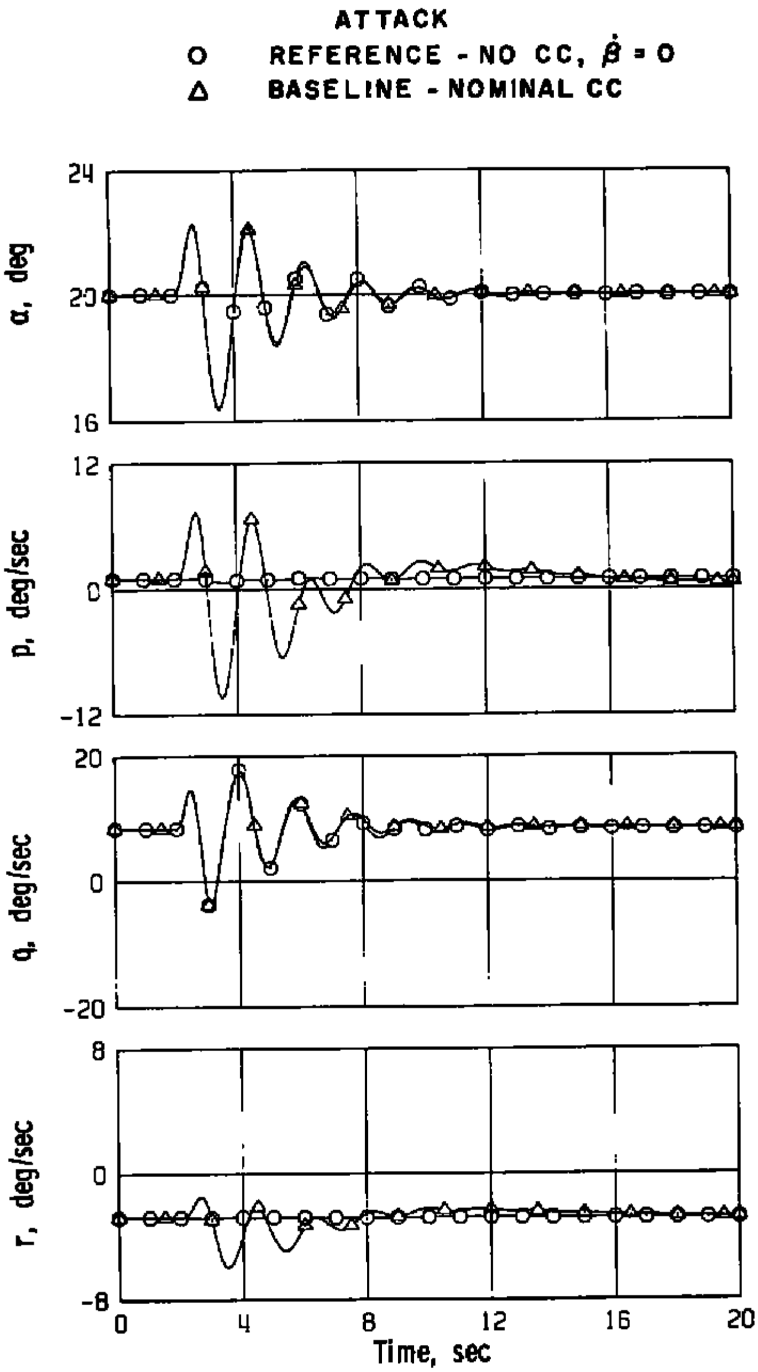

a. Elevator doublet

Figure 14. Attack baseline motion, 3-g turning flight, nominal cross-coupling derivatives, $\dot{\beta}$ derivatives zero.

ATTACK
○ REFERENCE - NO CC, $\dot{\beta} = 0$
△ BASELINE - NOMINAL CC

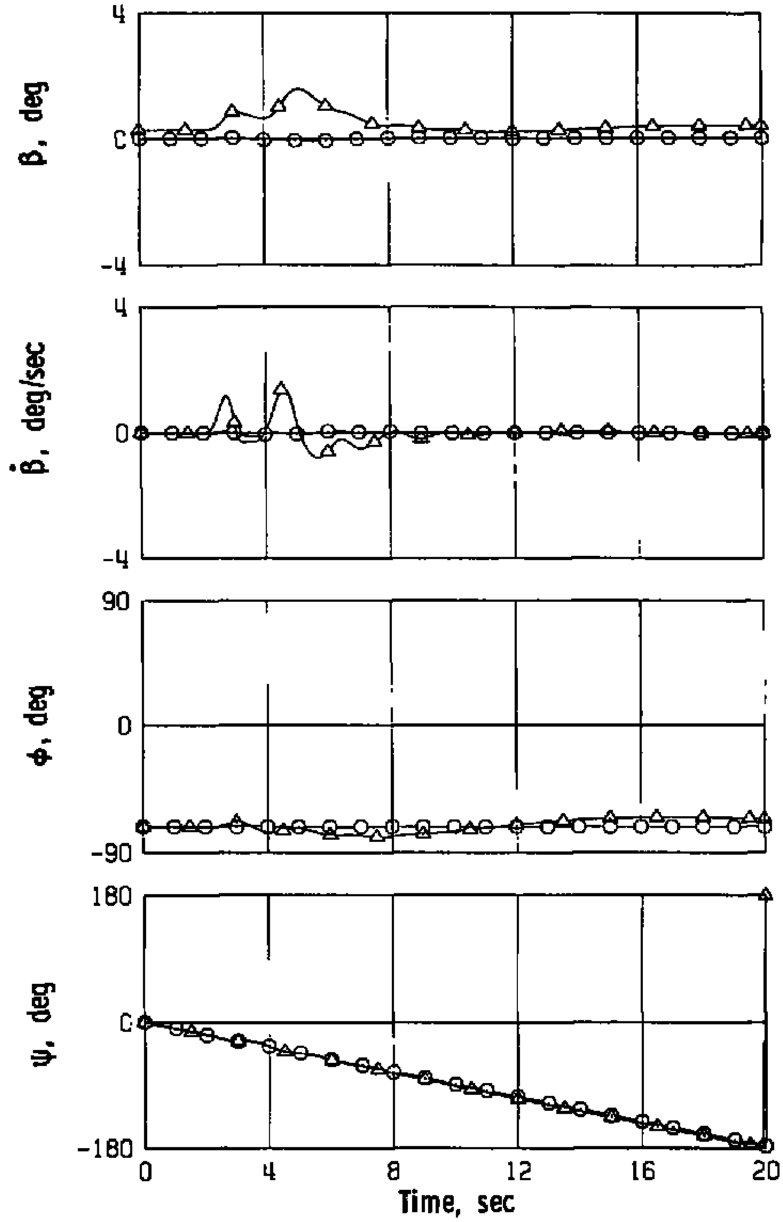

a. Continued
Figure 14. Continued.

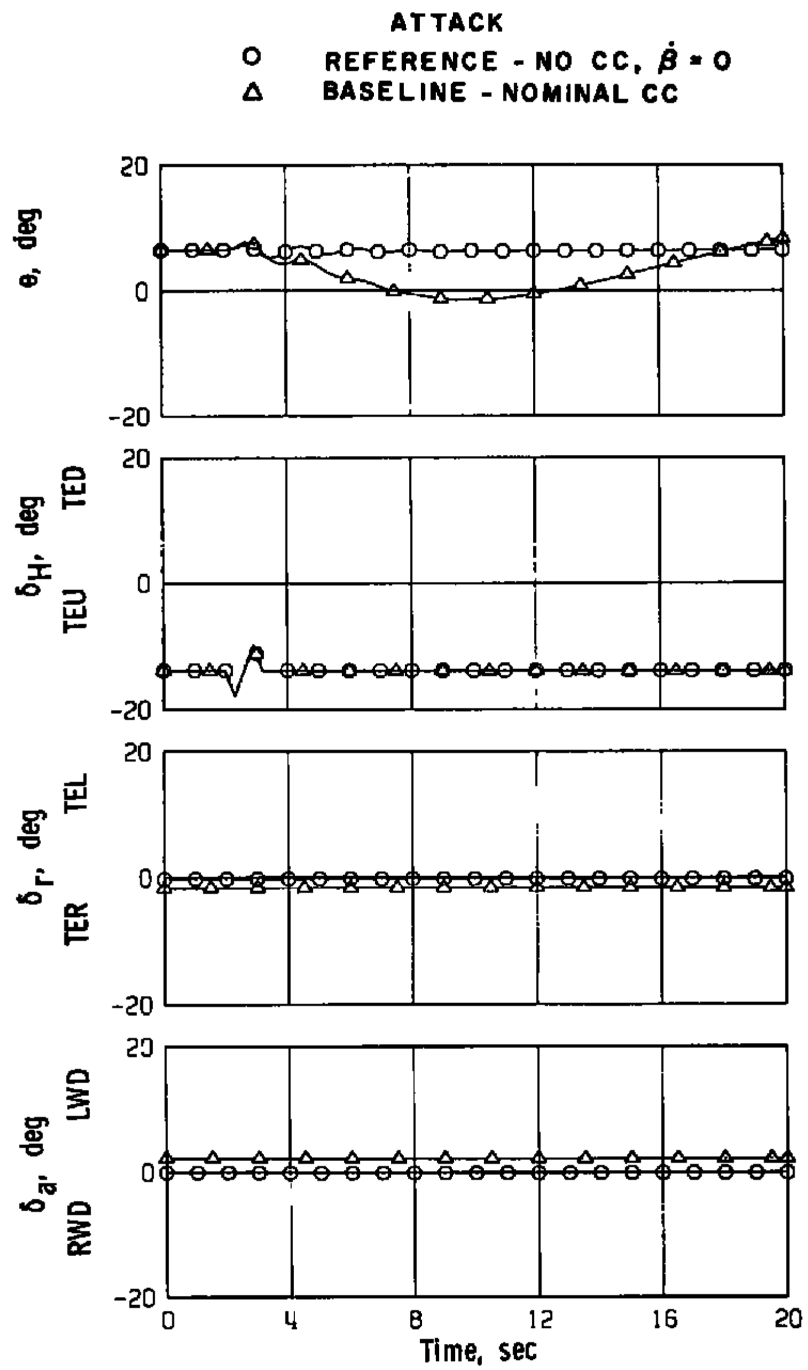

a. Concluded
Figure 14. Continued.

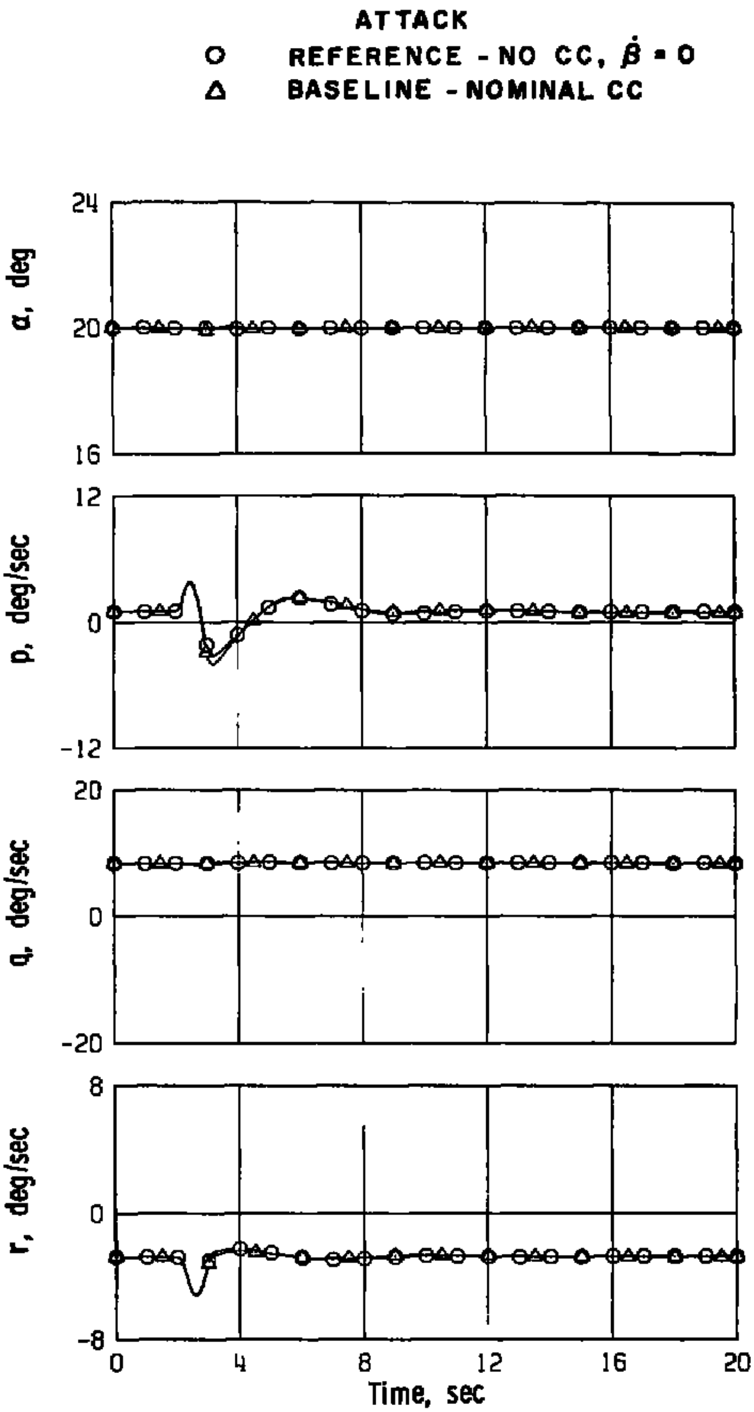

b. Rudder doublet
Figure 14. Continued.

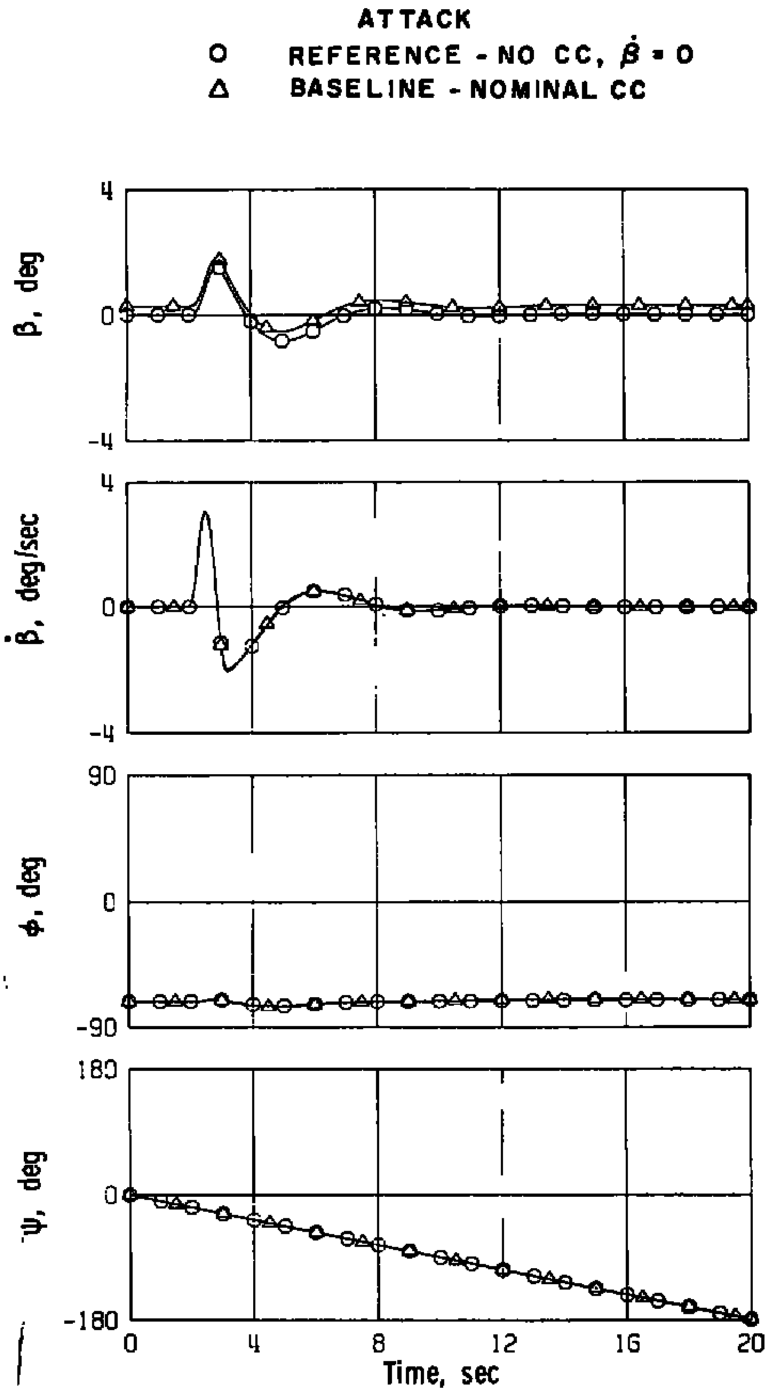

b. Continued
Figure 14. Continued.

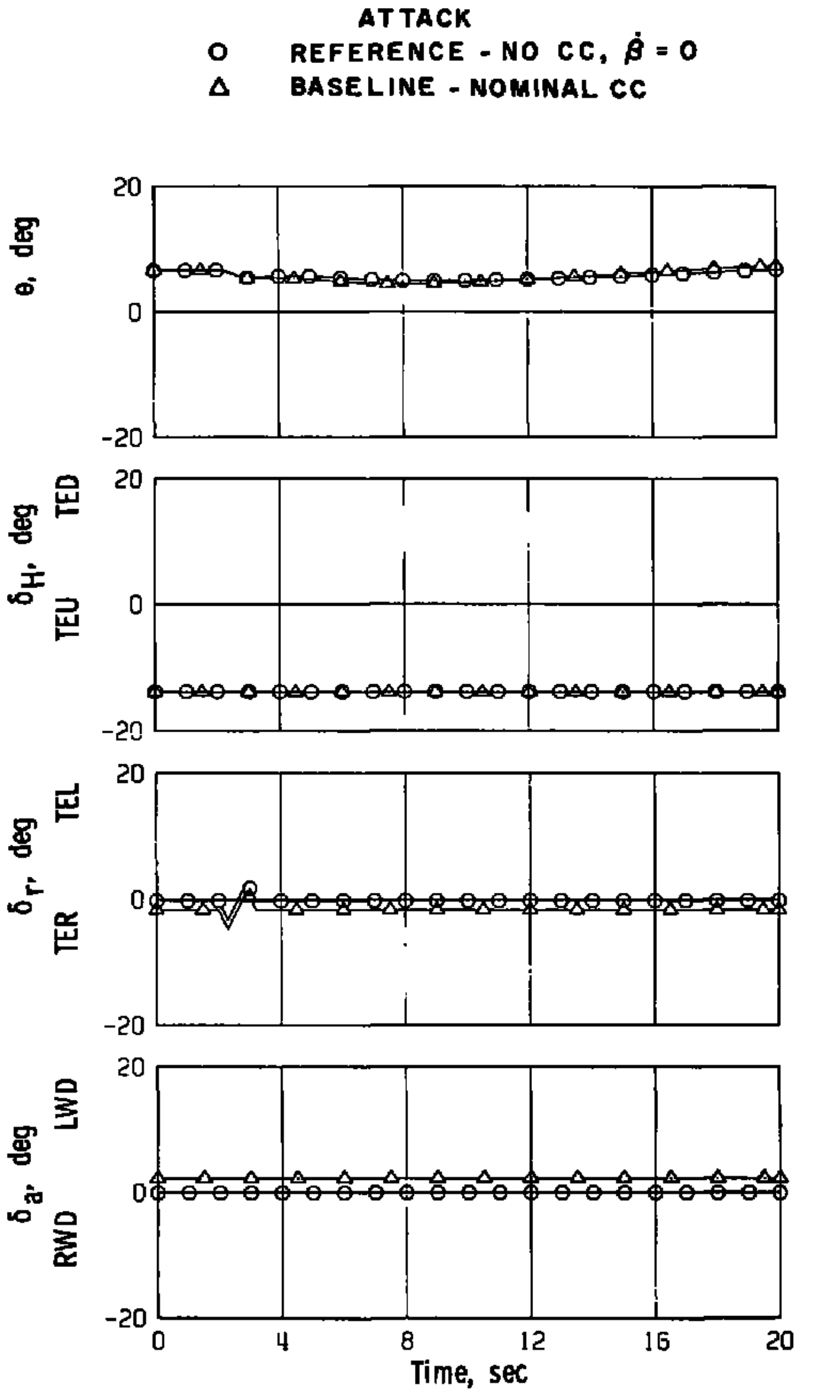

b. Concluded
Figure 14. Concluded.

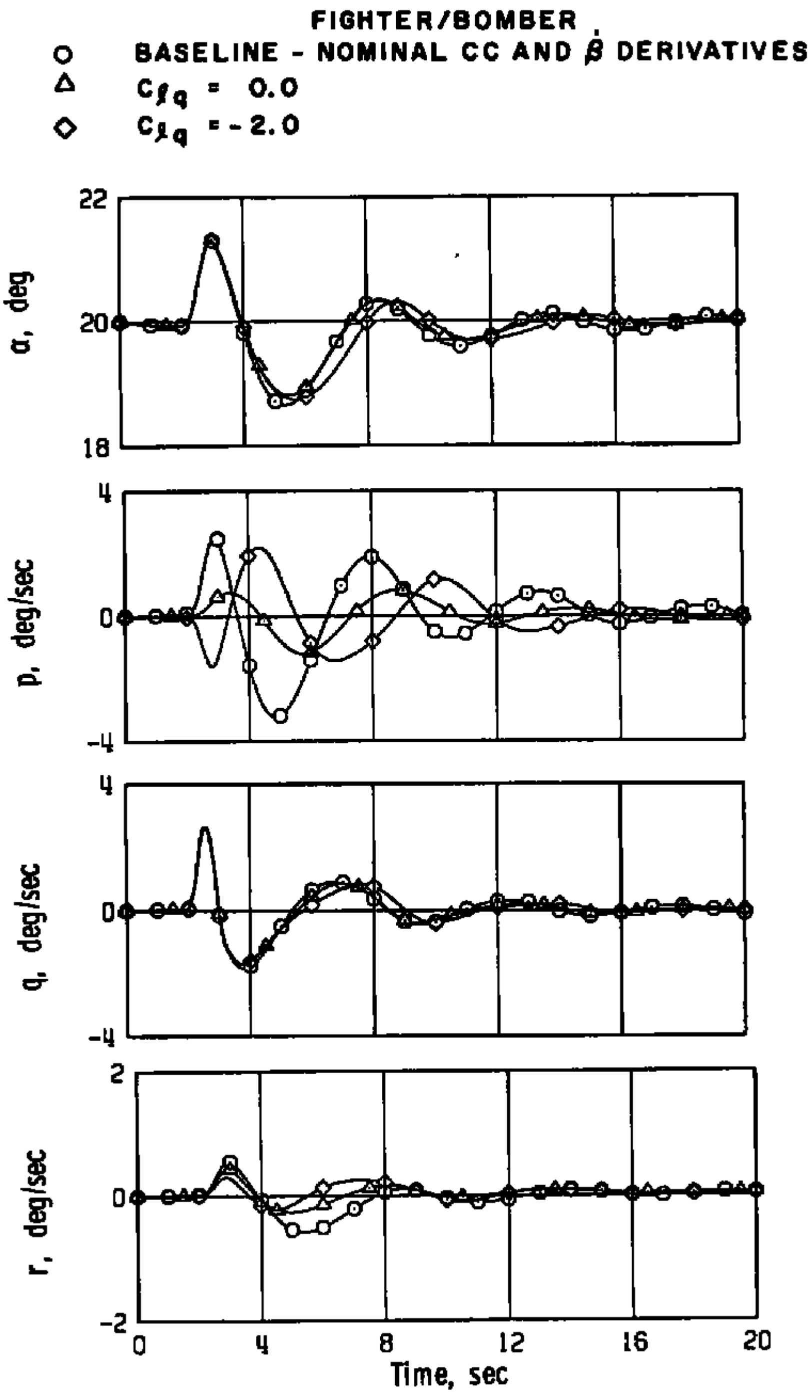

Figure 15. C_{ℓ_q} variation, fighter/bomber level flight with nominal cross-coupling and $\dot{\beta}$ derivatives, elevator doublet.

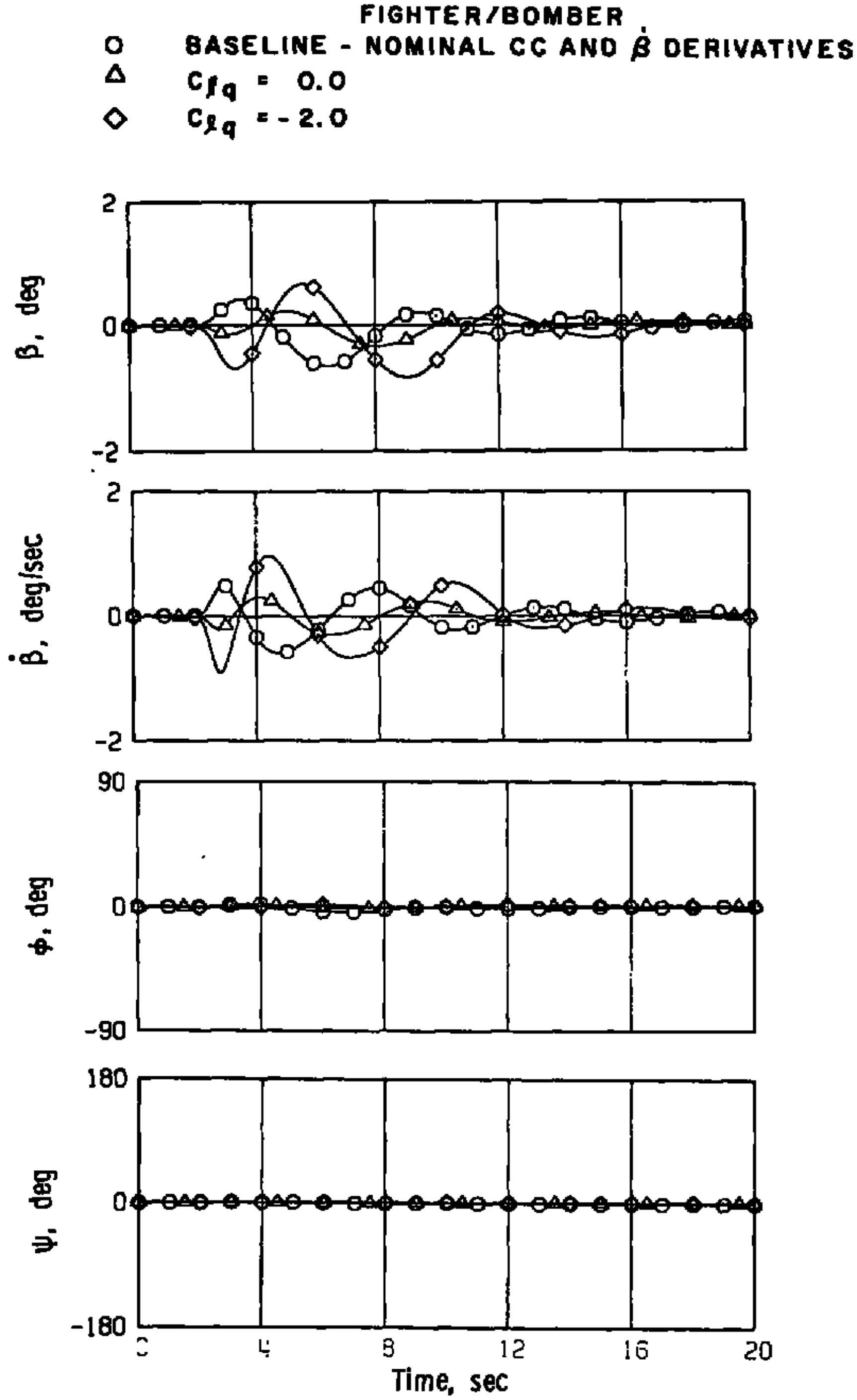

Figure 15. Continued.

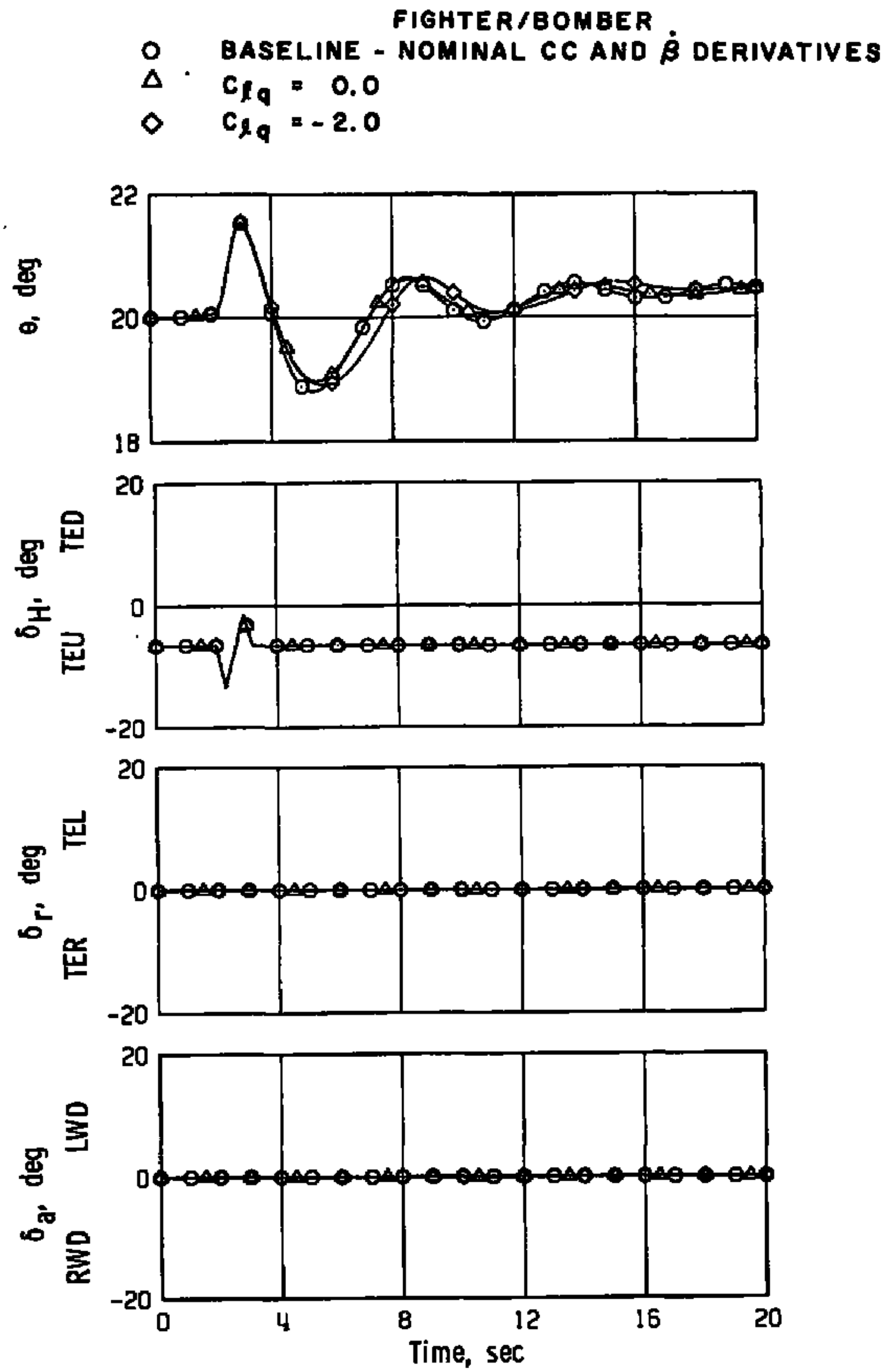

Figure 15. Concluded.

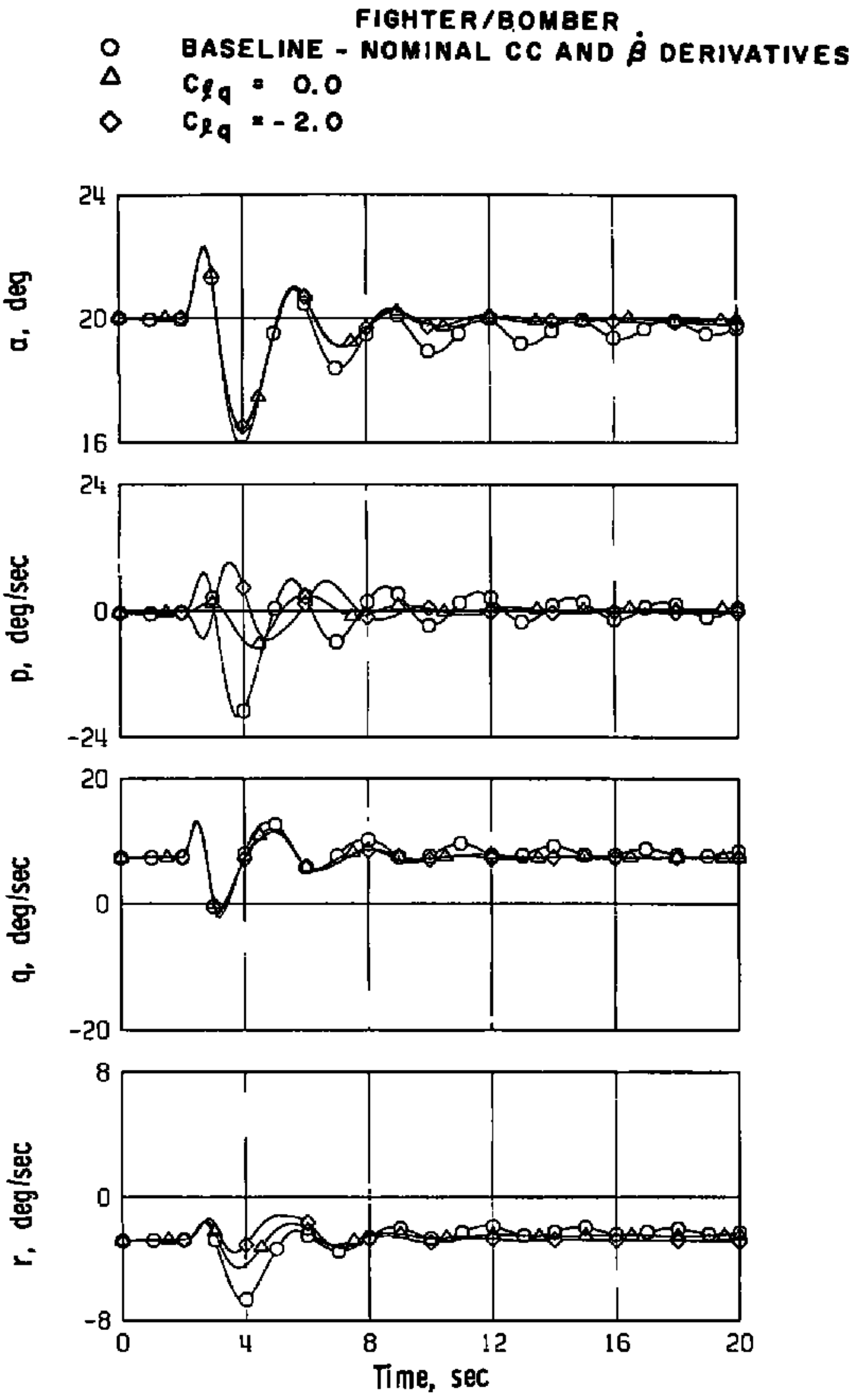

Figure 16. C_{ℓ_q} variation, fighter/bomber 3-g turning flight with nominal cross-coupling and $\dot{\beta}$ derivatives, elevator doublet.

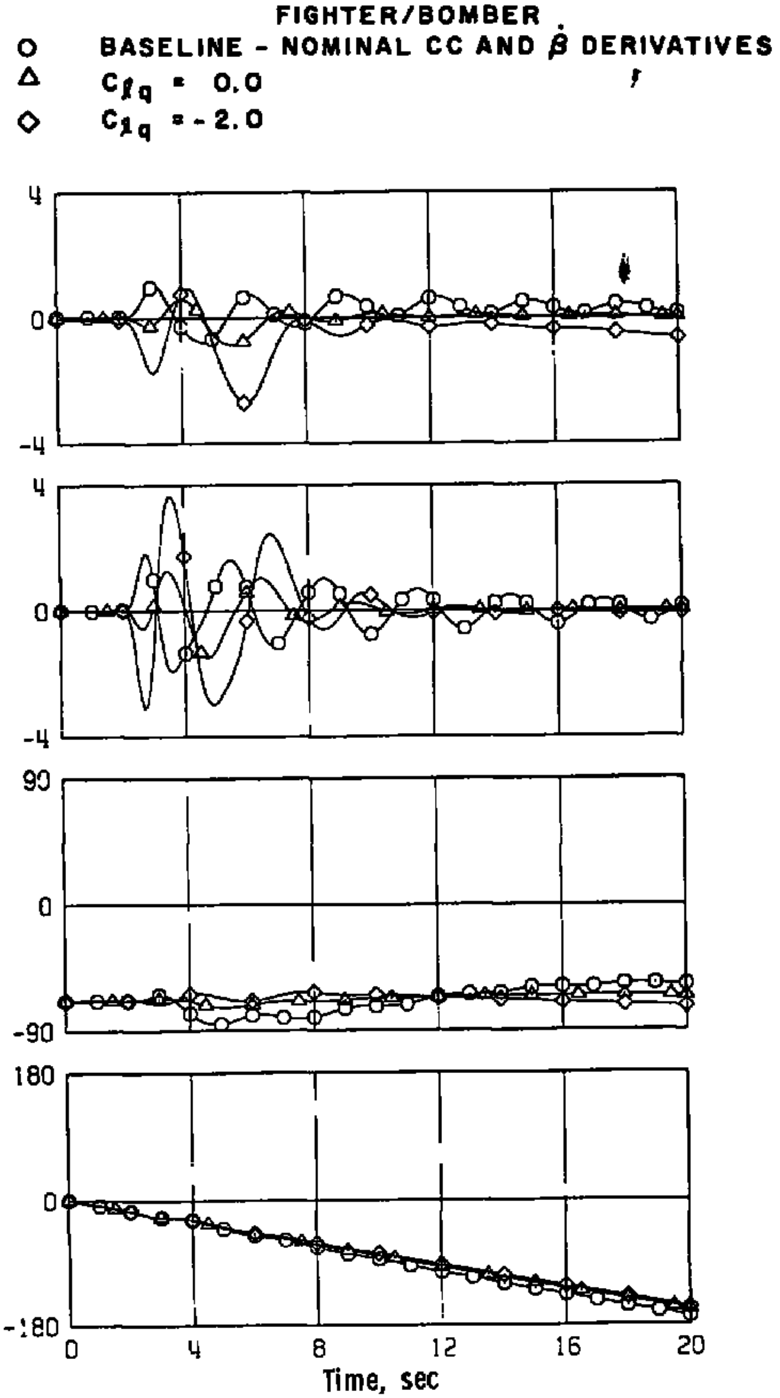

Figure 16. Continued.

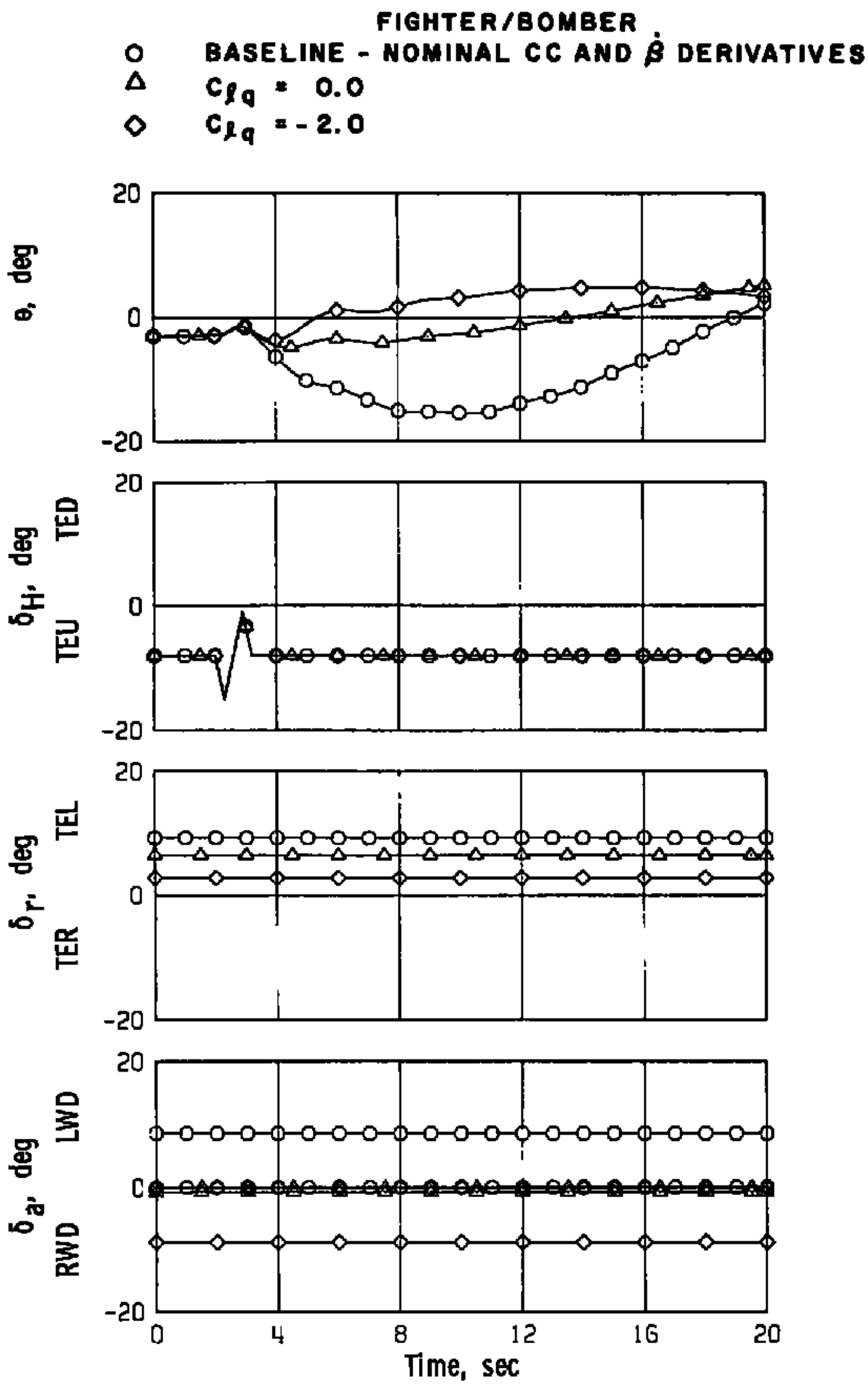

Figure 16. Concluded.

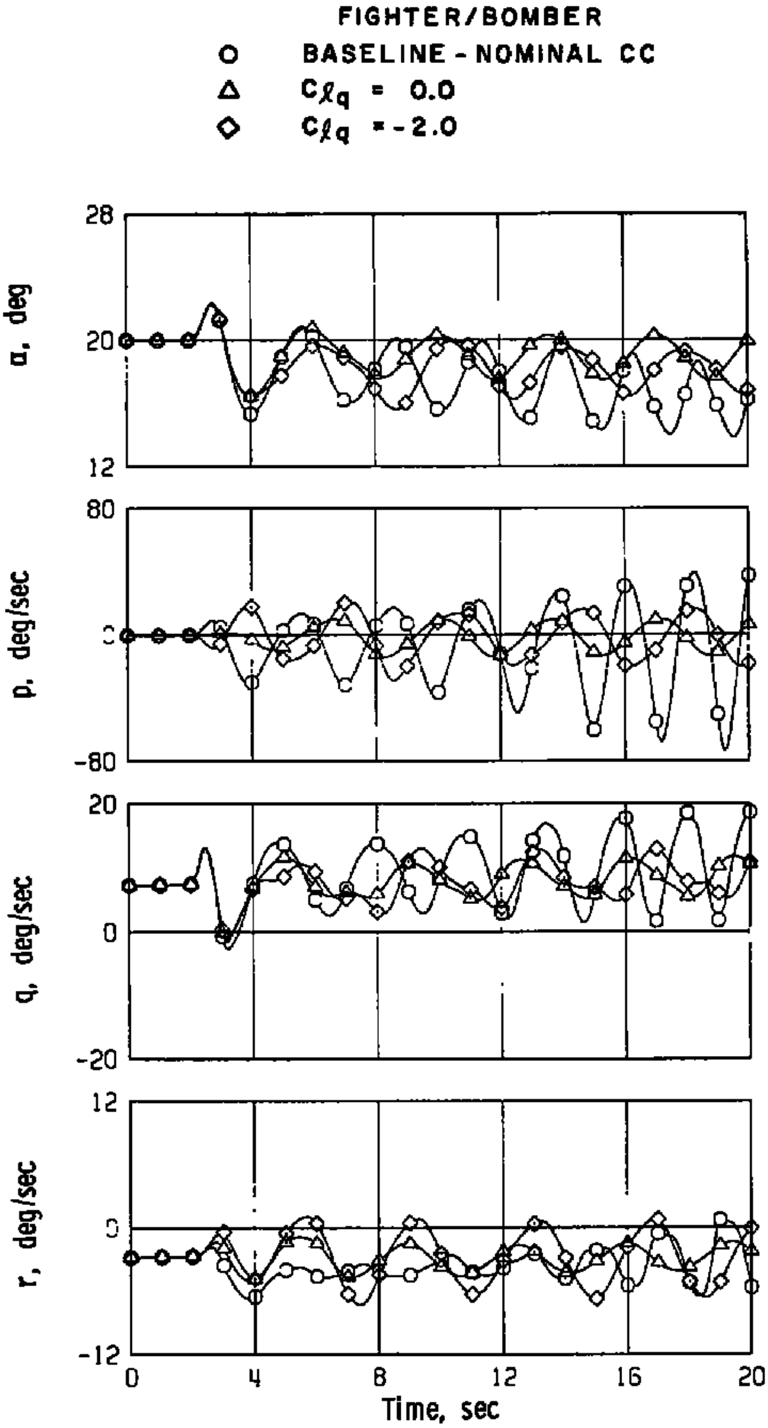

Figure 17. C_{ℓ_q} variation, fighter/bomber 3-g turning flight with nominal cross-coupling derivatives, $\dot{\beta}$ derivatives zero, elevator doublet.

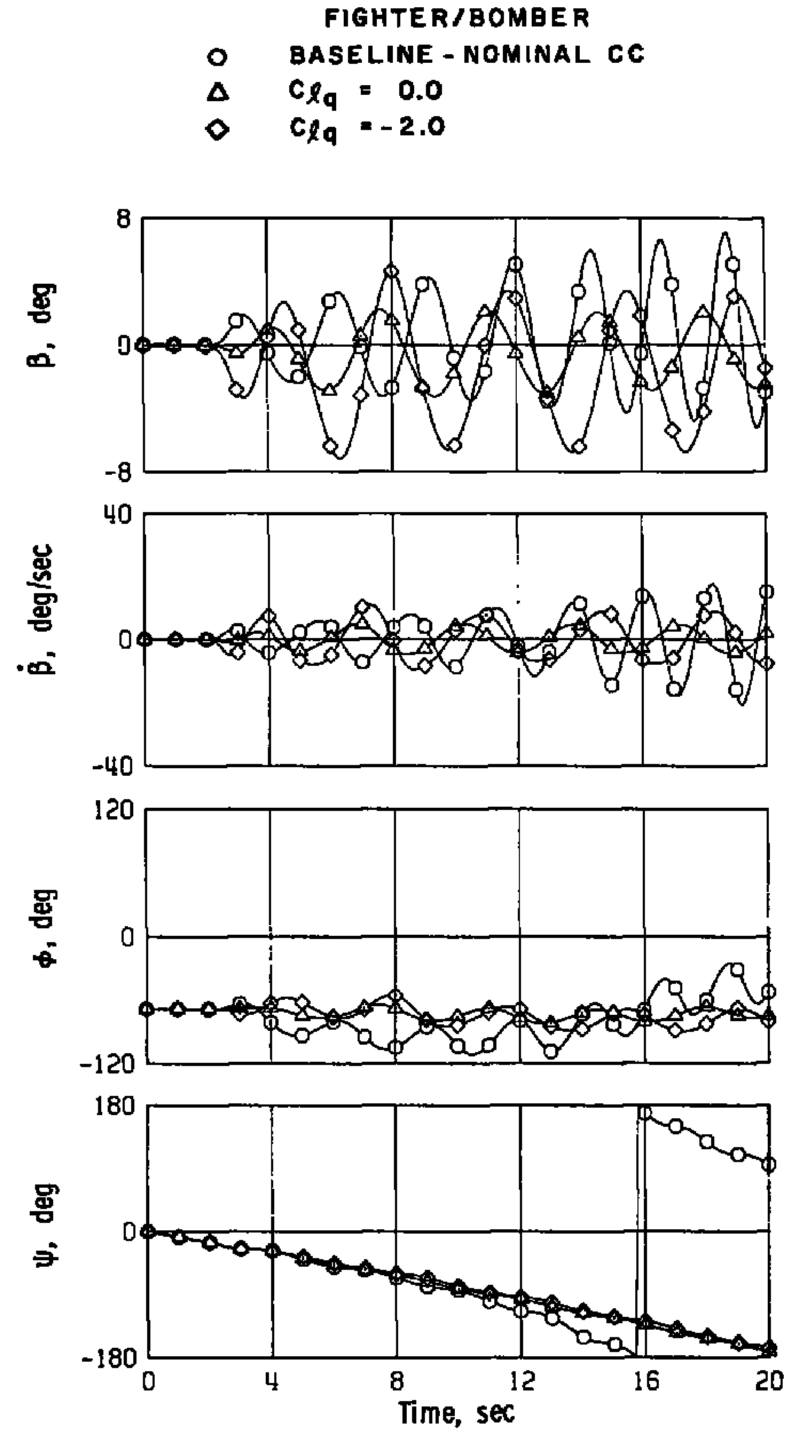

Figure 17. Continued.

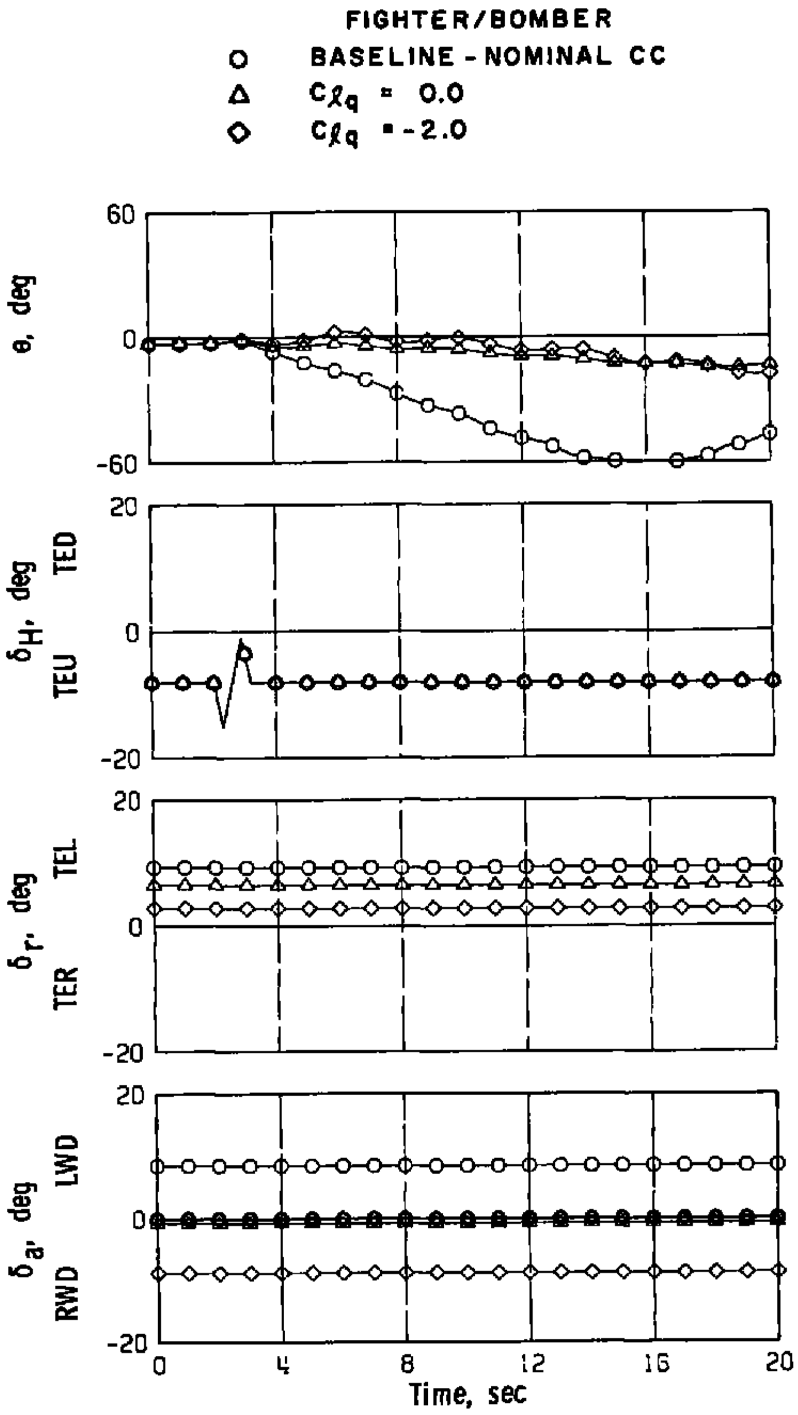

Figure 17. Concluded.

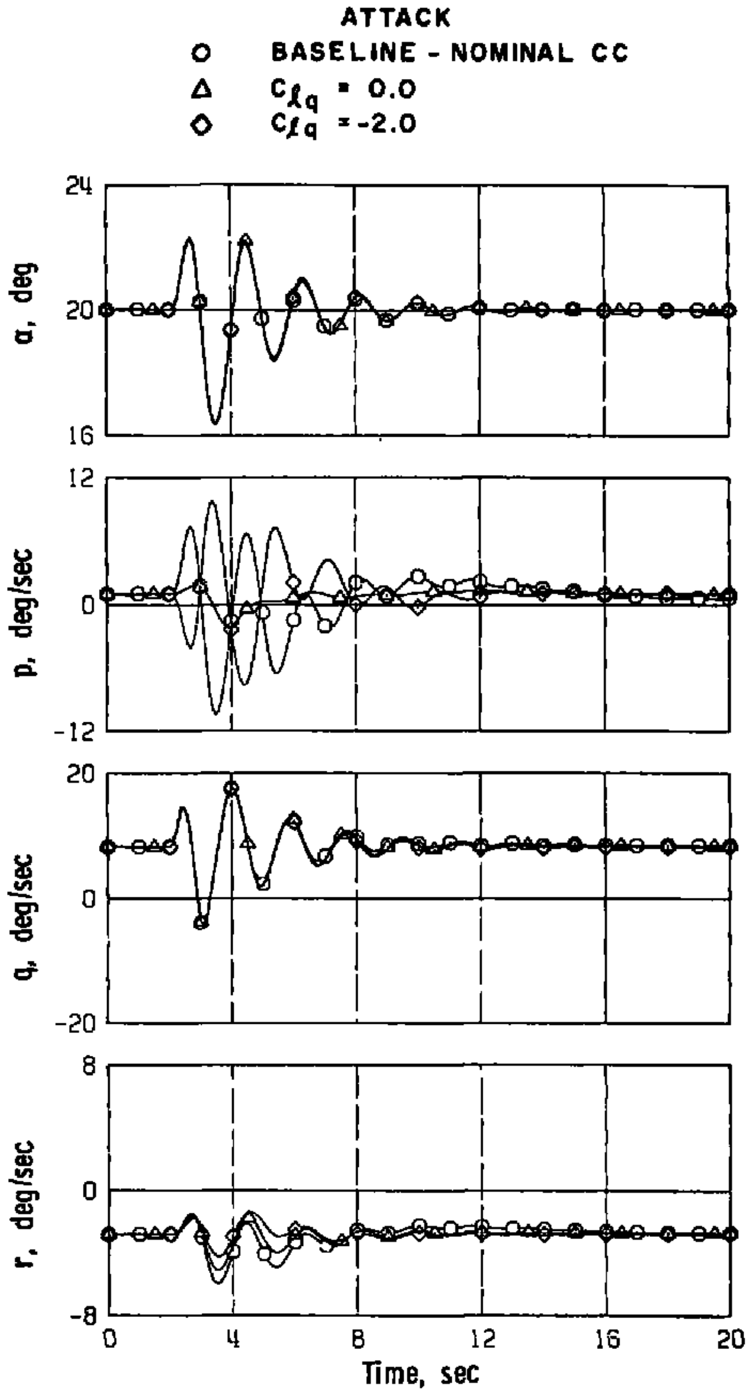

Figure 18. C_{ℓ_q} variation, attack 3-g turning flight with nominal cross-coupling derivatives, $\dot{\beta}$ derivatives zero, elevator doublet.

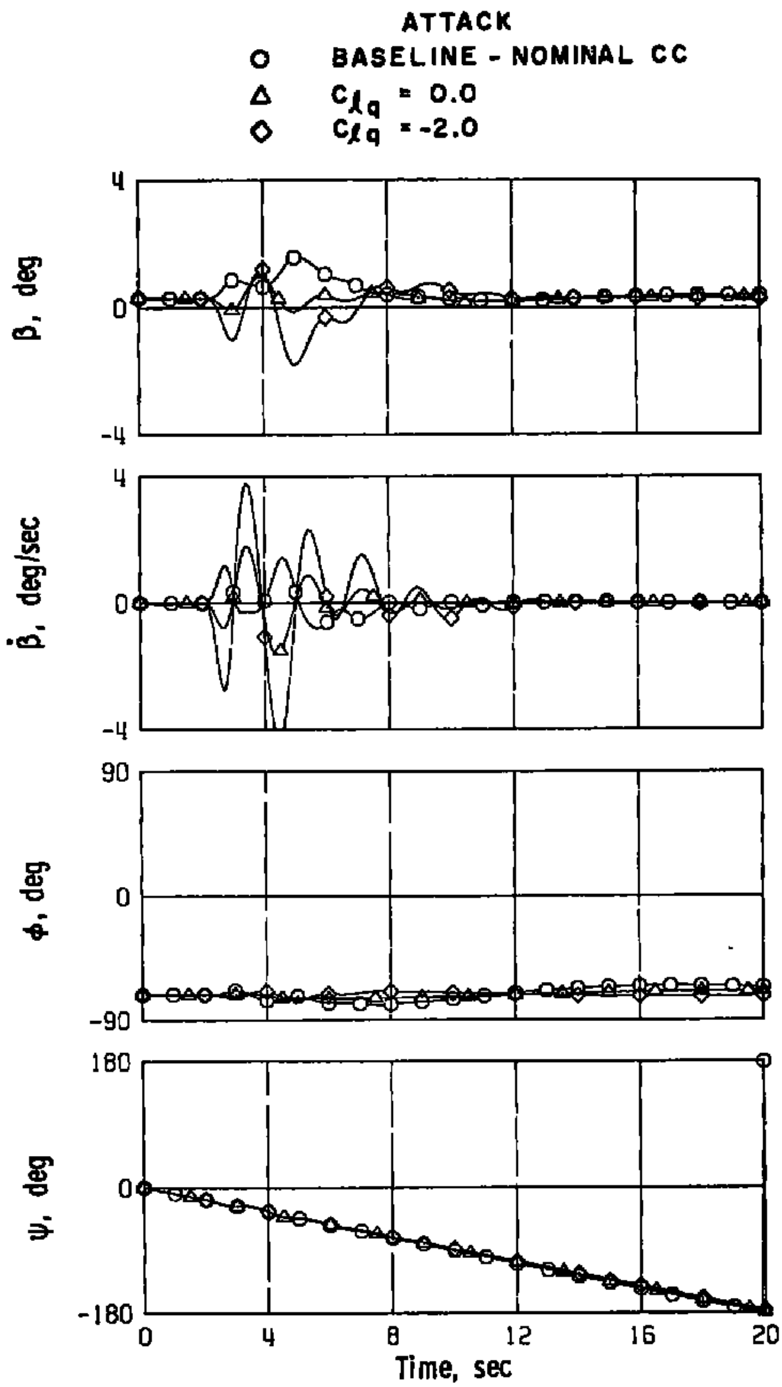

Figure 18. Continued.

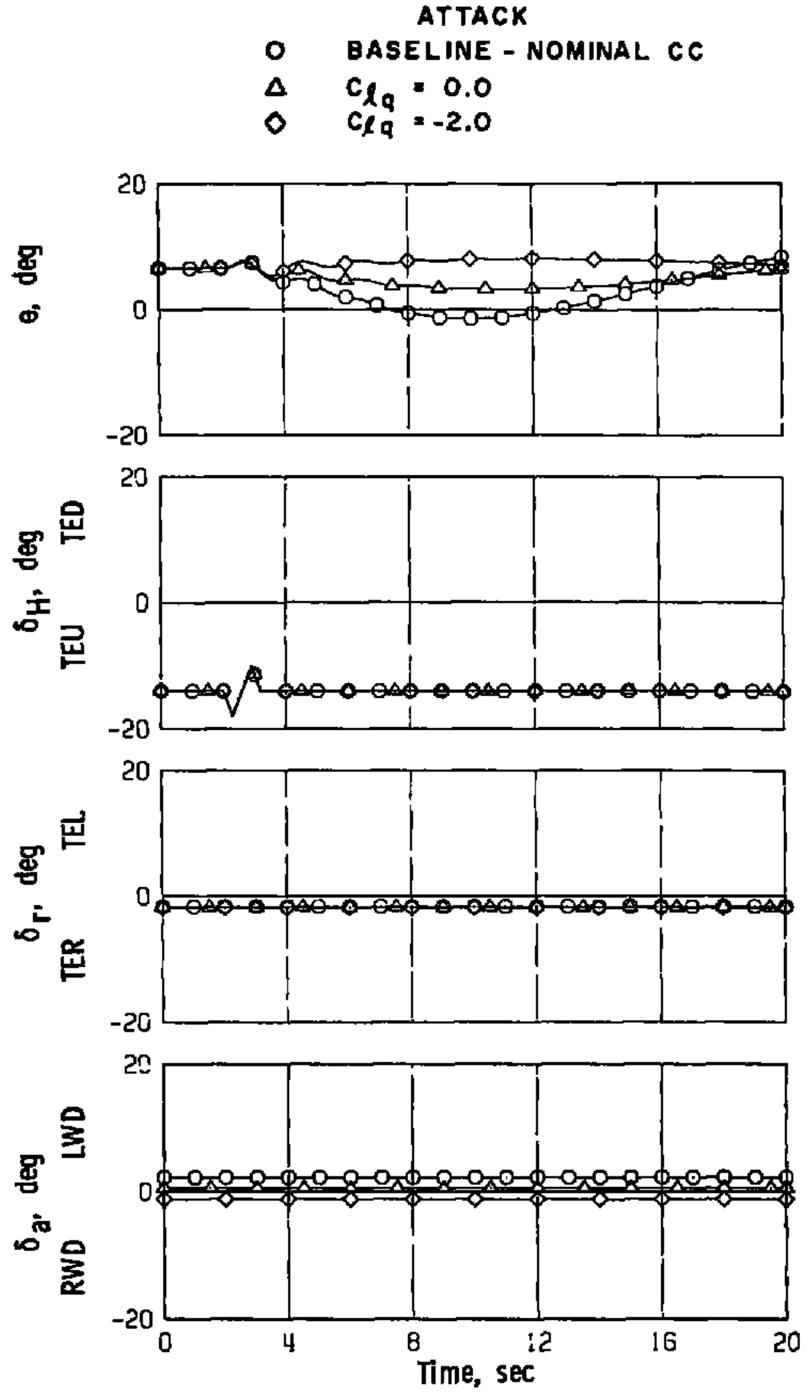

Figure 18. Concluded.

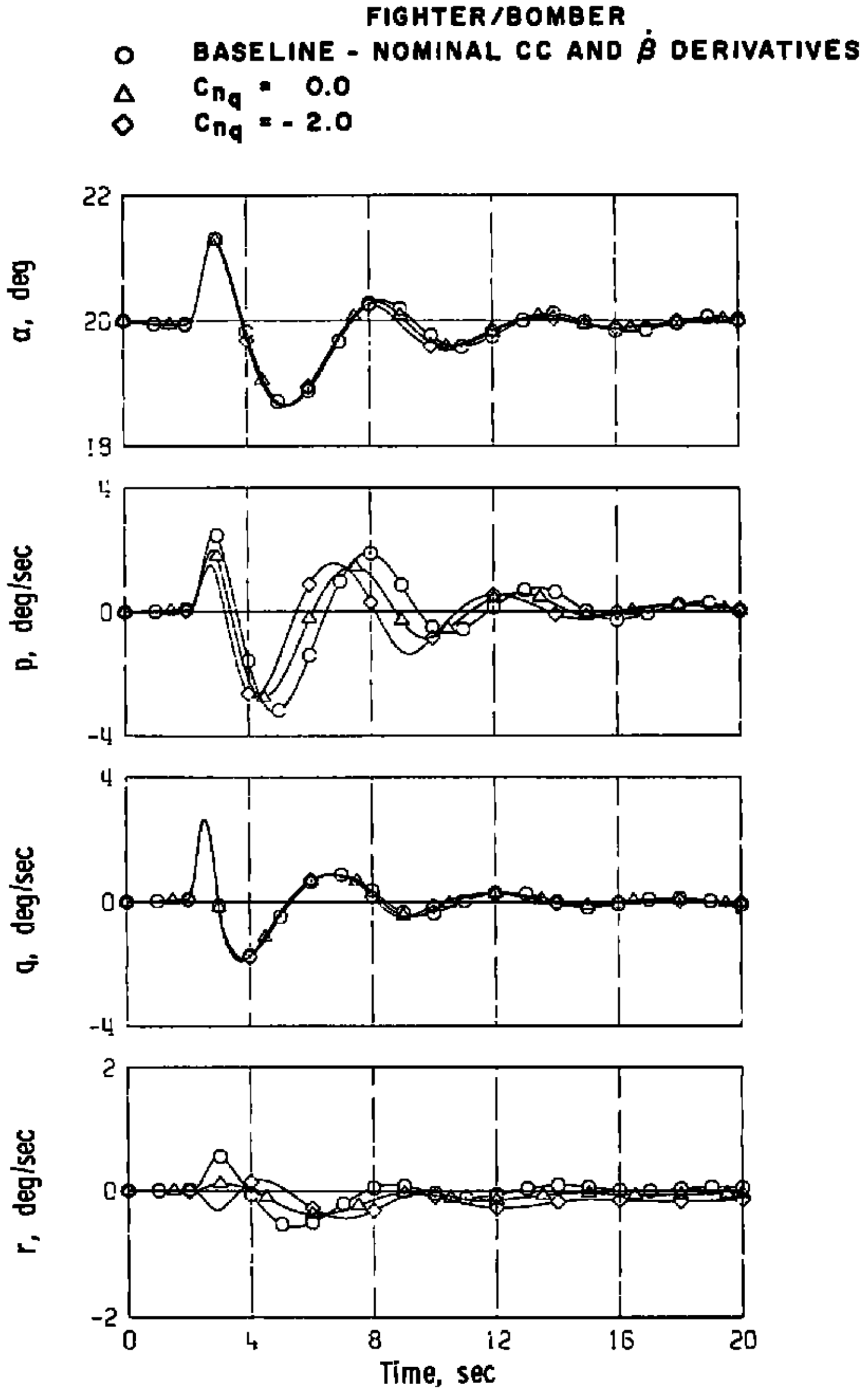

Figure 19. C_{n_q} variation, fighter/bomber level flight with nominal cross-coupling and $\dot{\beta}$ derivatives, elevator doublet.

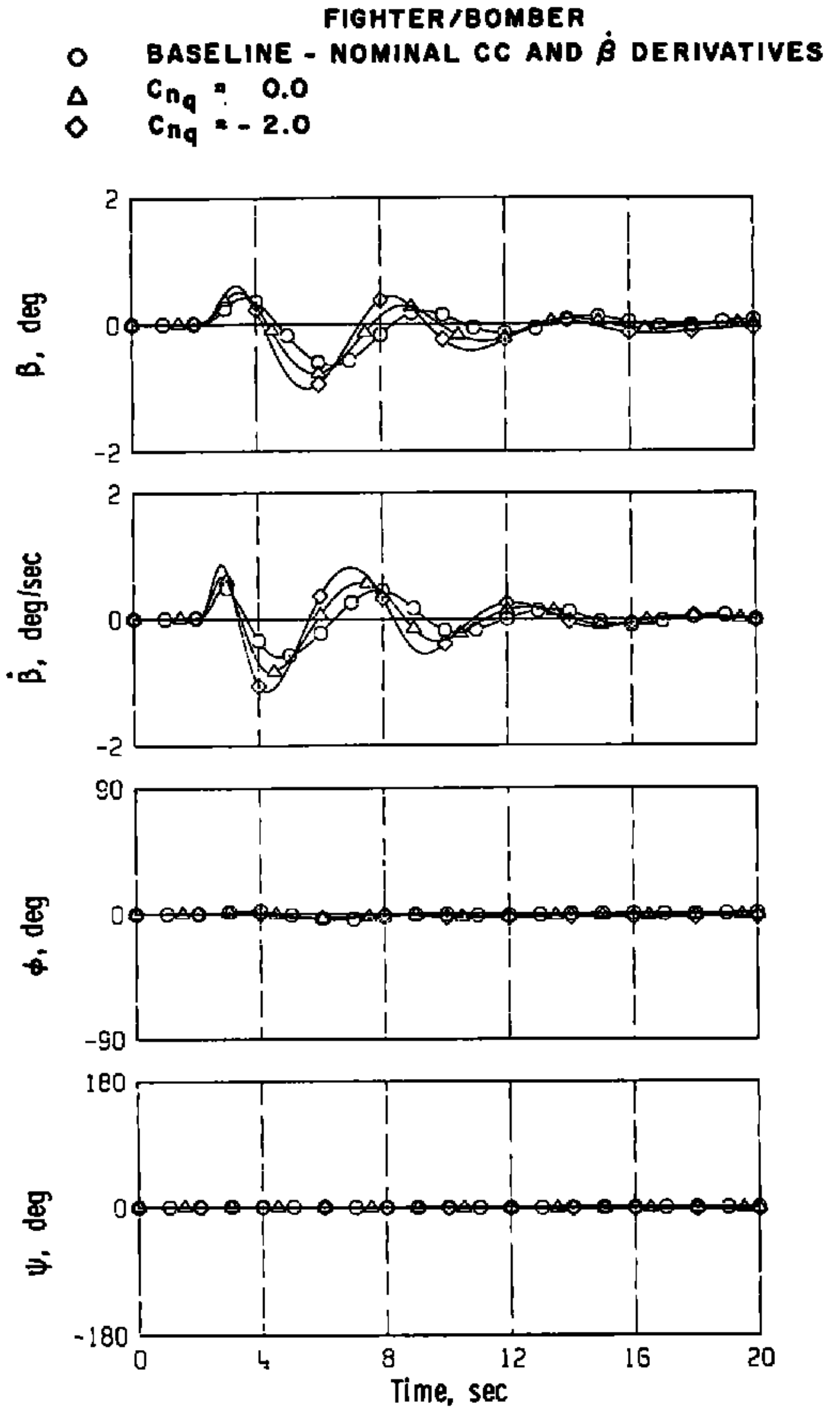

Figure 19. Continued.

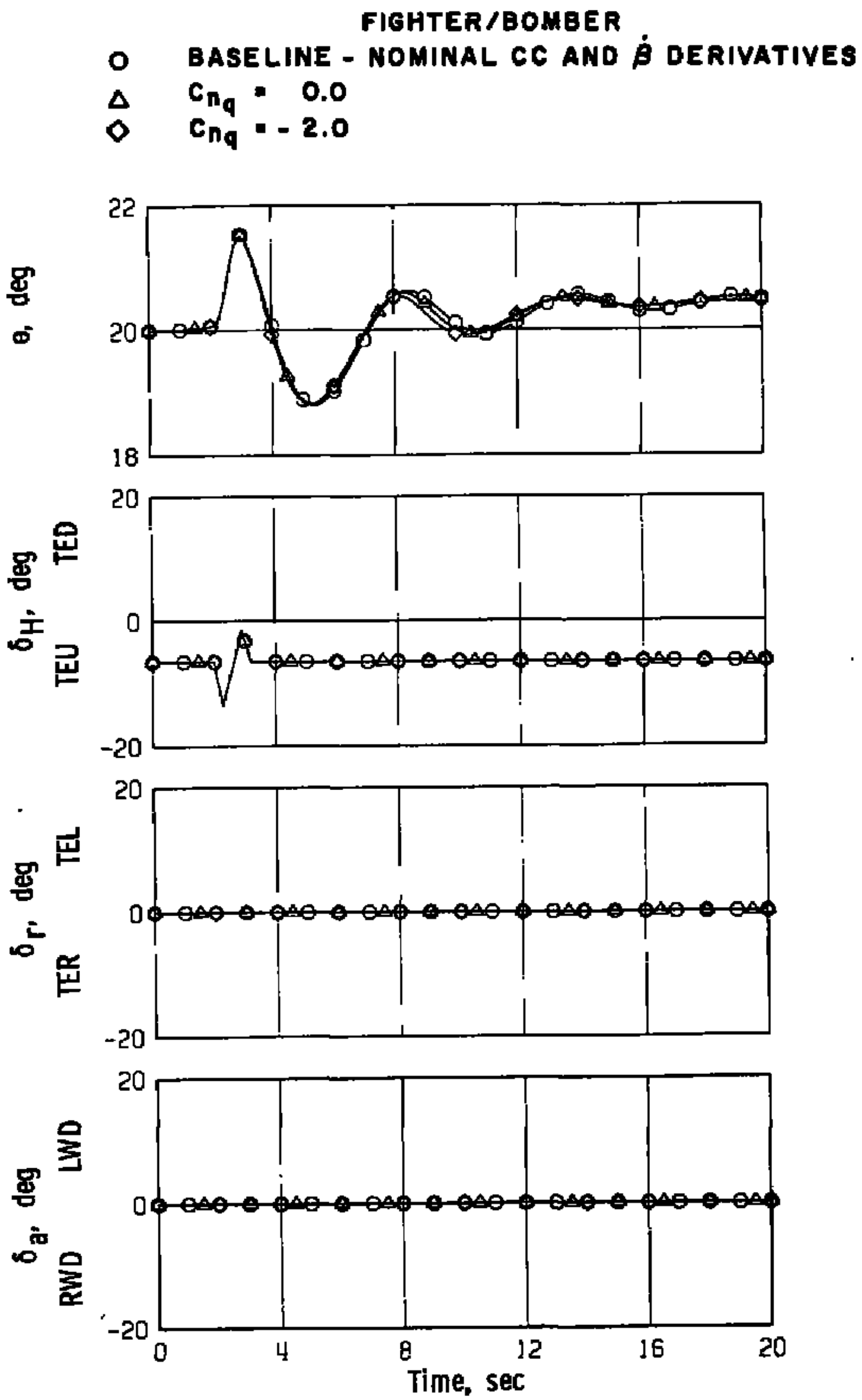

Figure 19. Concluded.

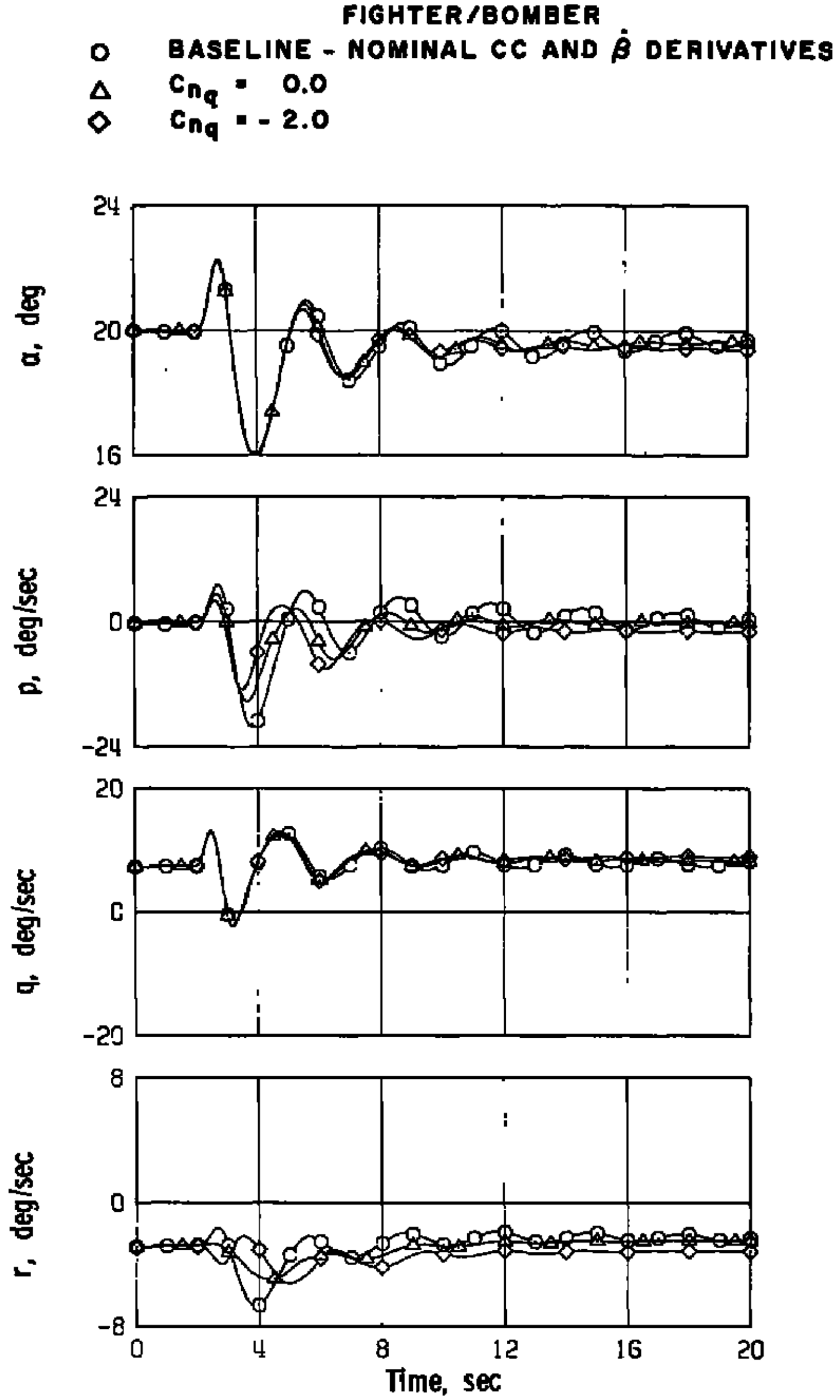

Figure 20. C_{n_q} variation, fighter/bomber 3-g turning flight with nominal cross-coupling and $\dot{\beta}$ derivatives, elevator doublet.

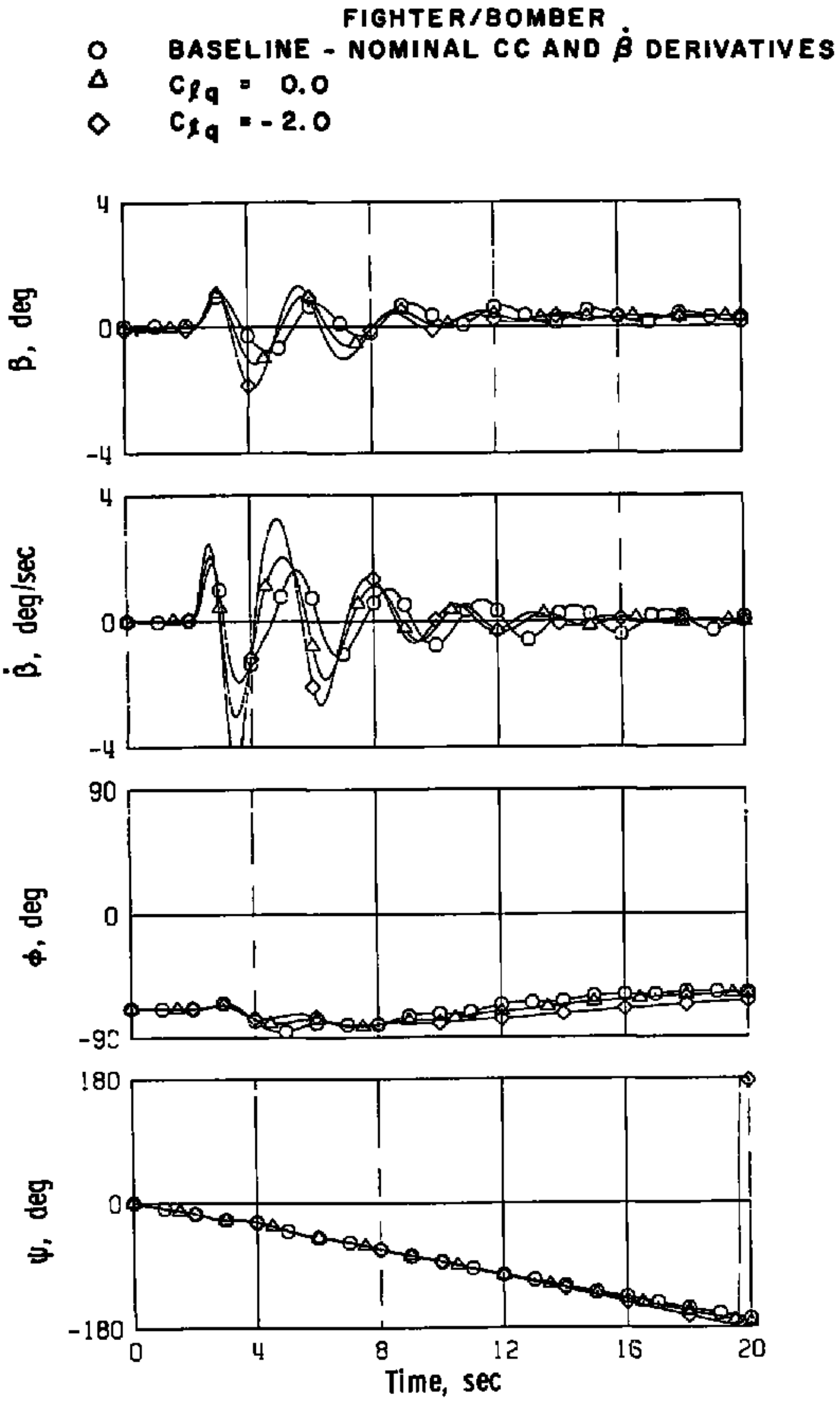

Figure 20. Continued.

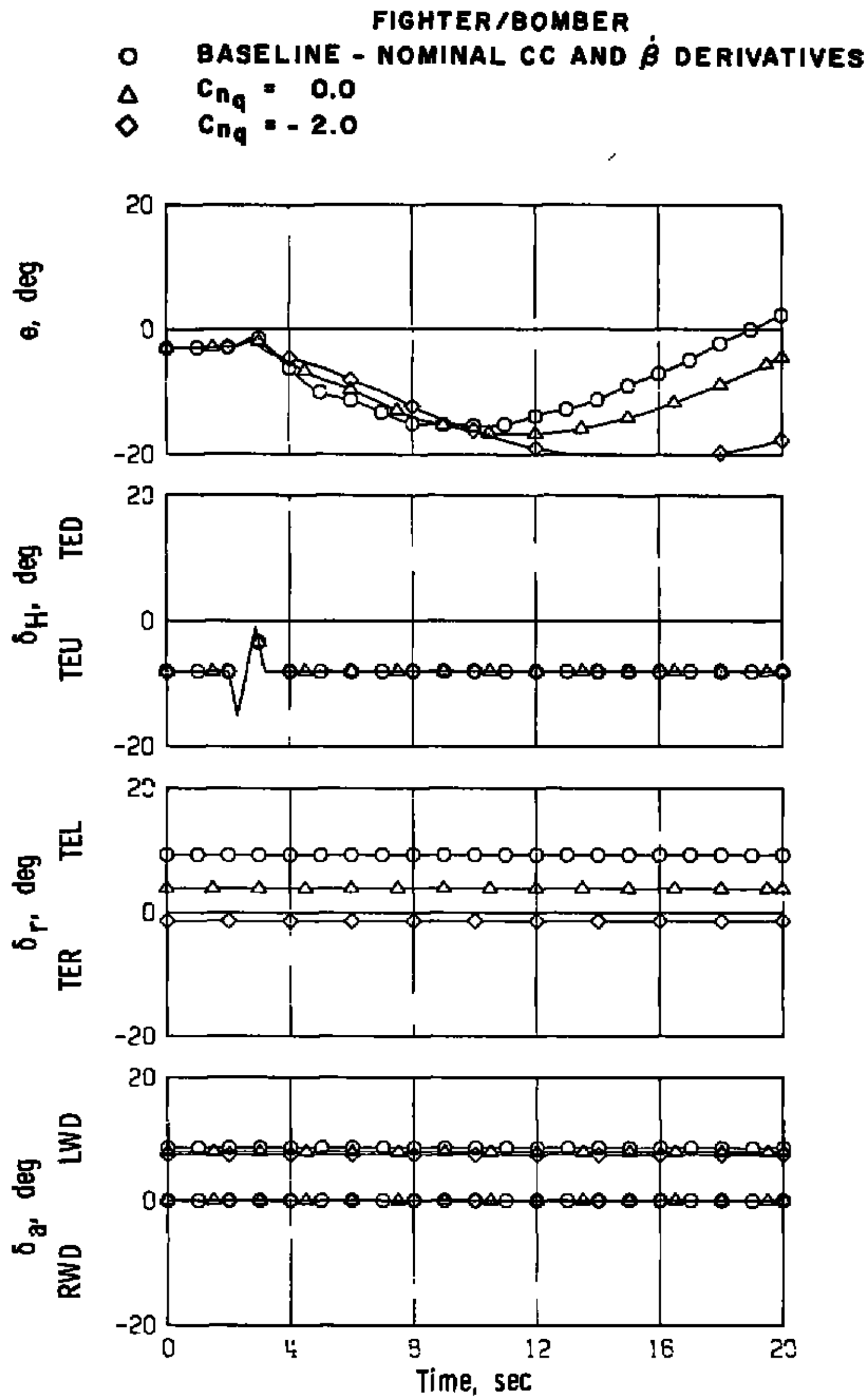

Figure 20. Concluded.

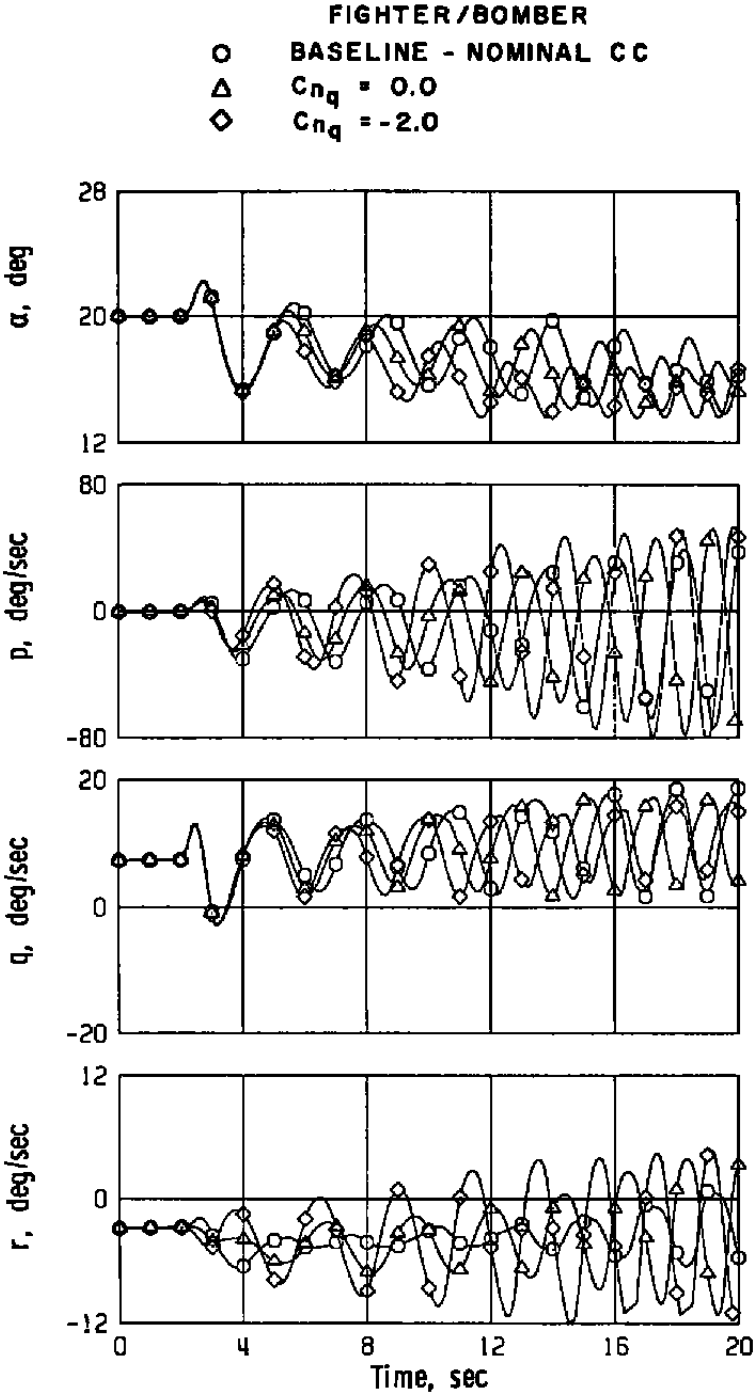

Figure 21. C_{n_q} variation, fighter/bomber 3-g turning flight with nominal cross-coupling derivatives, $\dot{\beta}$ derivatives zero, elevator doublet.

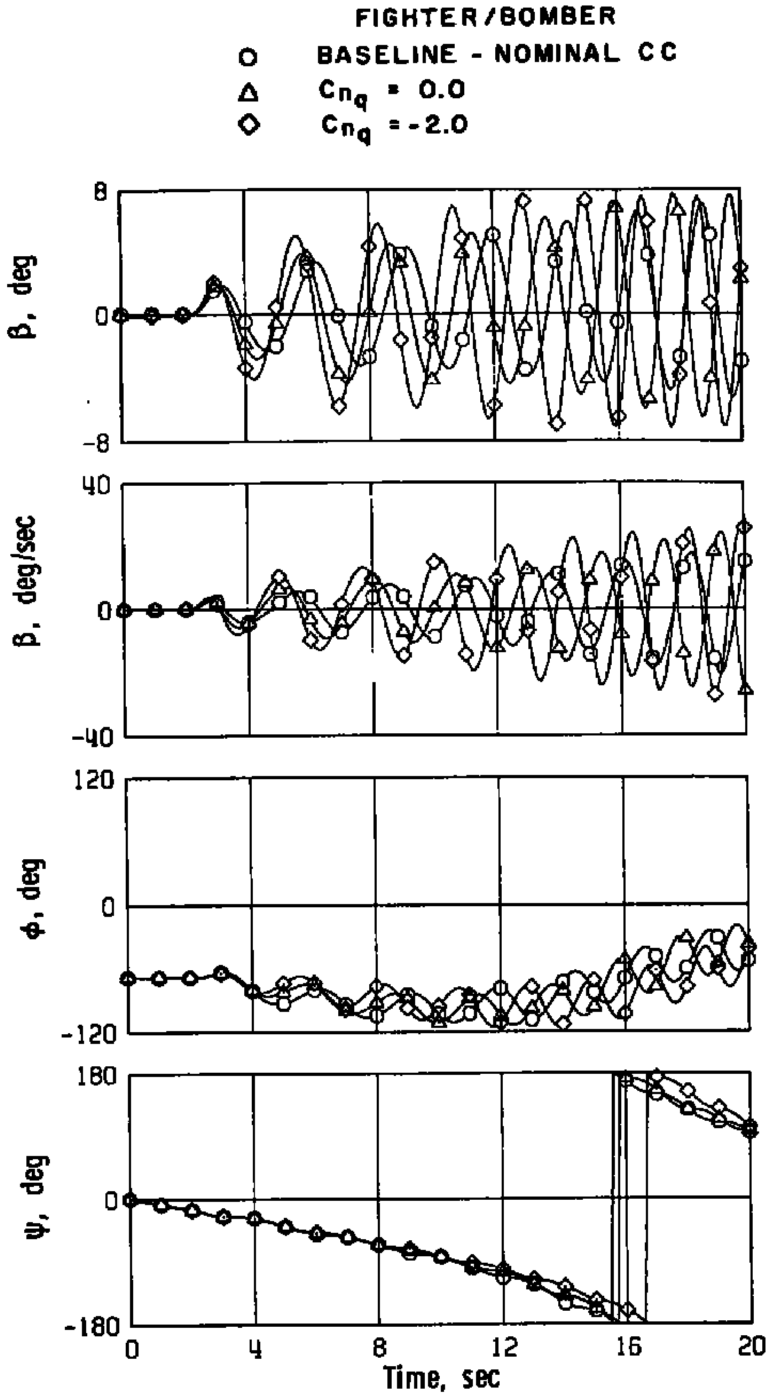

Figure 21. Continued.

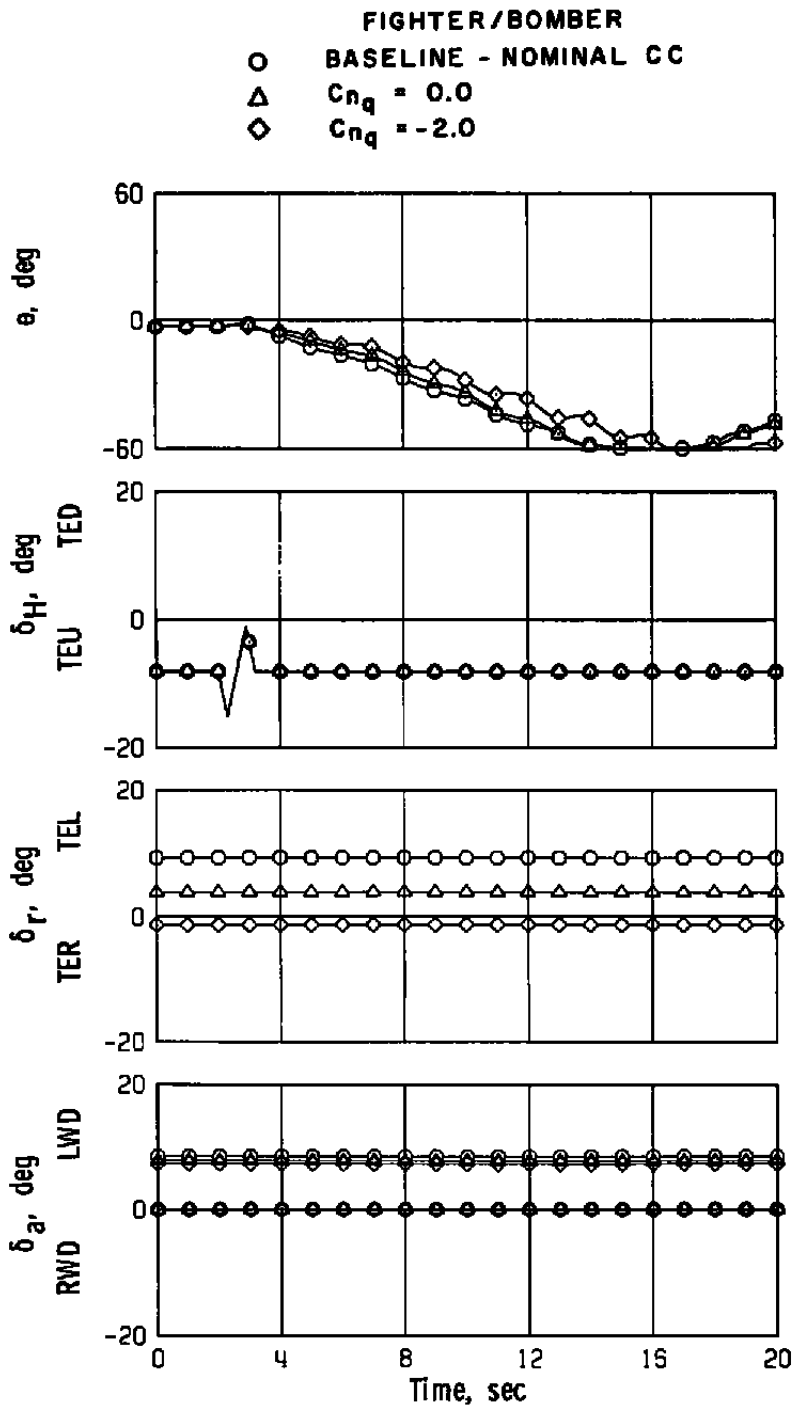

Figure 21. Concluded.

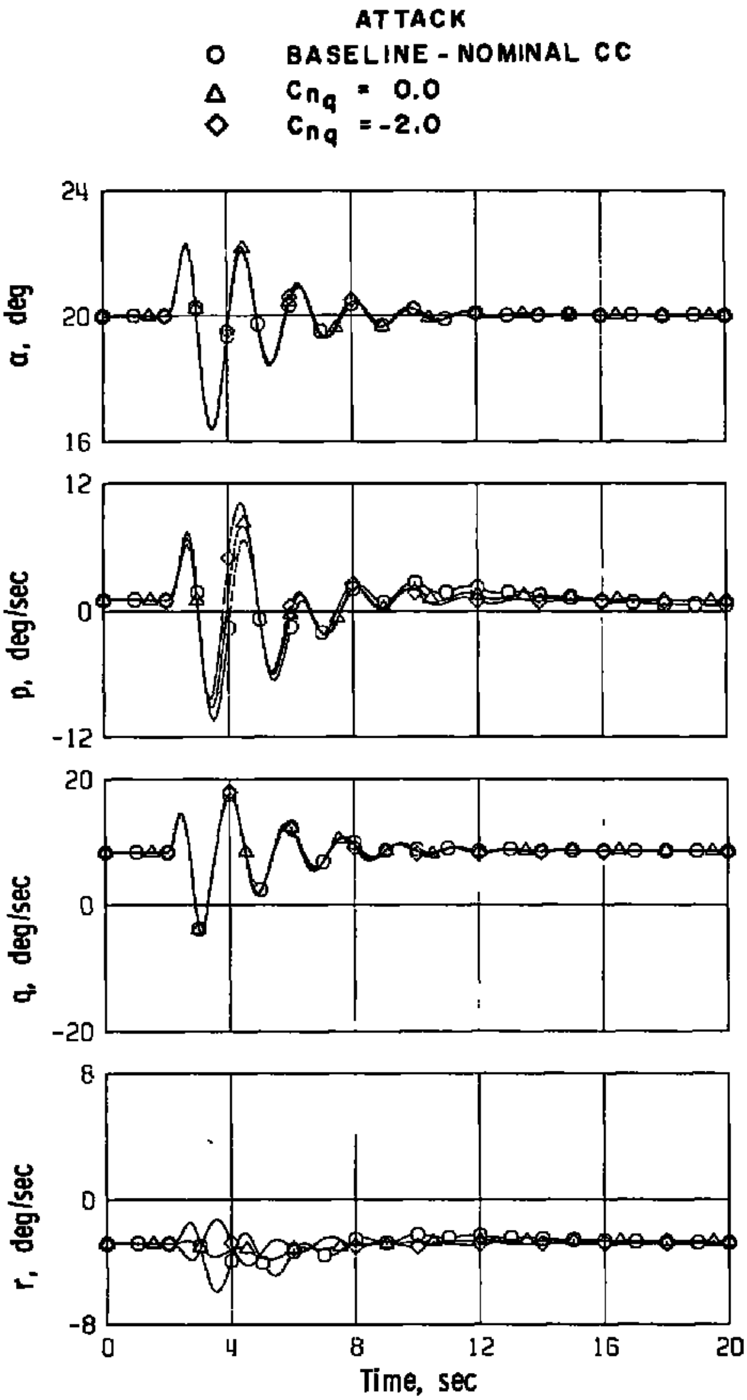

Figure 22. C_{n_q} variation, attack 3-g turning flight with nominal cross-coupling derivatives, $\dot{\beta}$ derivatives zero, elevator doublet.

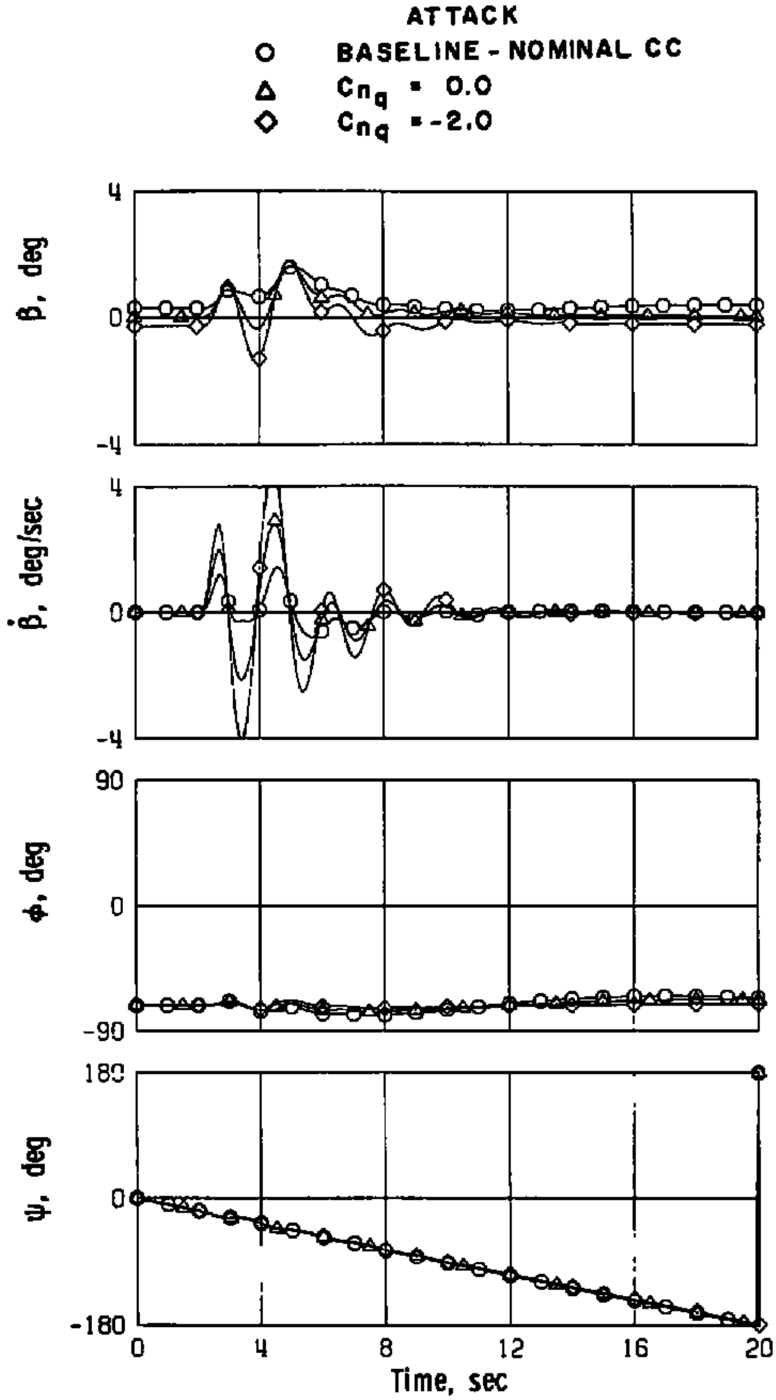

Figure 22. Continued.

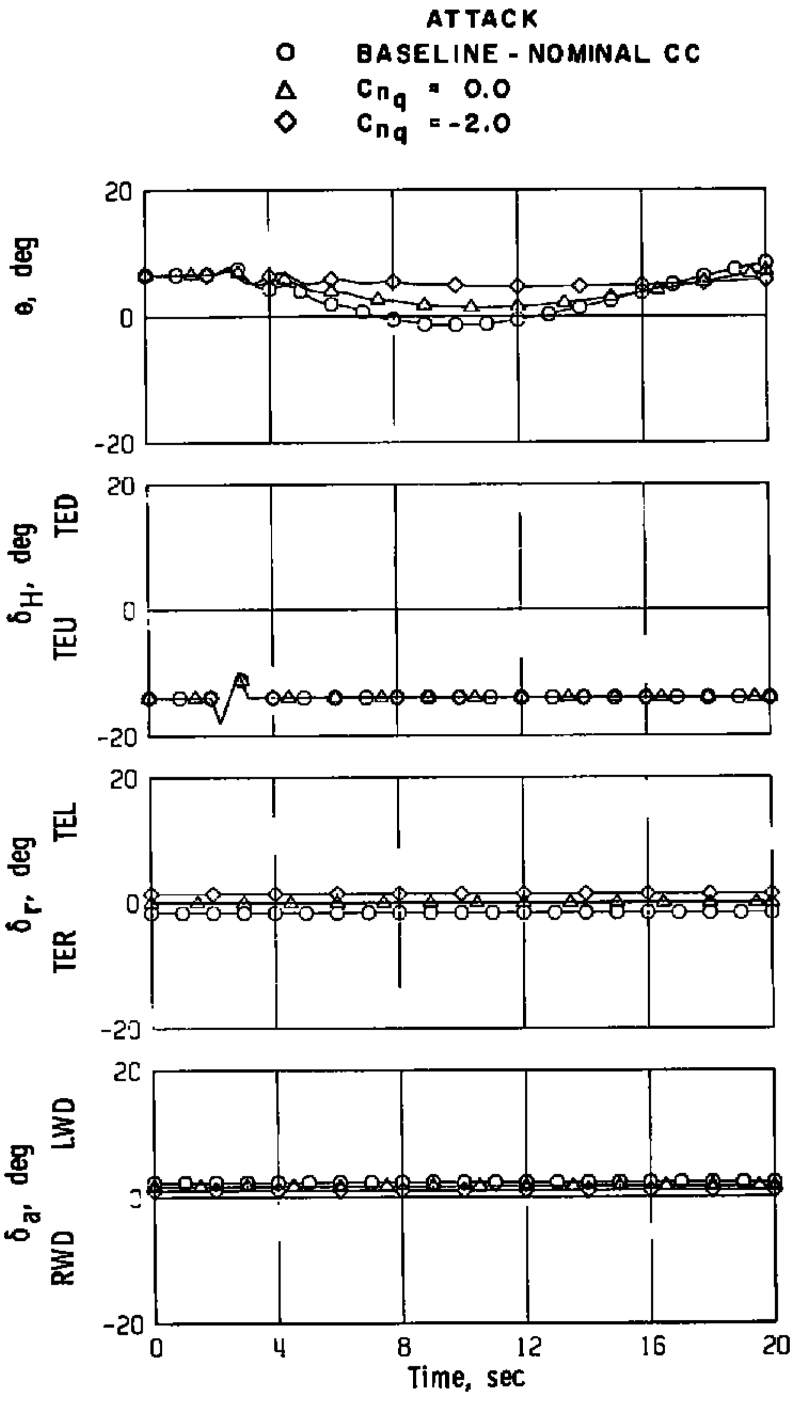

Figure 22. Concluded.

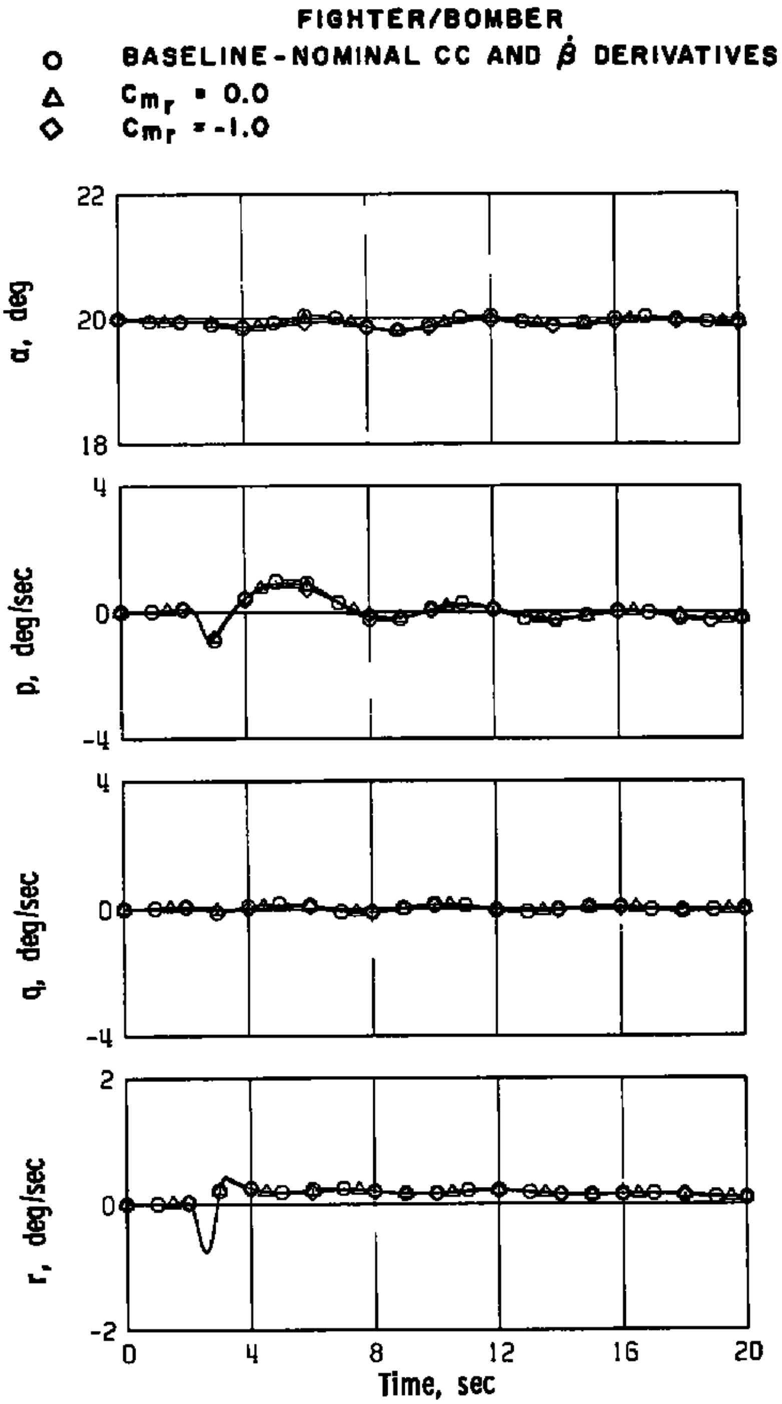

Figure 23. C_{m_r} variation, fighter/bomber level flight with nominal cross-coupling and $\dot{\beta}$ derivatives, rudder doublet.

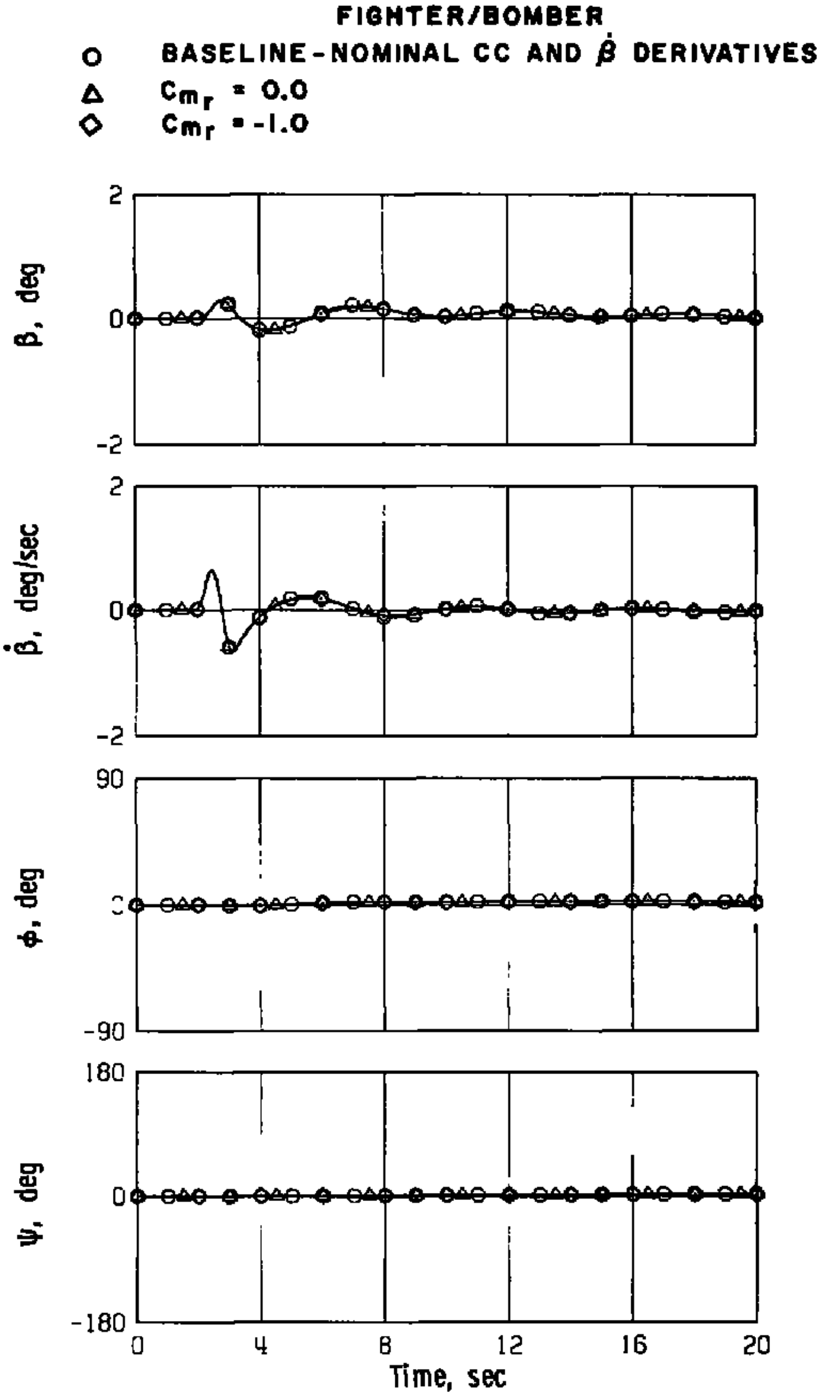

Figure 23. Continued.

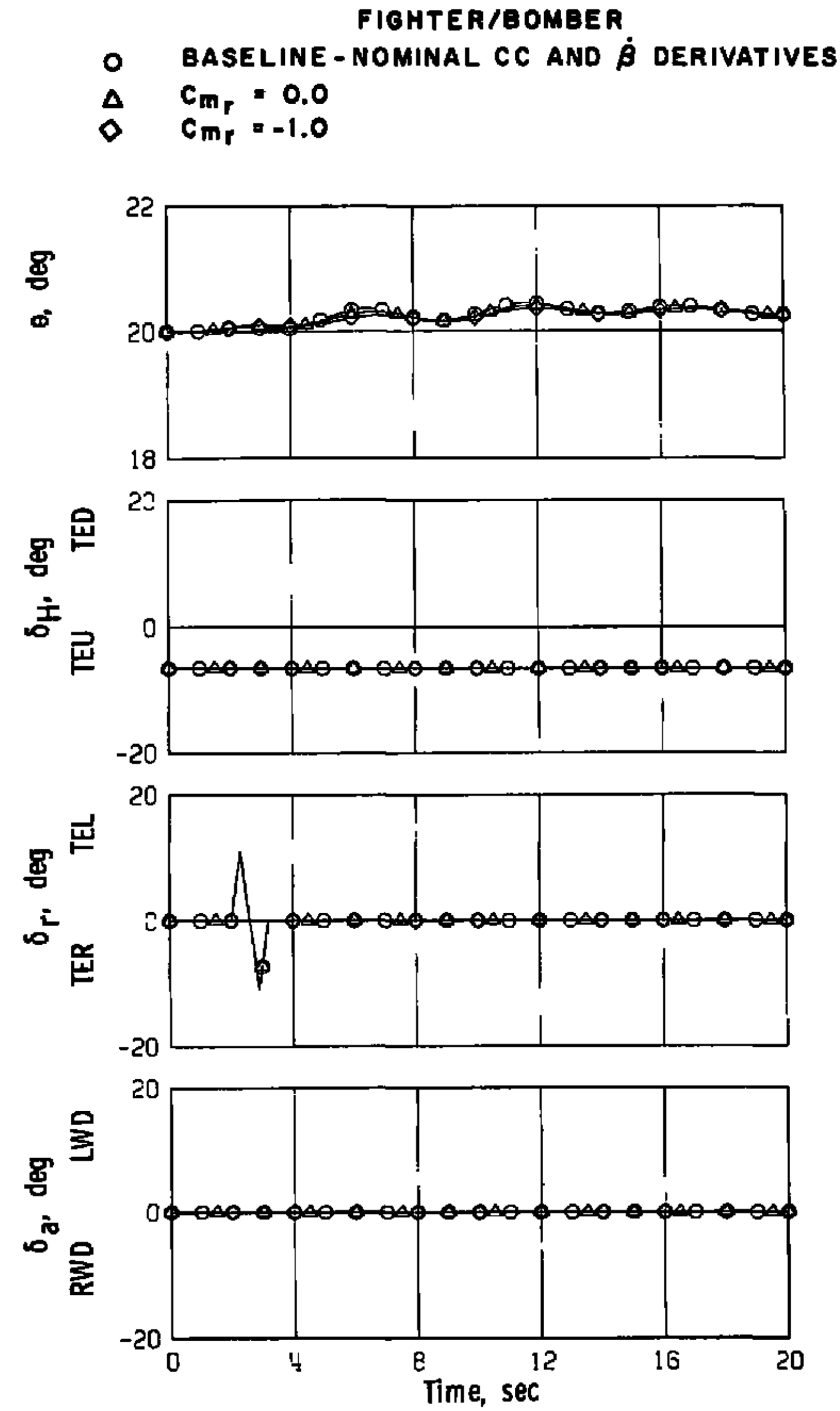

Figure 23. Concluded.

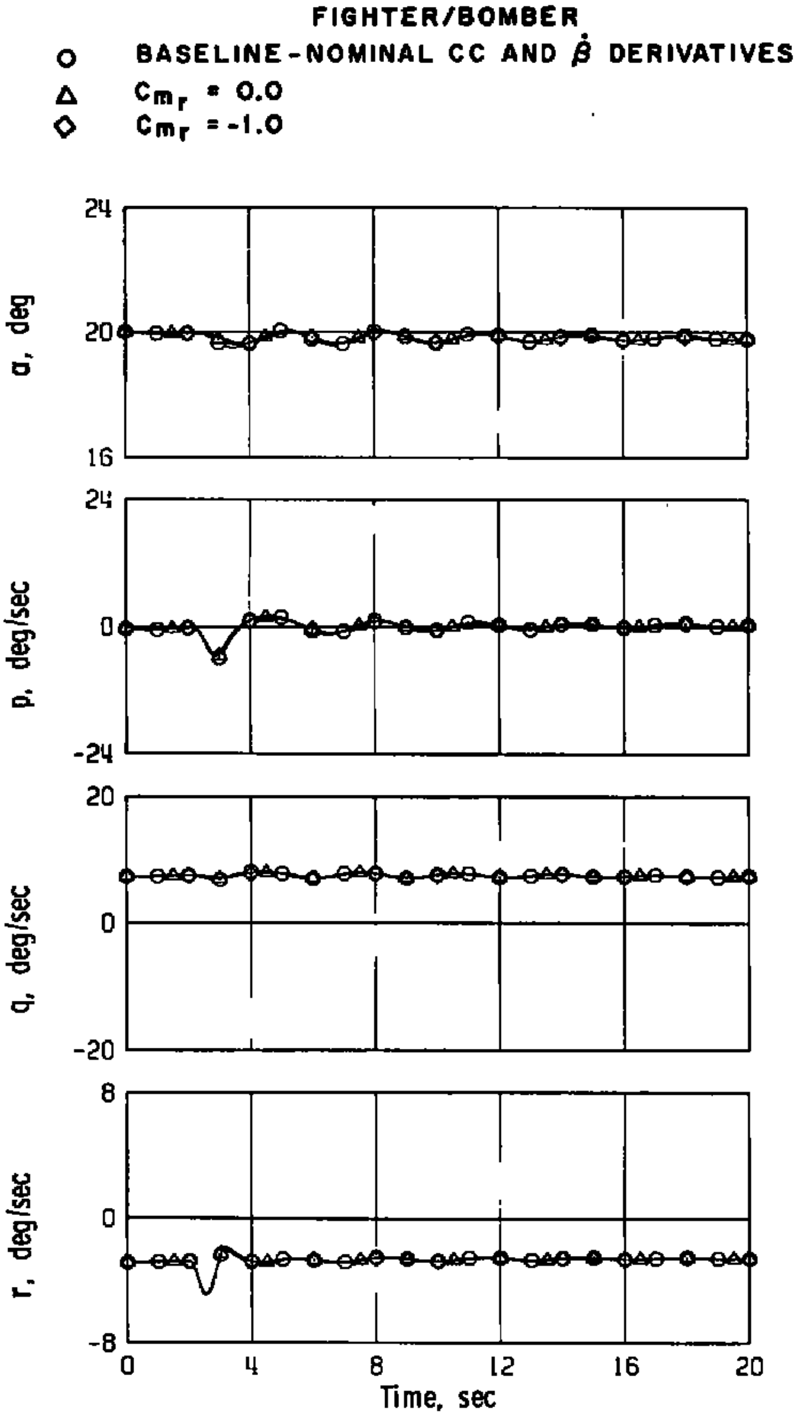

Figure 24. C_{m_r} variation, fighter/bomber 3-g turning flight with nominal cross-coupling and $\dot{\beta}$ derivatives, rudder doublet.

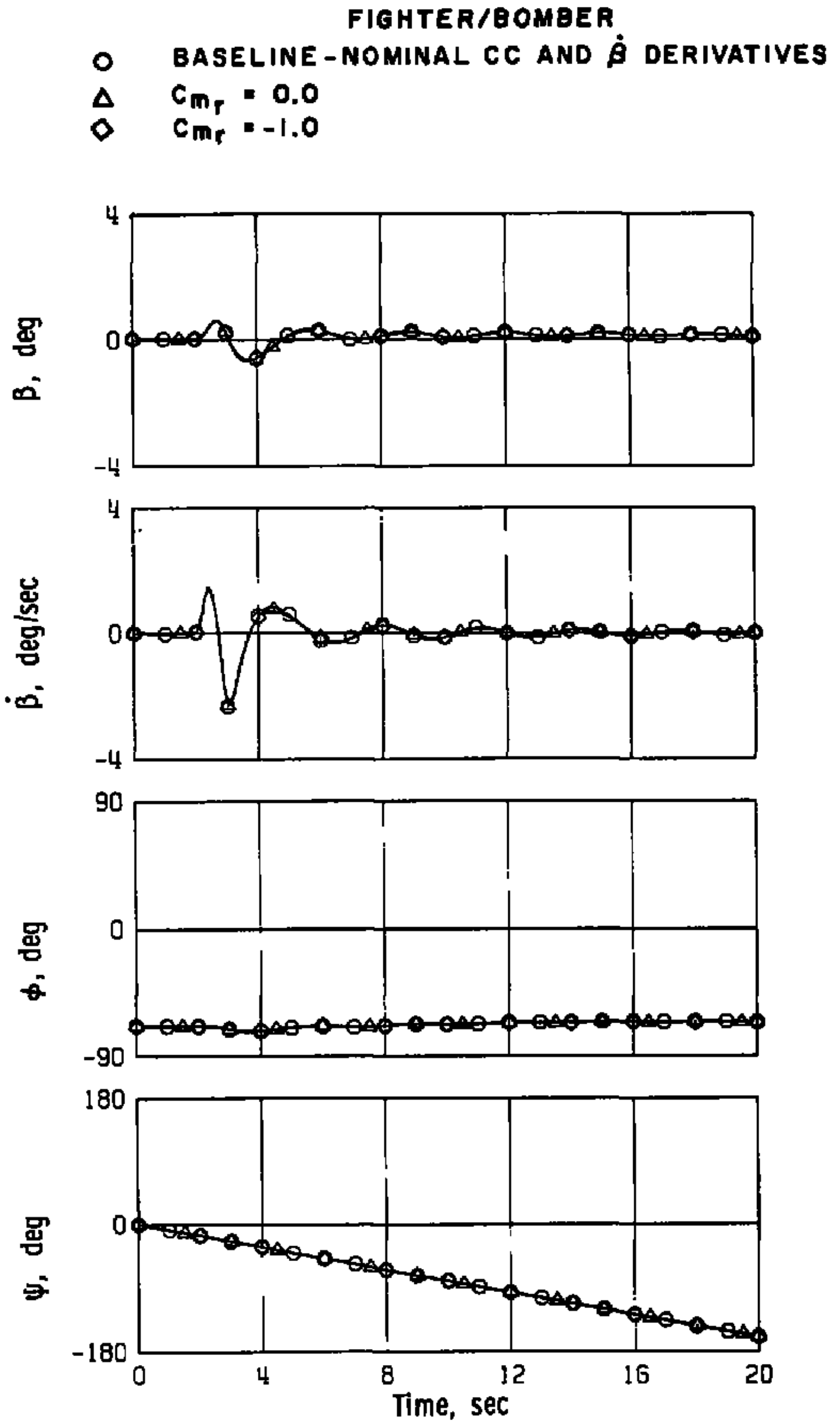

Figure 24. Continued.

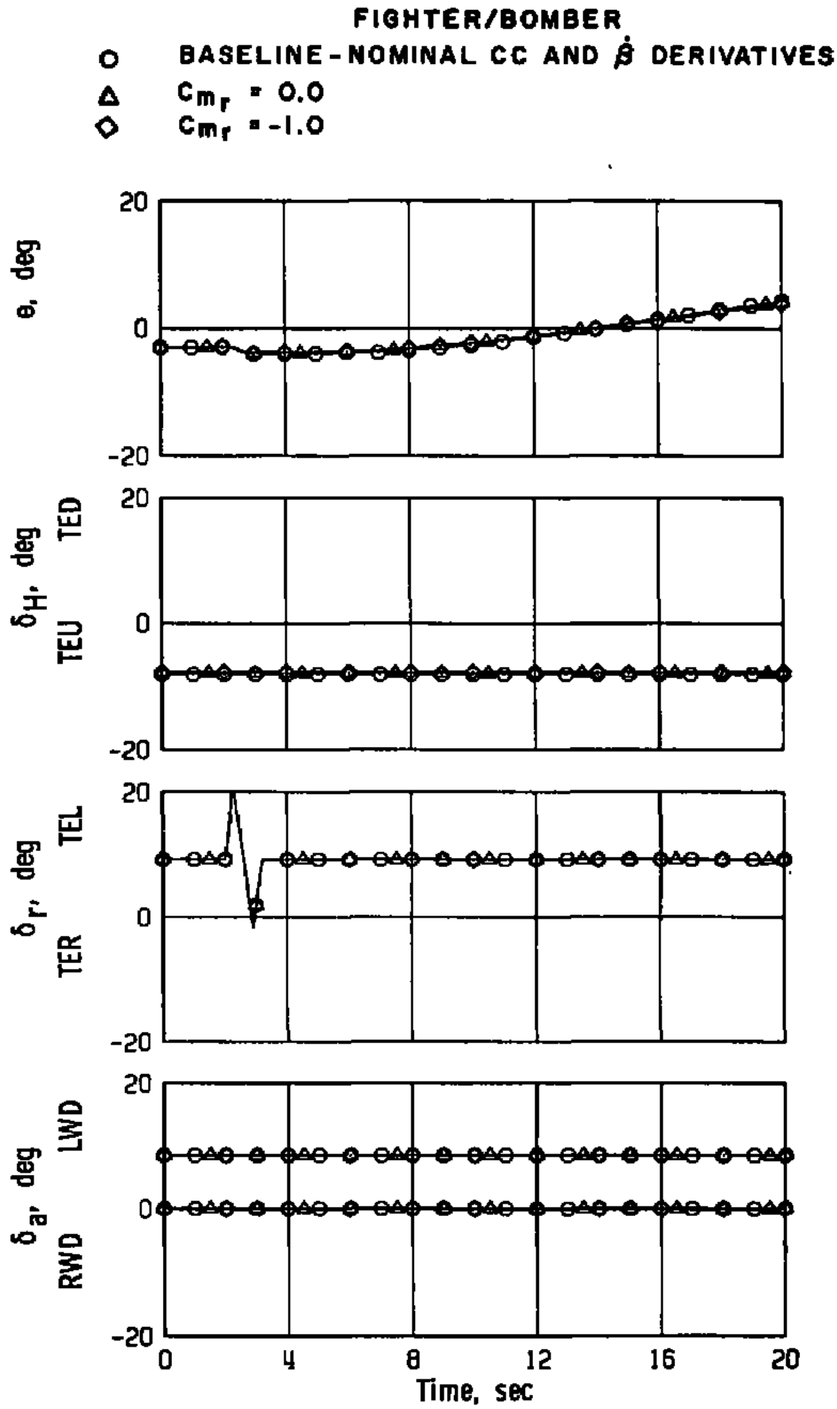

Figure 24. Concluded.

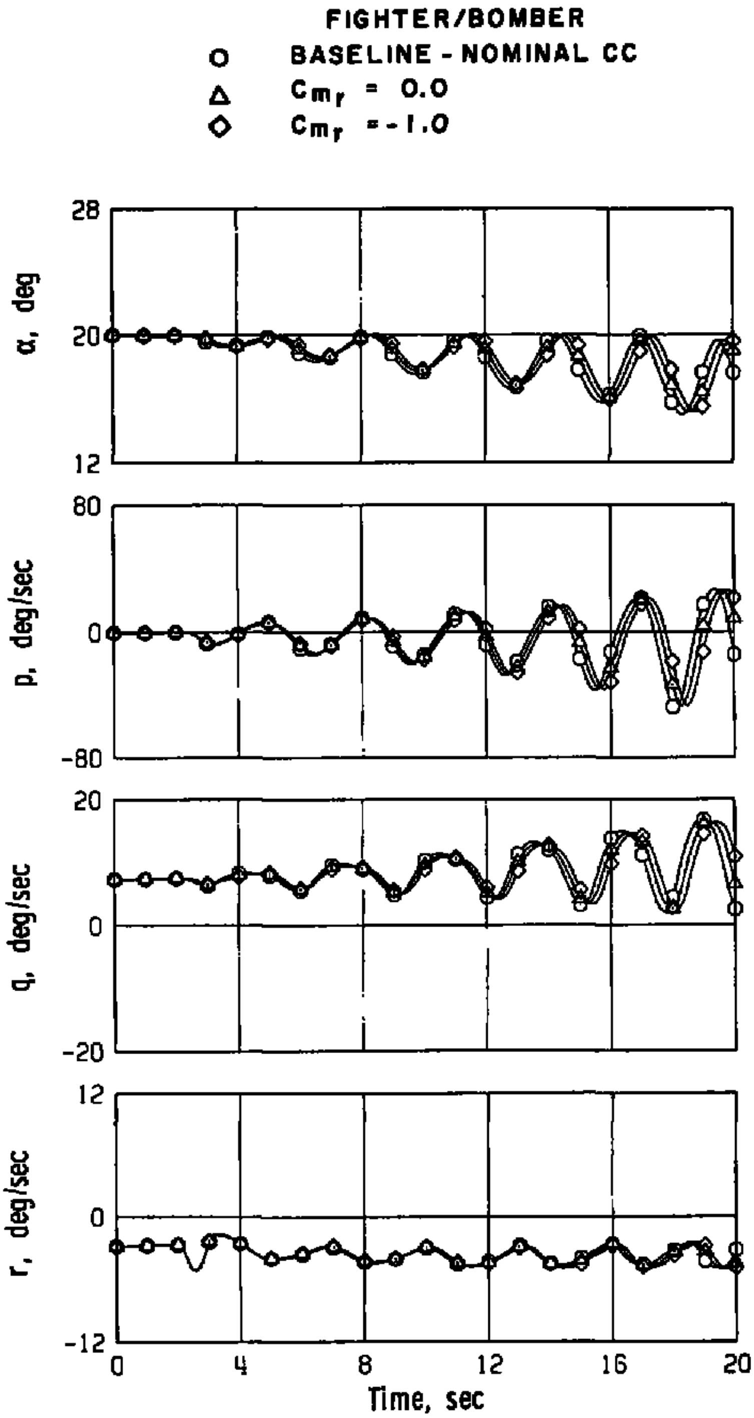

Figure 25. C_{m_r} variation, fighter/bomber 3-g turning flight with nominal cross-coupling derivatives, $\dot{\beta}$ derivatives zero, rudder doublet.

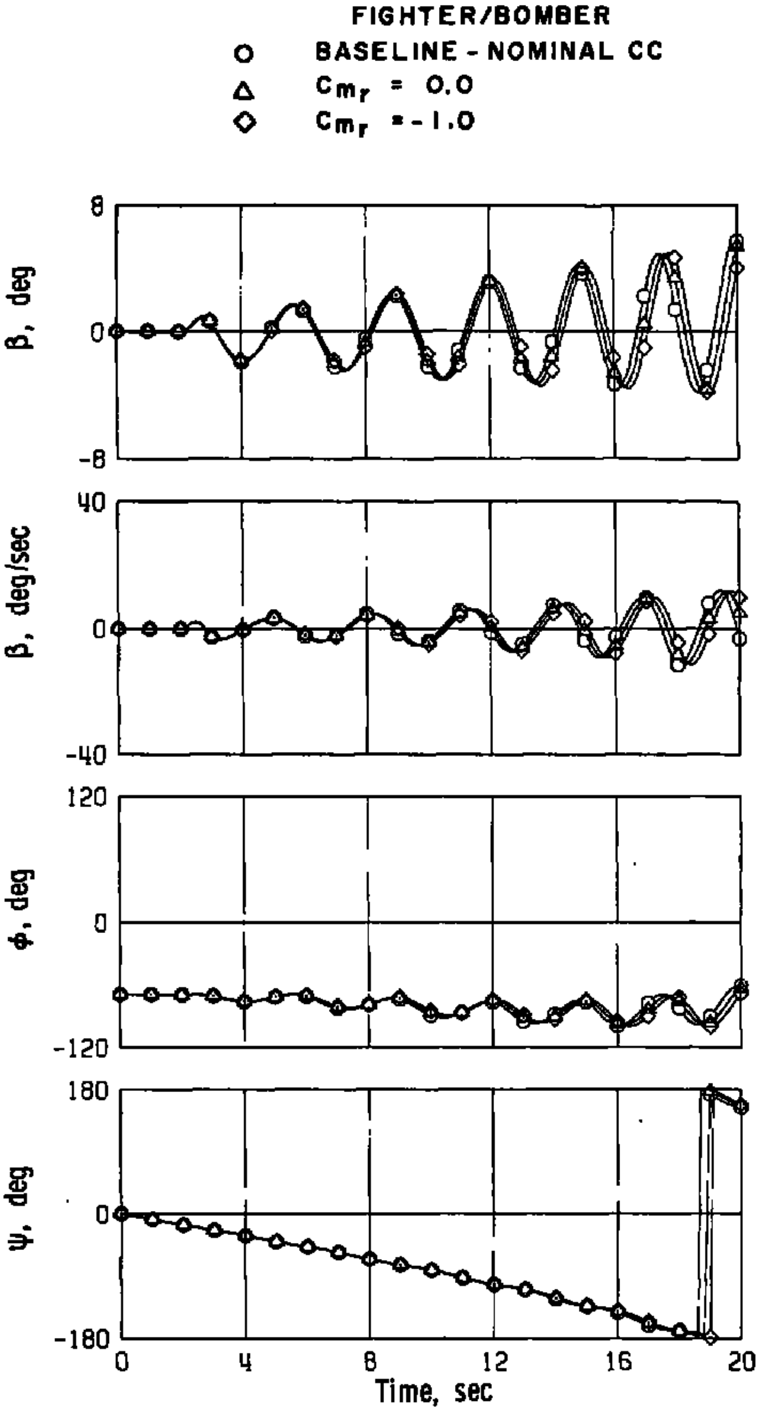

Figure 25. Continued.

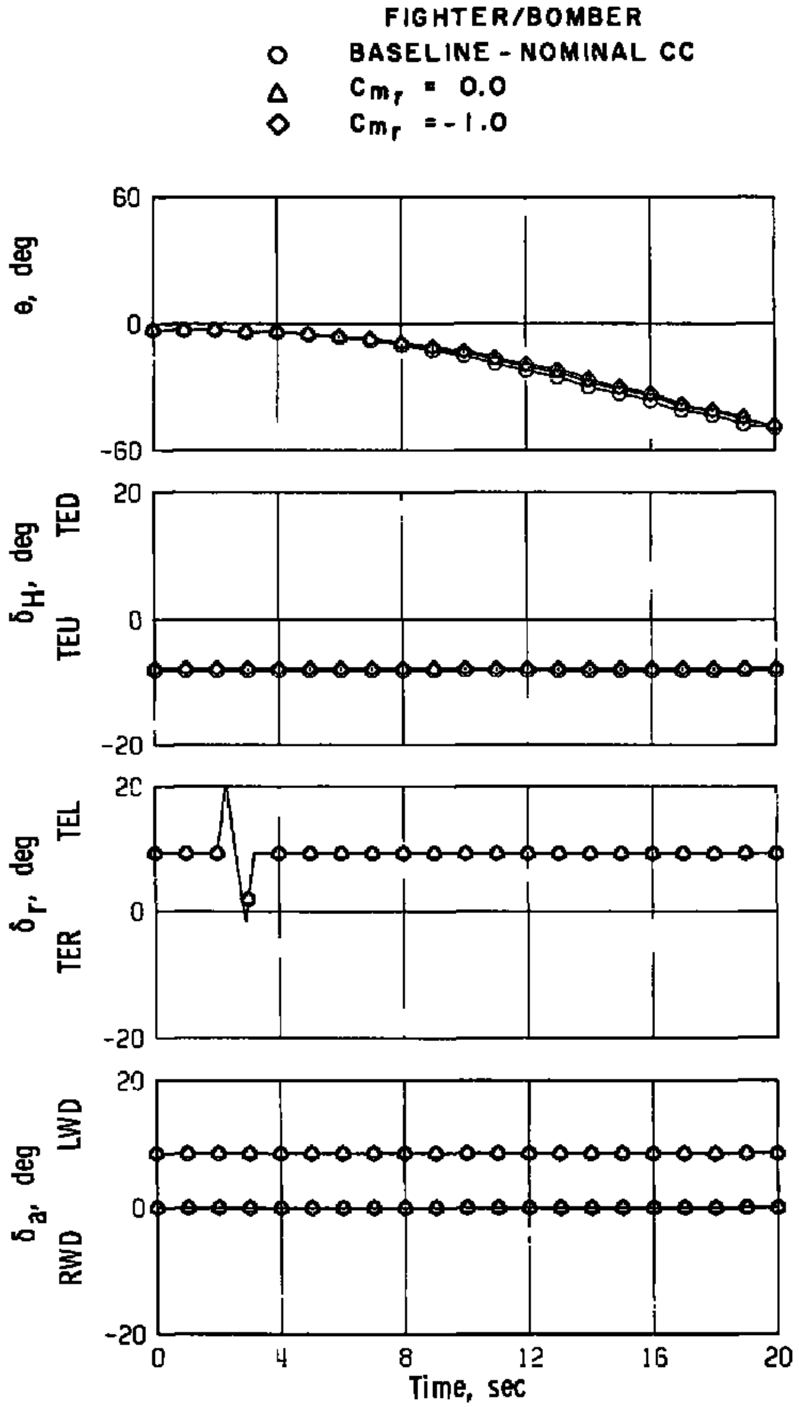

Figure 25. Concluded.

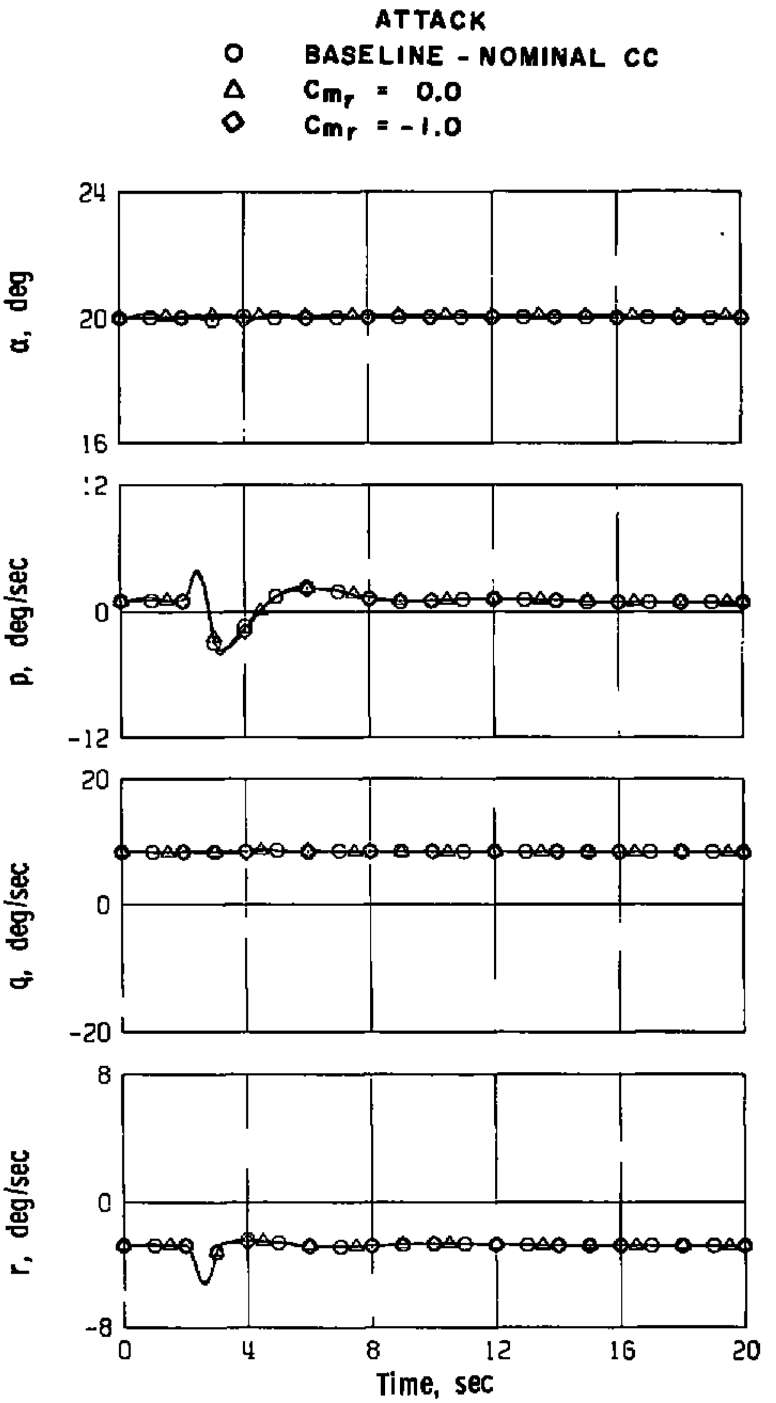

Figure 26. C_{m_r} variation, attack 3-g turning flight with nominal cross-coupling derivatives, $\dot{\beta}$ derivatives zero, rudder doublet.

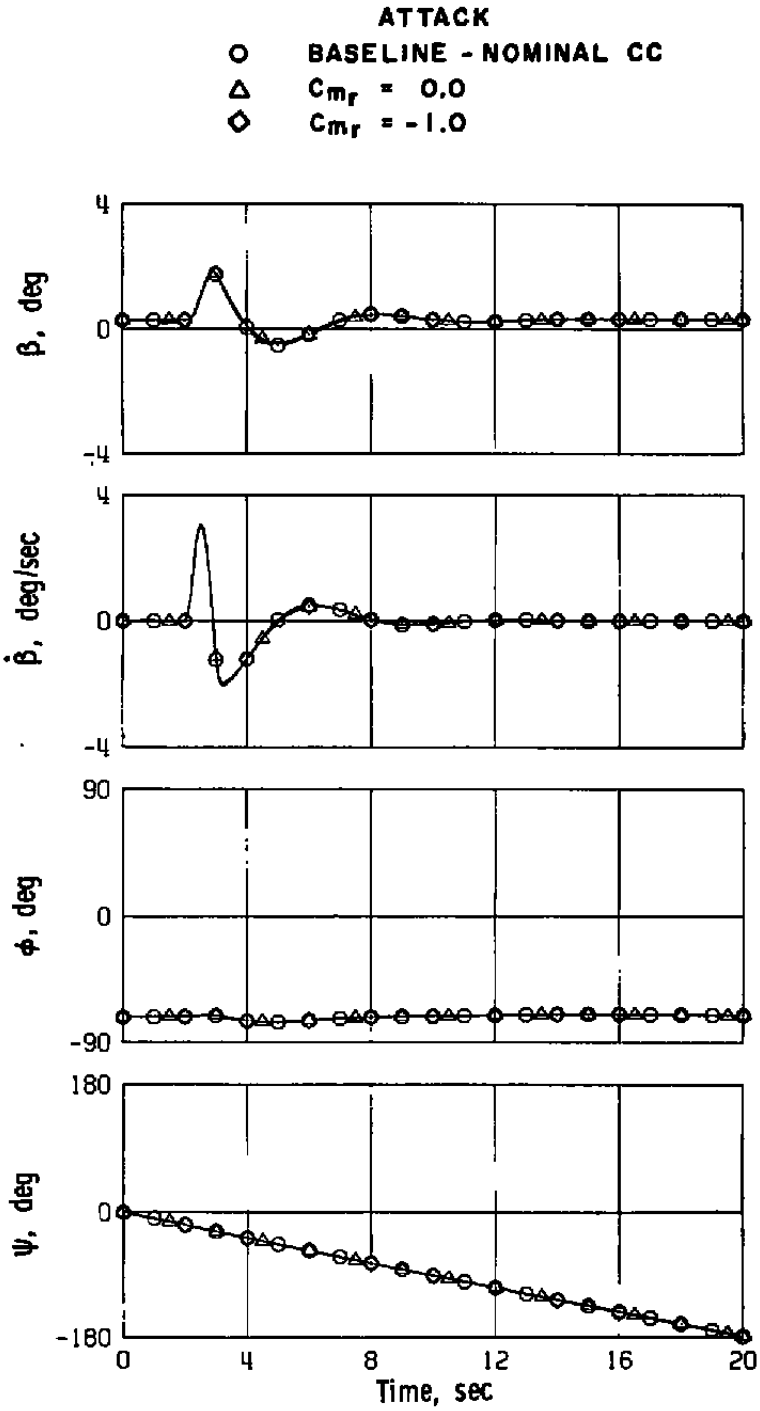

Figure 26. Continued.

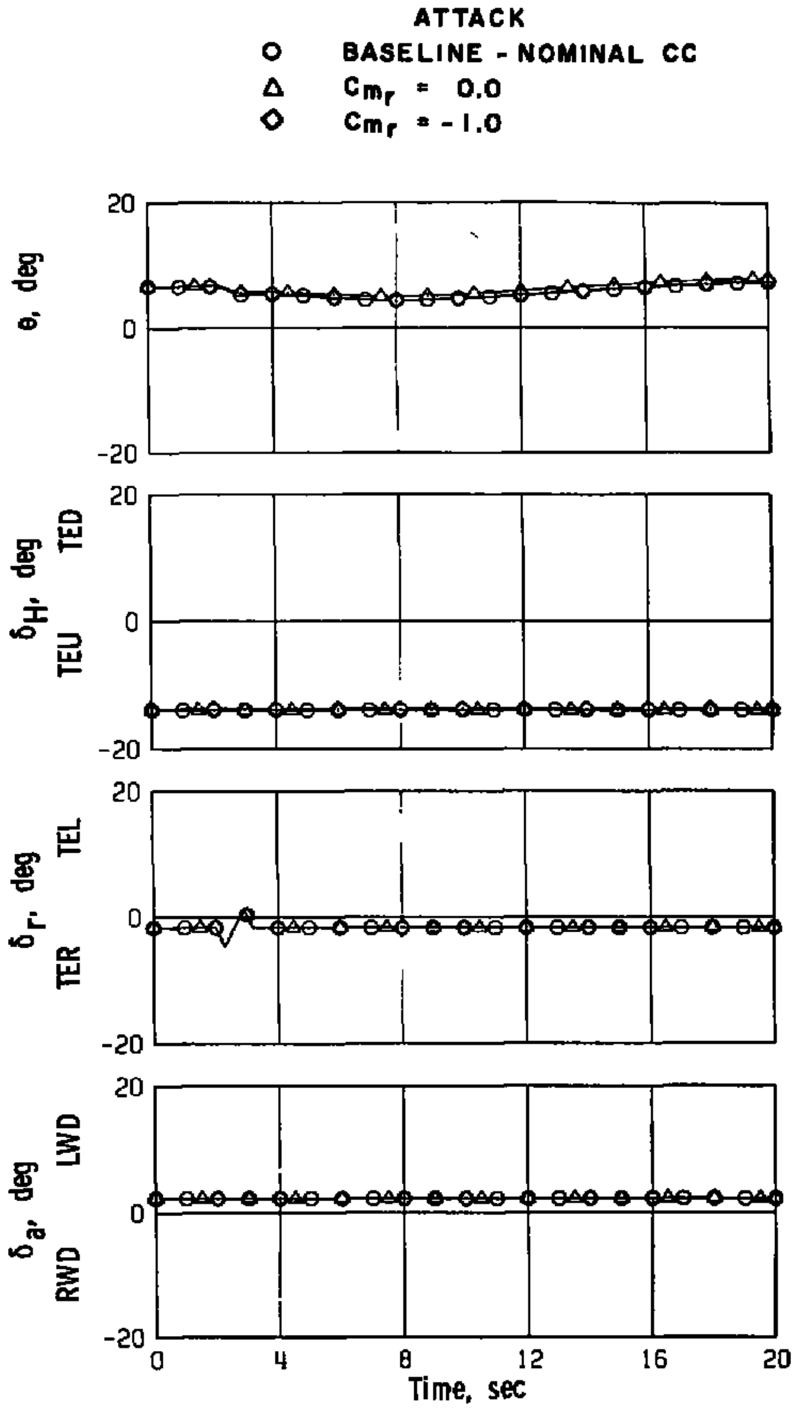

Figure 26. Concluded.

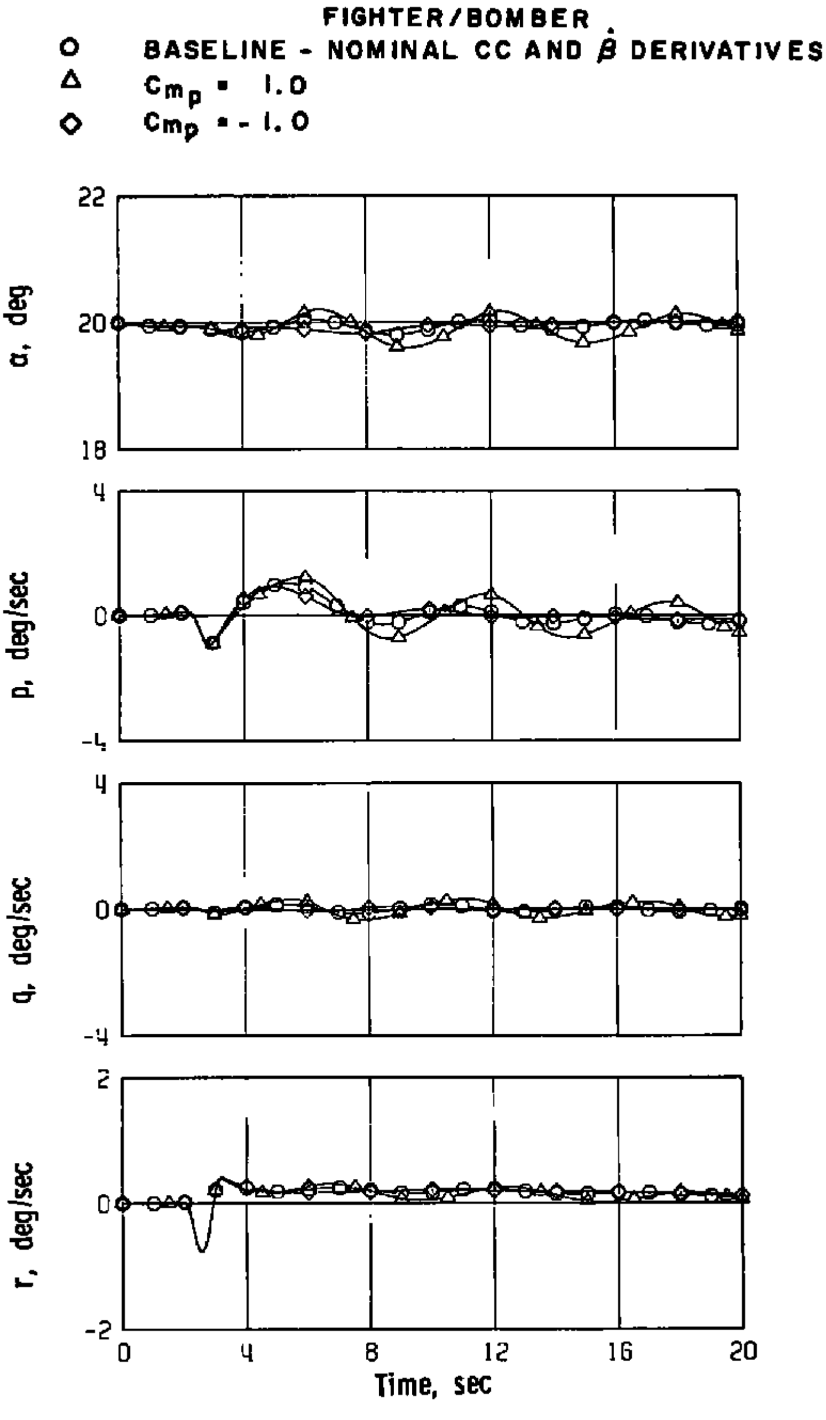

Figure 27. C_{m_p} variation, fighter/bomber level flight with nominal cross-coupling and $\dot{\beta}$ derivatives, rudder doublet.

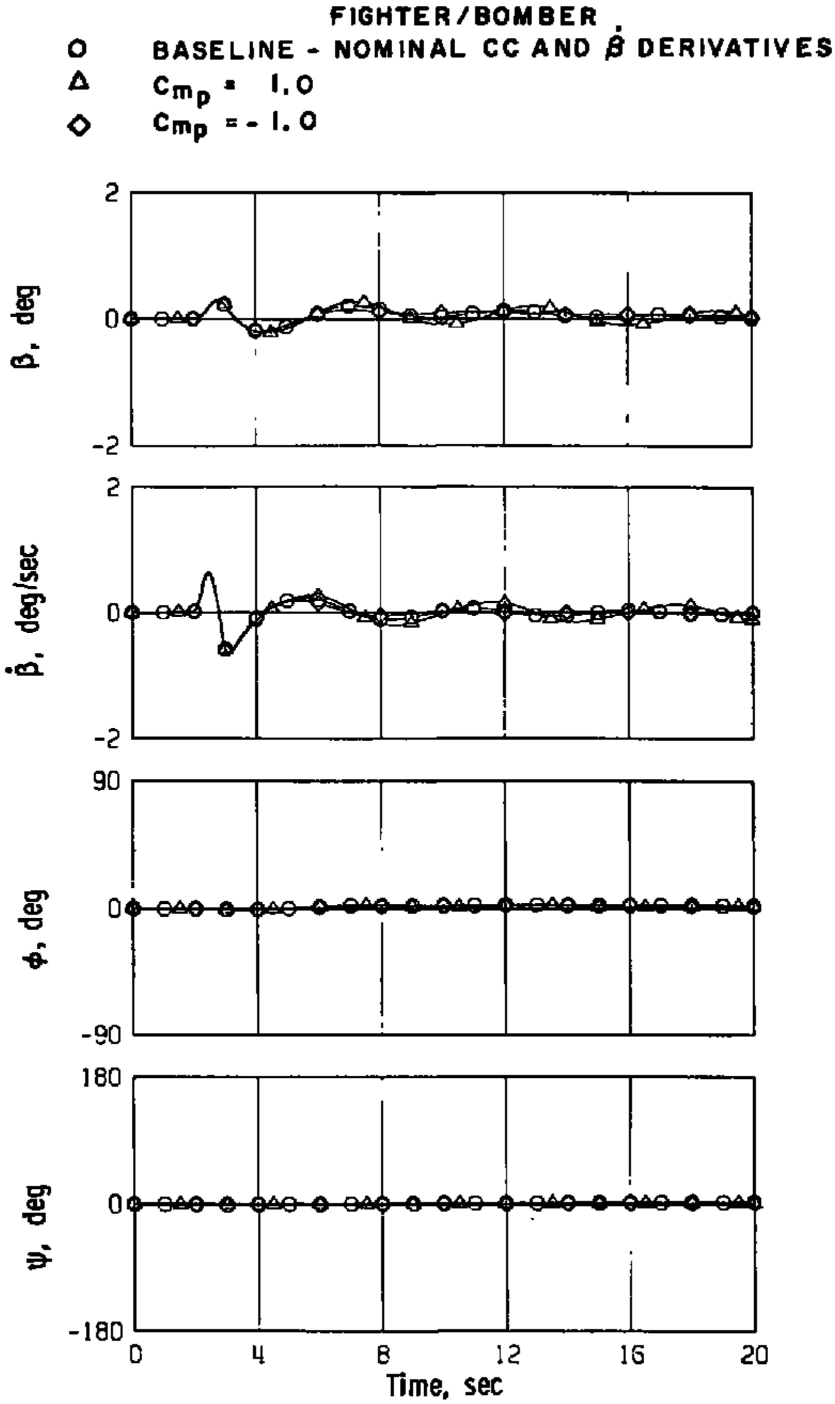

Figure 27. Continued.

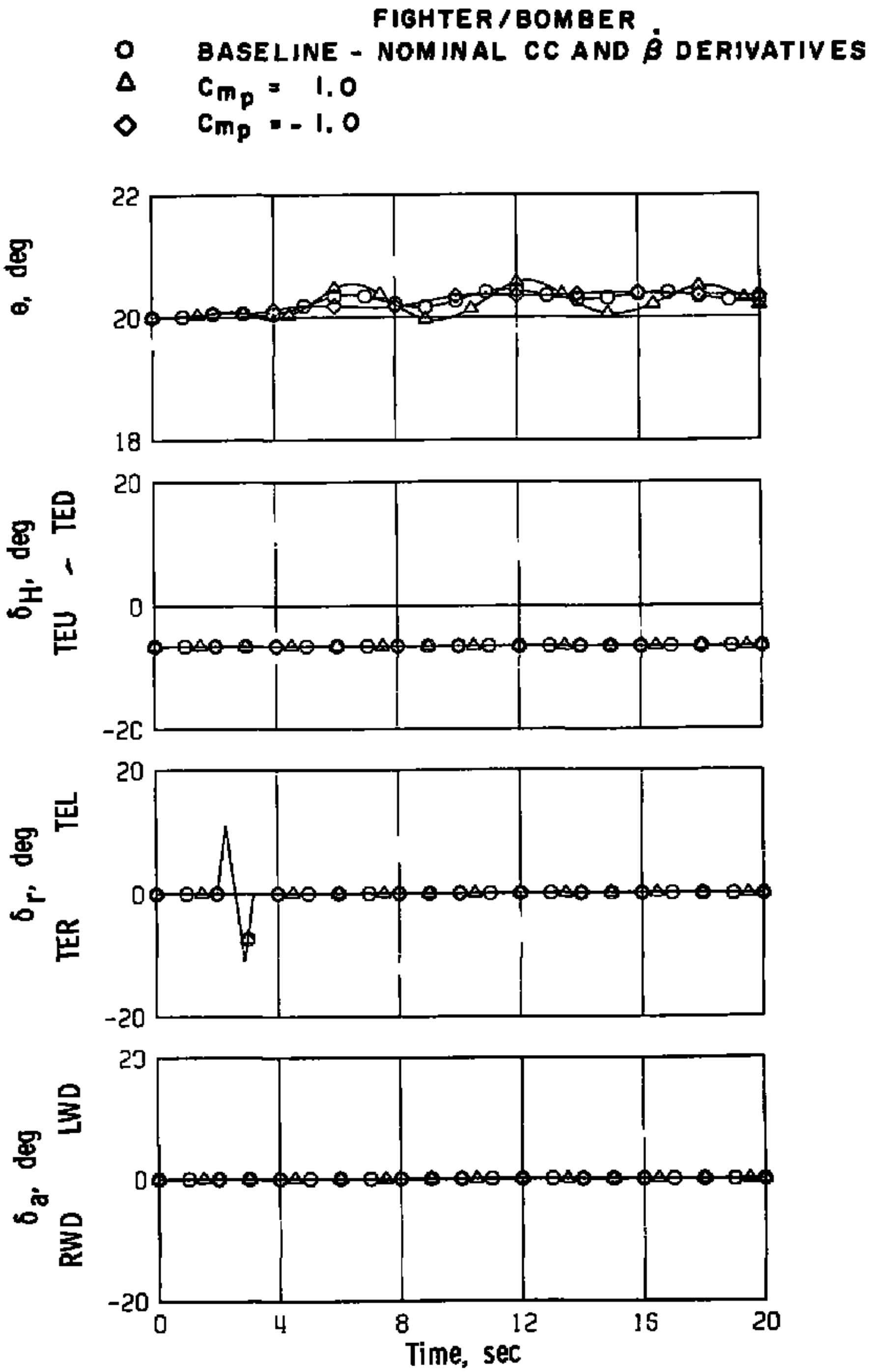

Figure 27. Concluded.

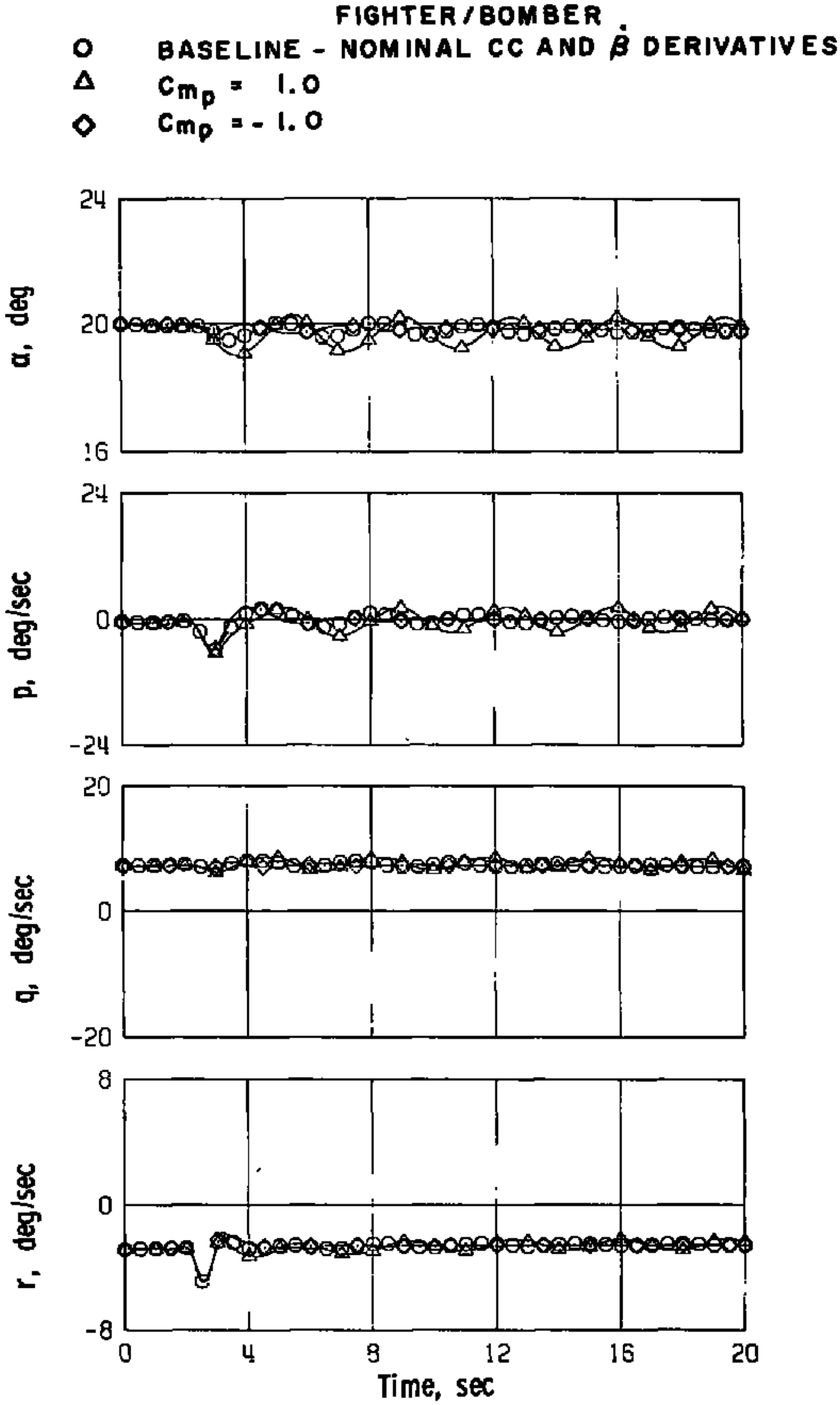

Figure 28. C_{m_p} variation, fighter/bomber 3-g turning flight with nominal cross-coupling and $\dot{\beta}$ derivatives, rudder doublet.

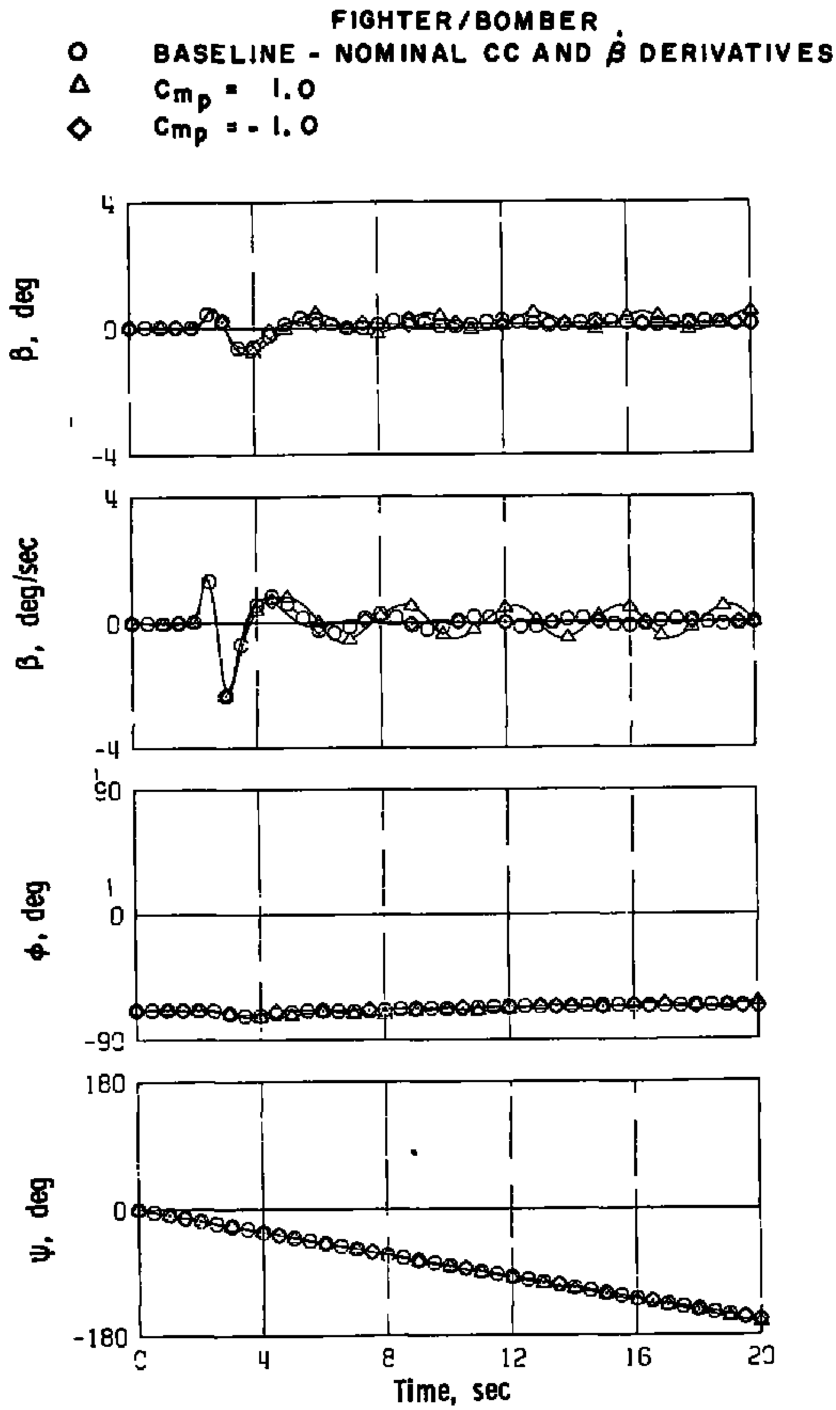

Figure 28. Continued.

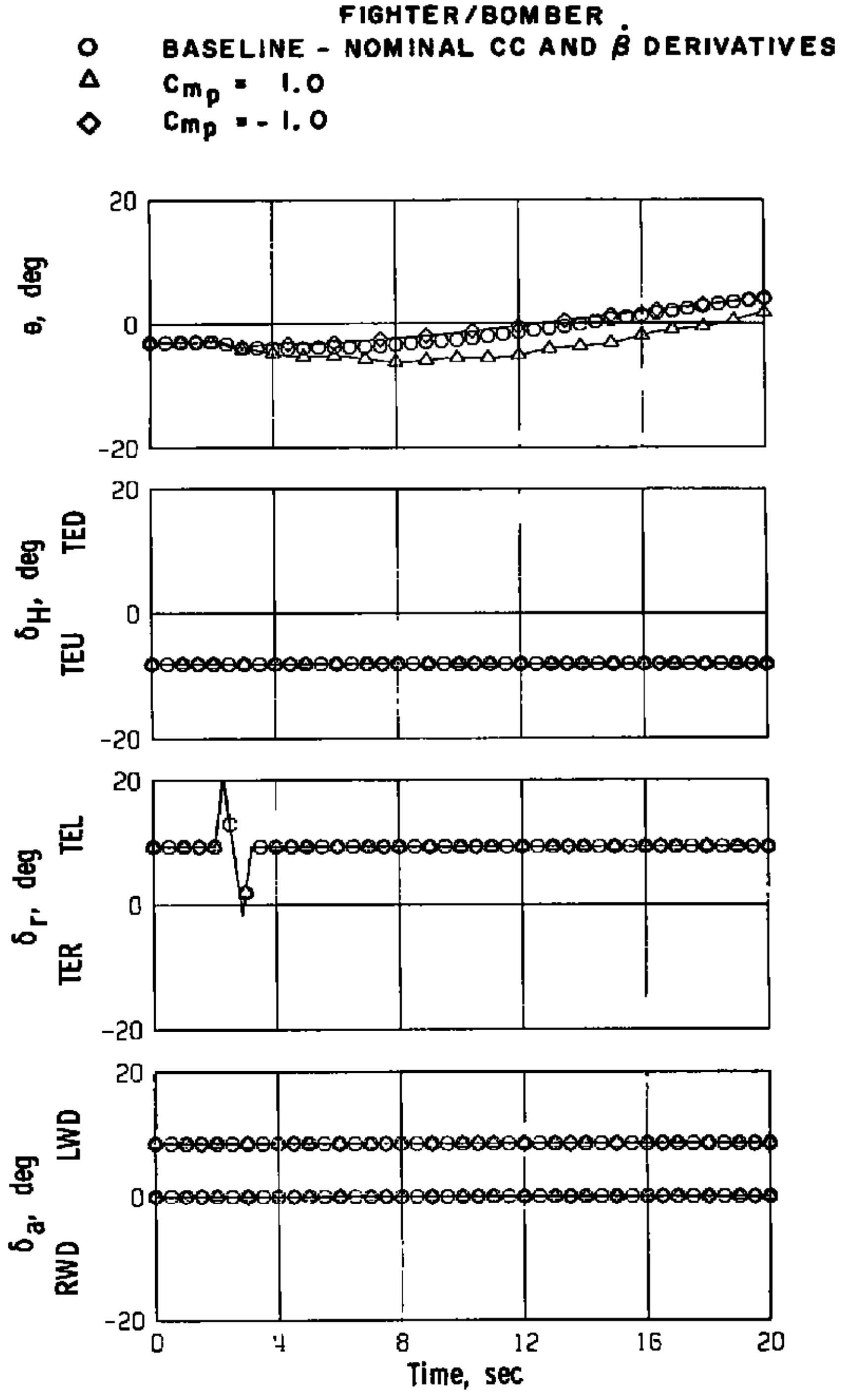

Figure 28. Concluded.

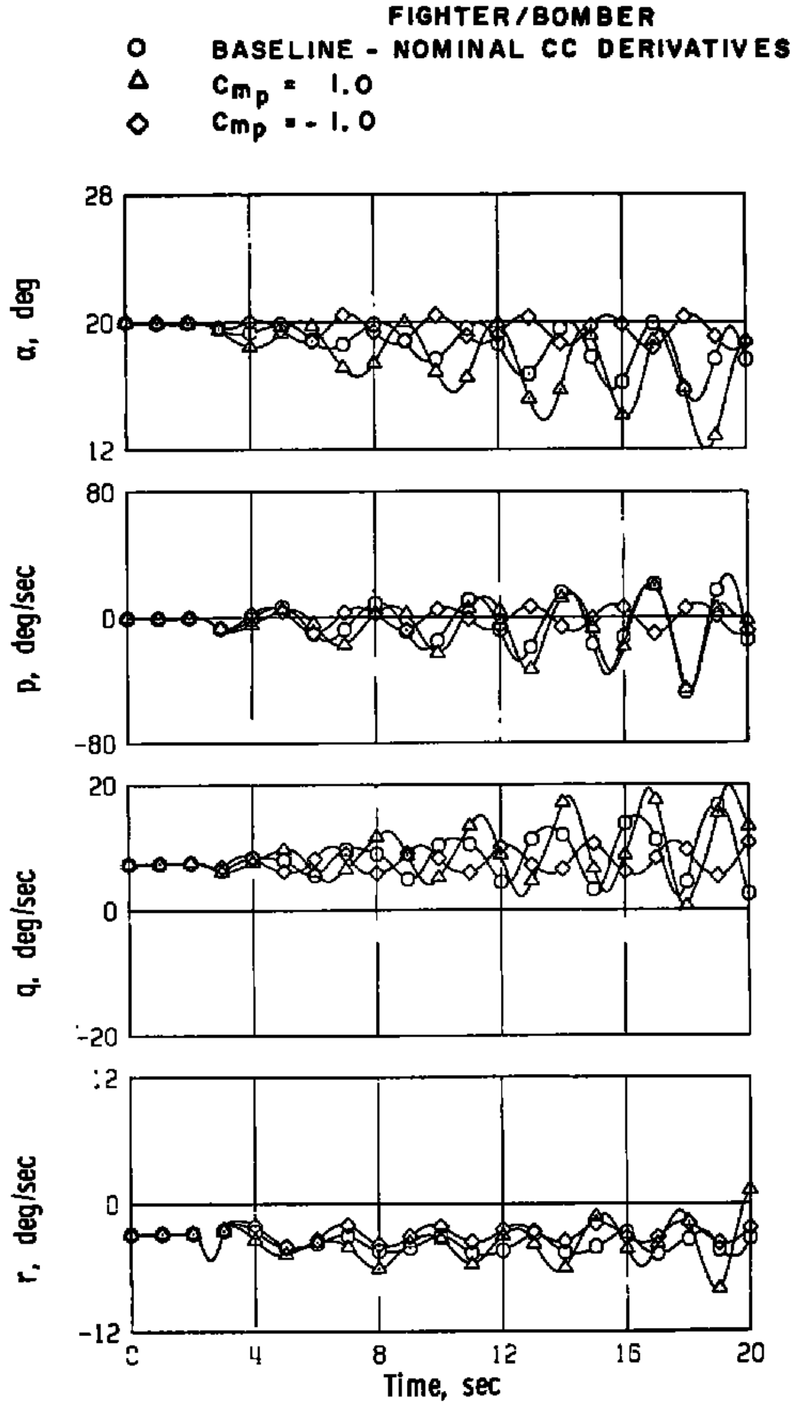

Figure 29. C_{m_p} variation, fighter/bomber 3-g turning flight with nominal cross-coupling derivatives, $\dot{\beta}$ derivatives zero, rudder doublet.

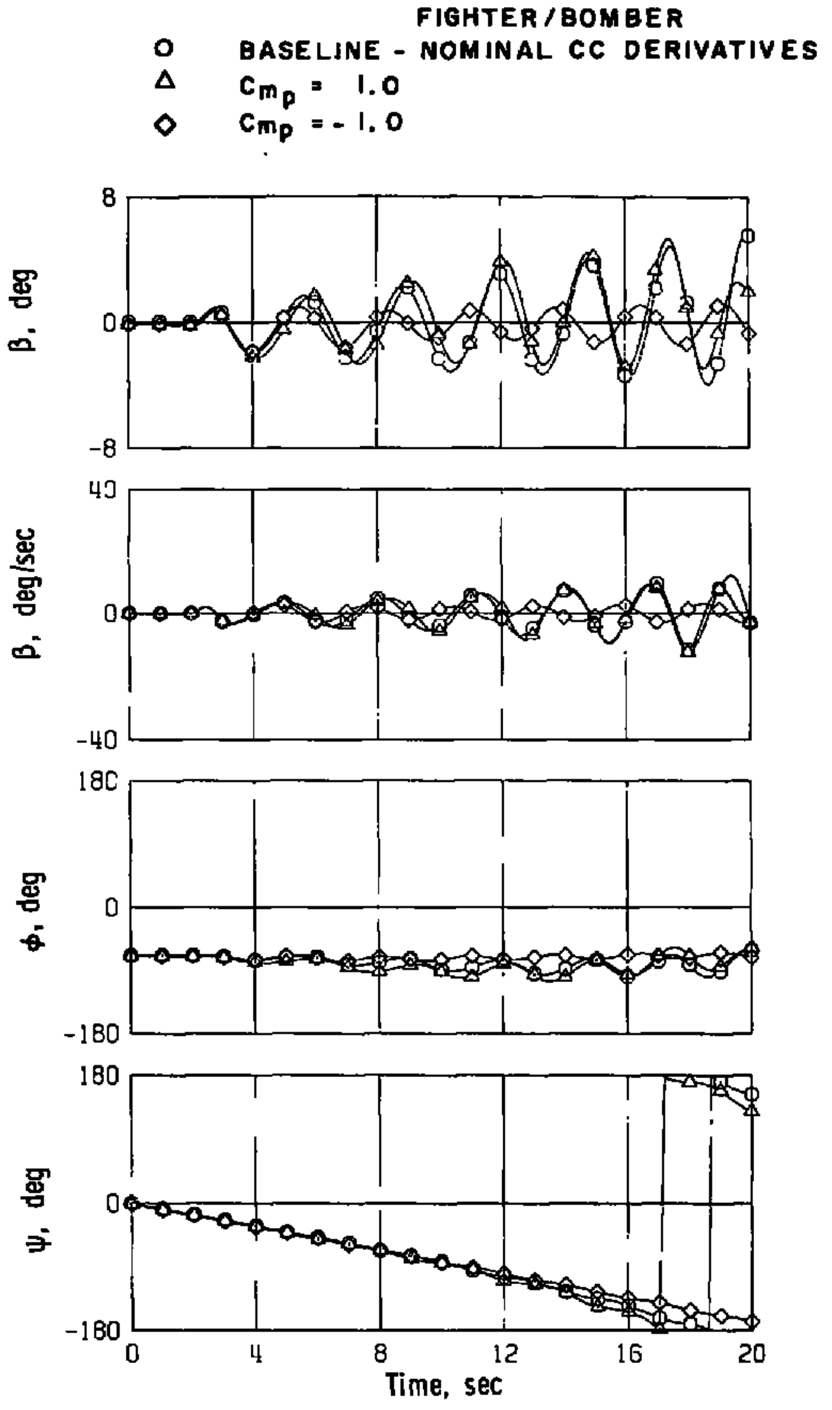

Figure 29. Continued.

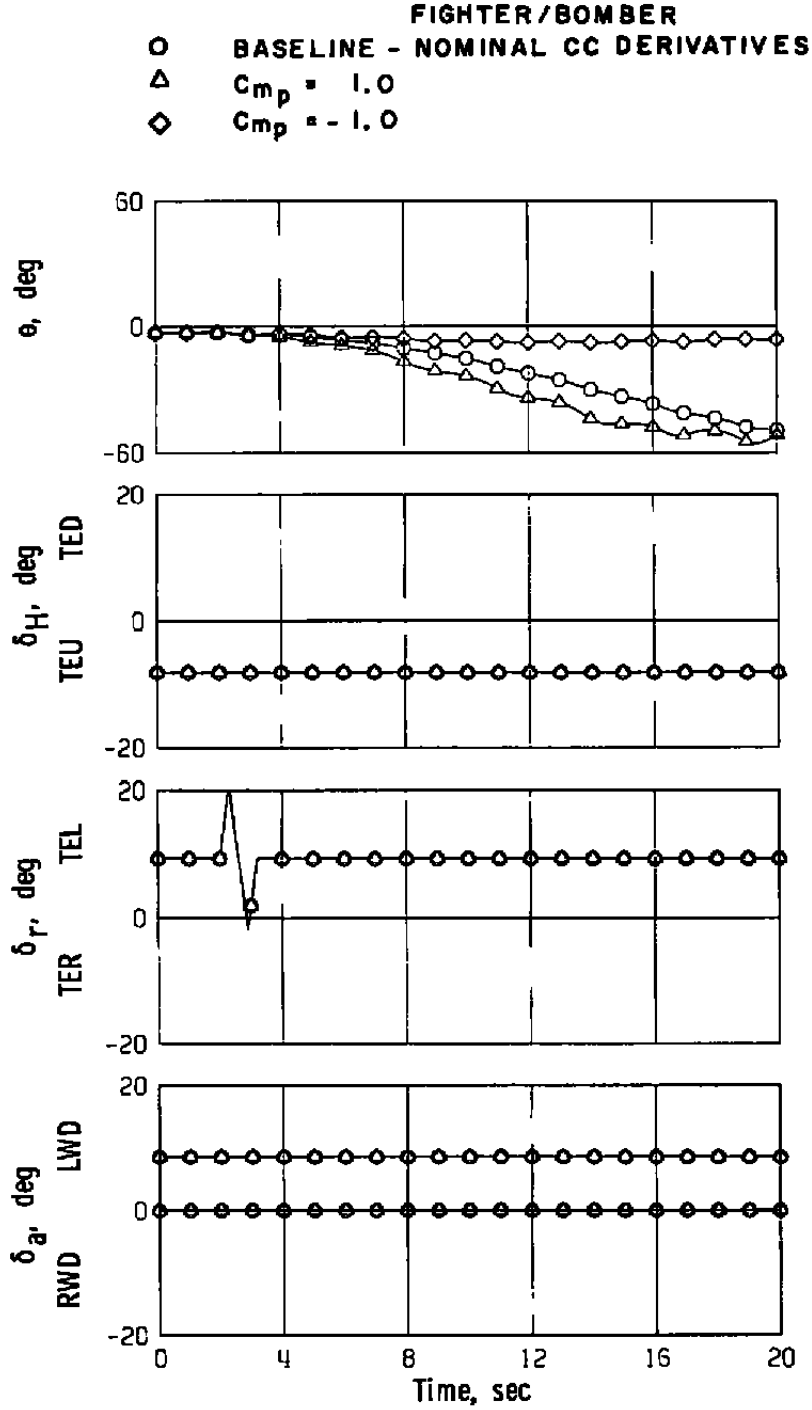

Figure 29. Concluded.

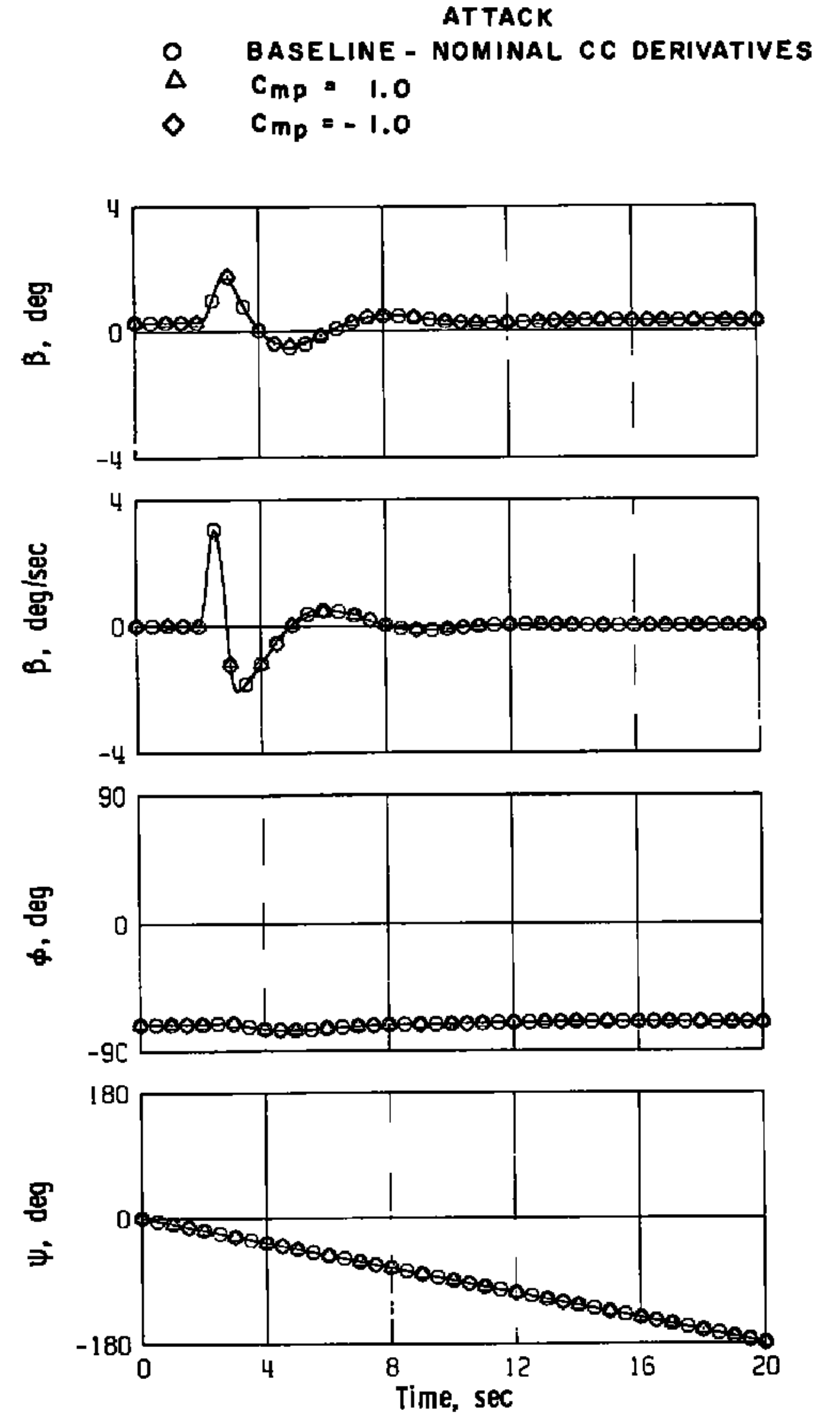

Figure 30. C_{m_p} variation, attack 3-g turning flight with nominal cross-coupling derivatives, $\dot{\beta}$ derivatives zero, rudder doublet.

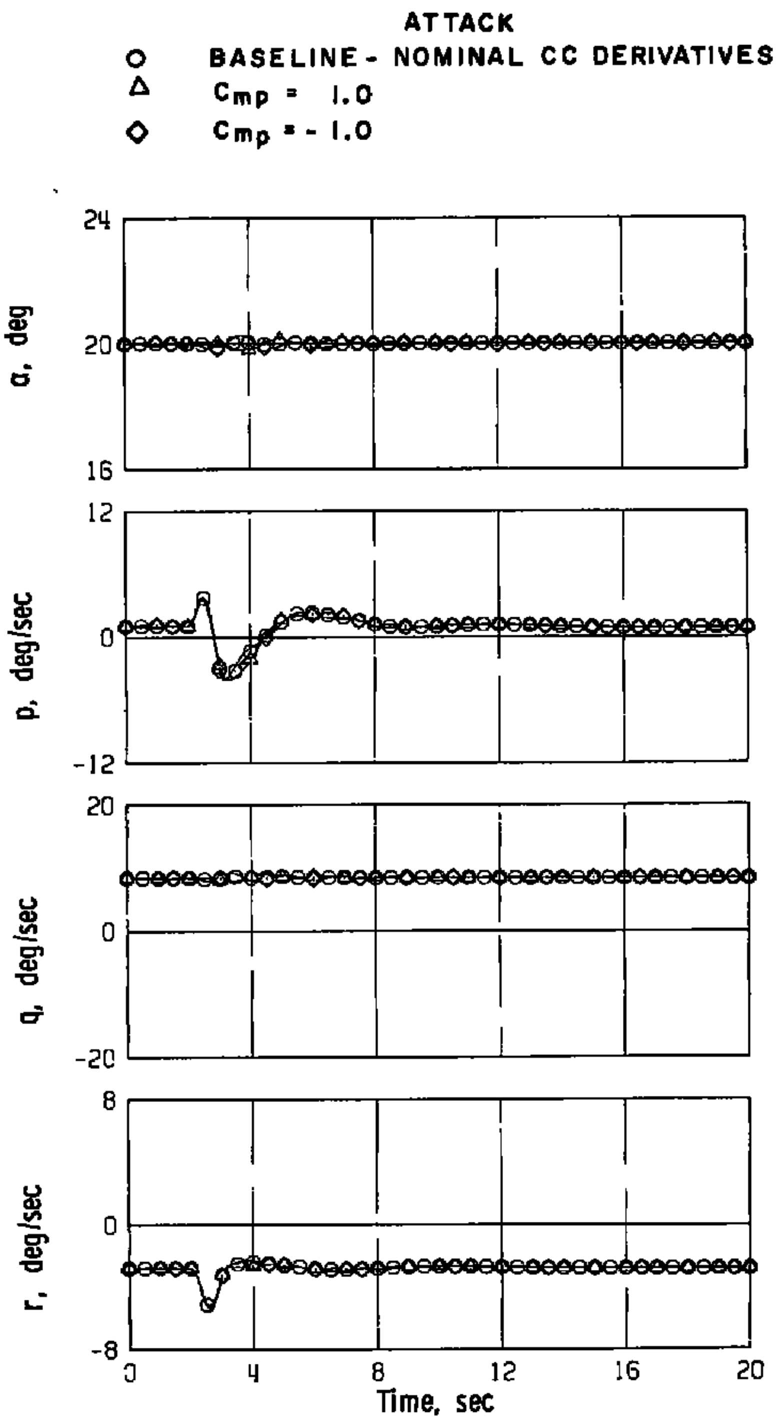

Figure 30. Continued.

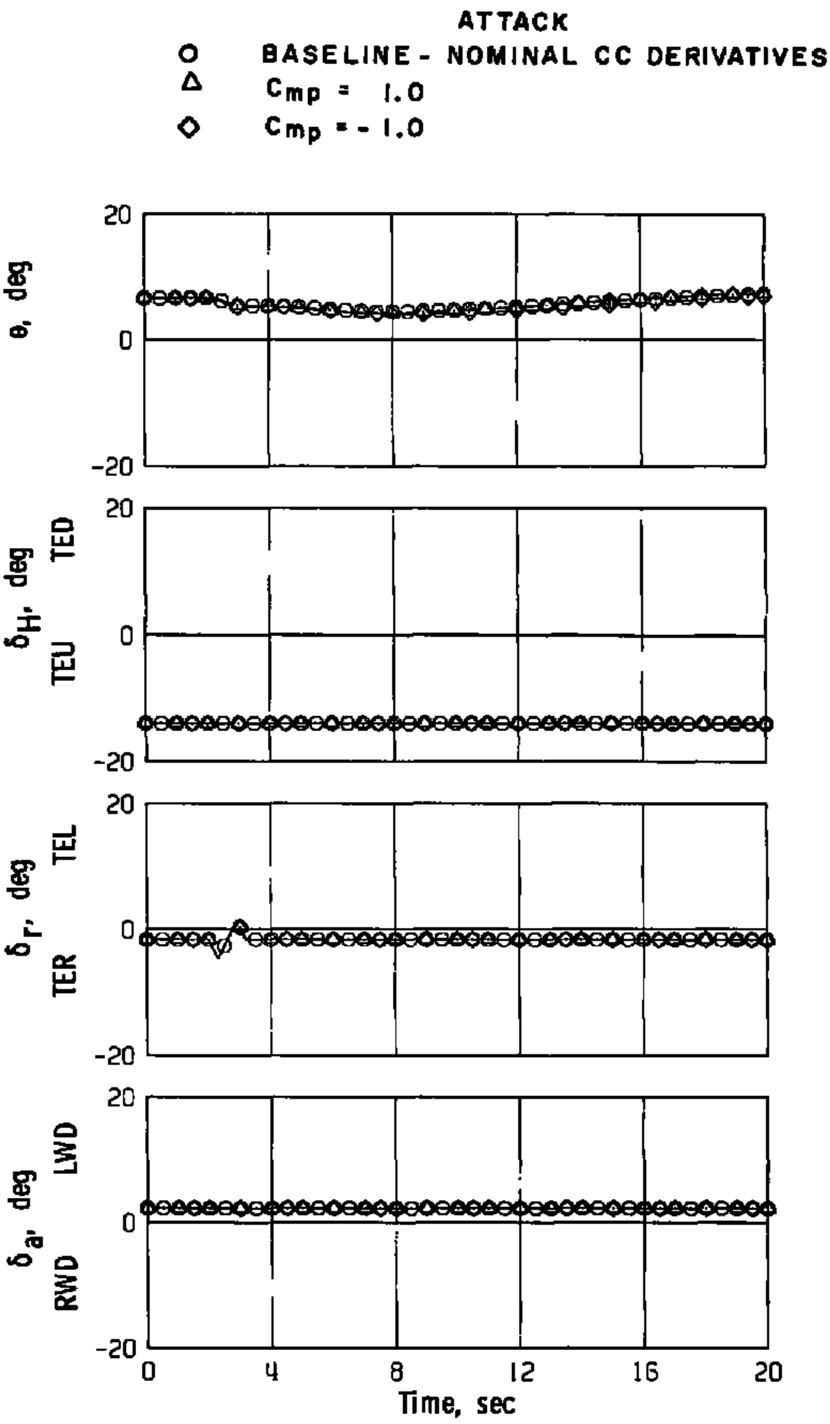

Figure 30. Concluded.

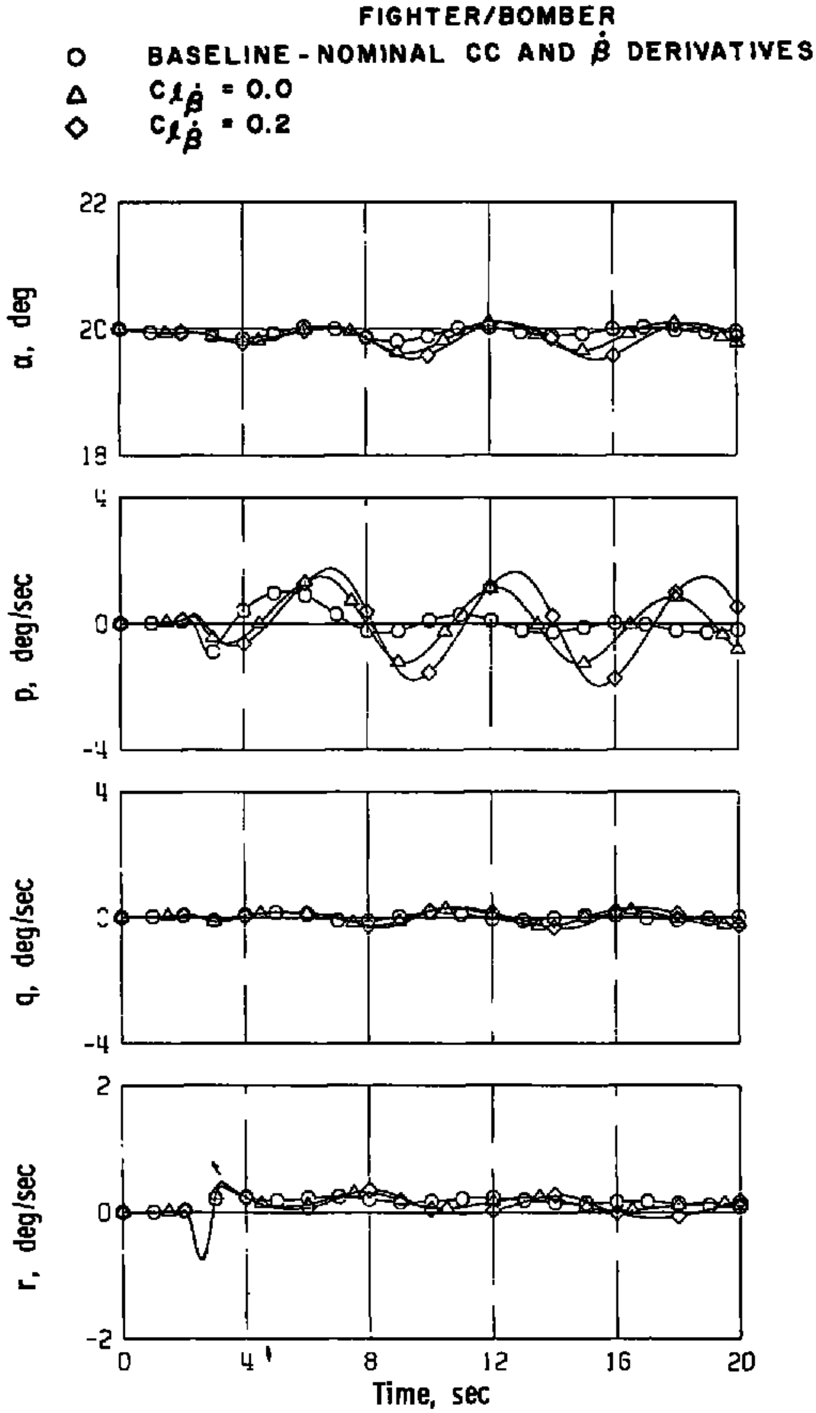

Figure 31. $C_{\ell_{\dot{\beta}}}$ variation, fighter/bomber level flight with nominal cross-coupling and $\dot{\beta}$ derivatives, rudder doublet.

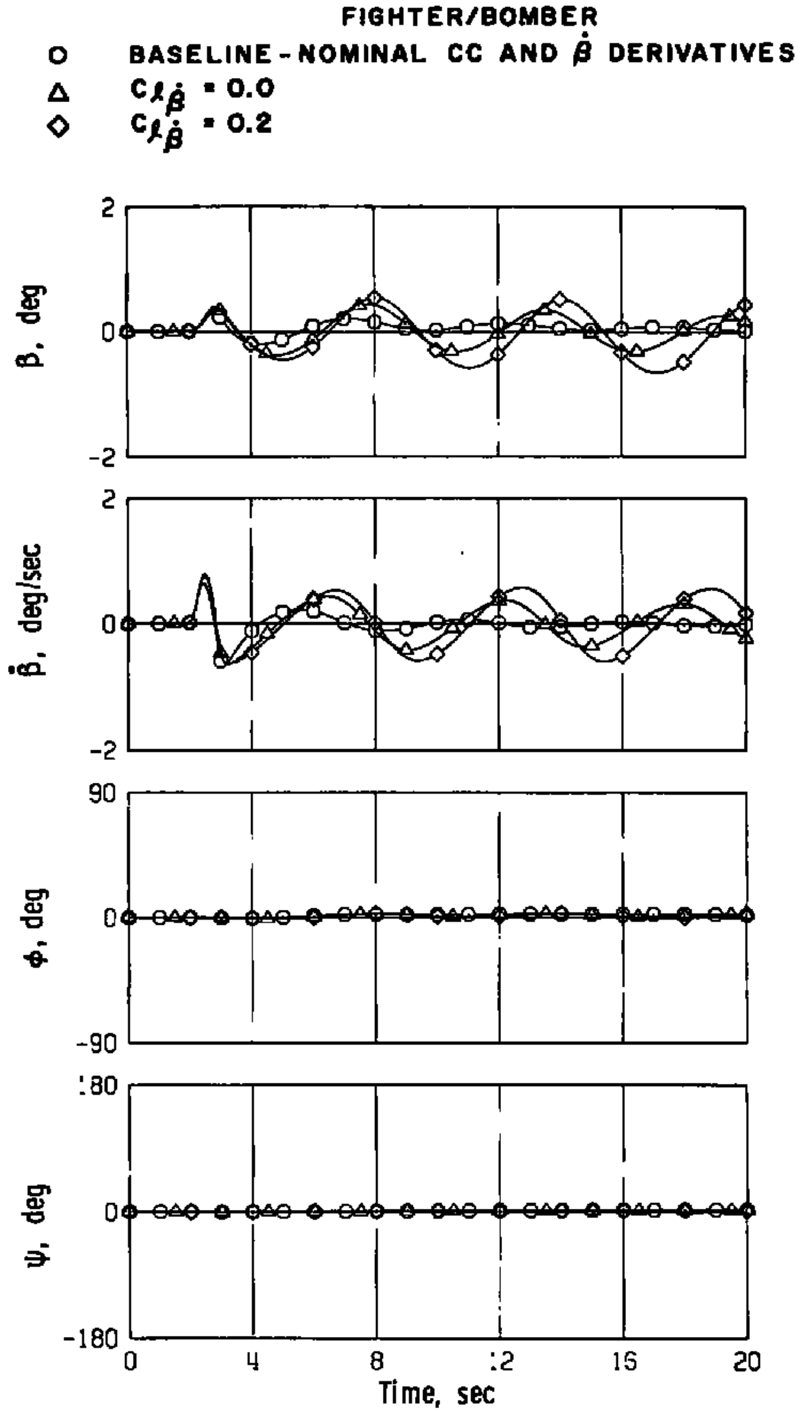

Figure 31. Continued.

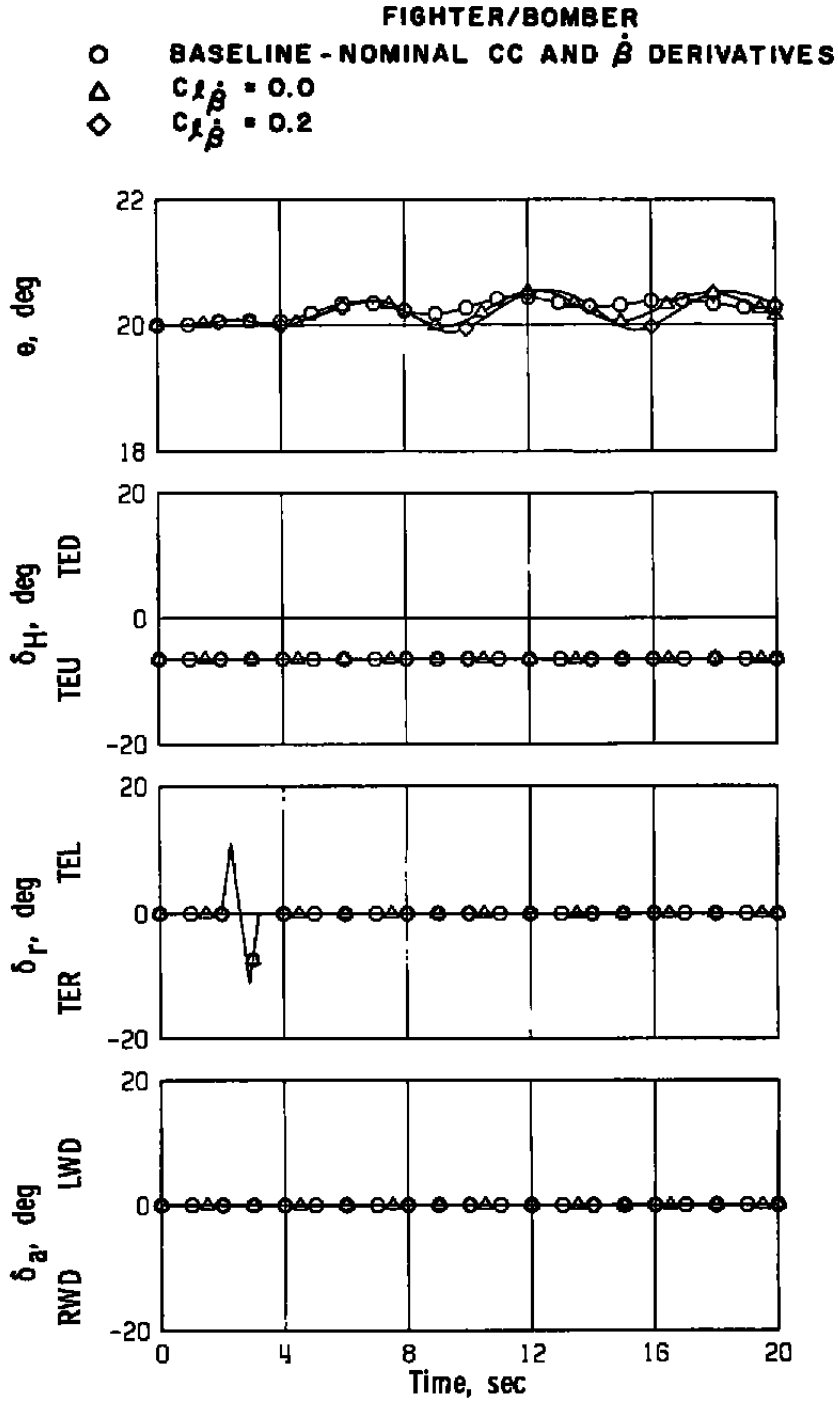

Figure 31. Concluded.

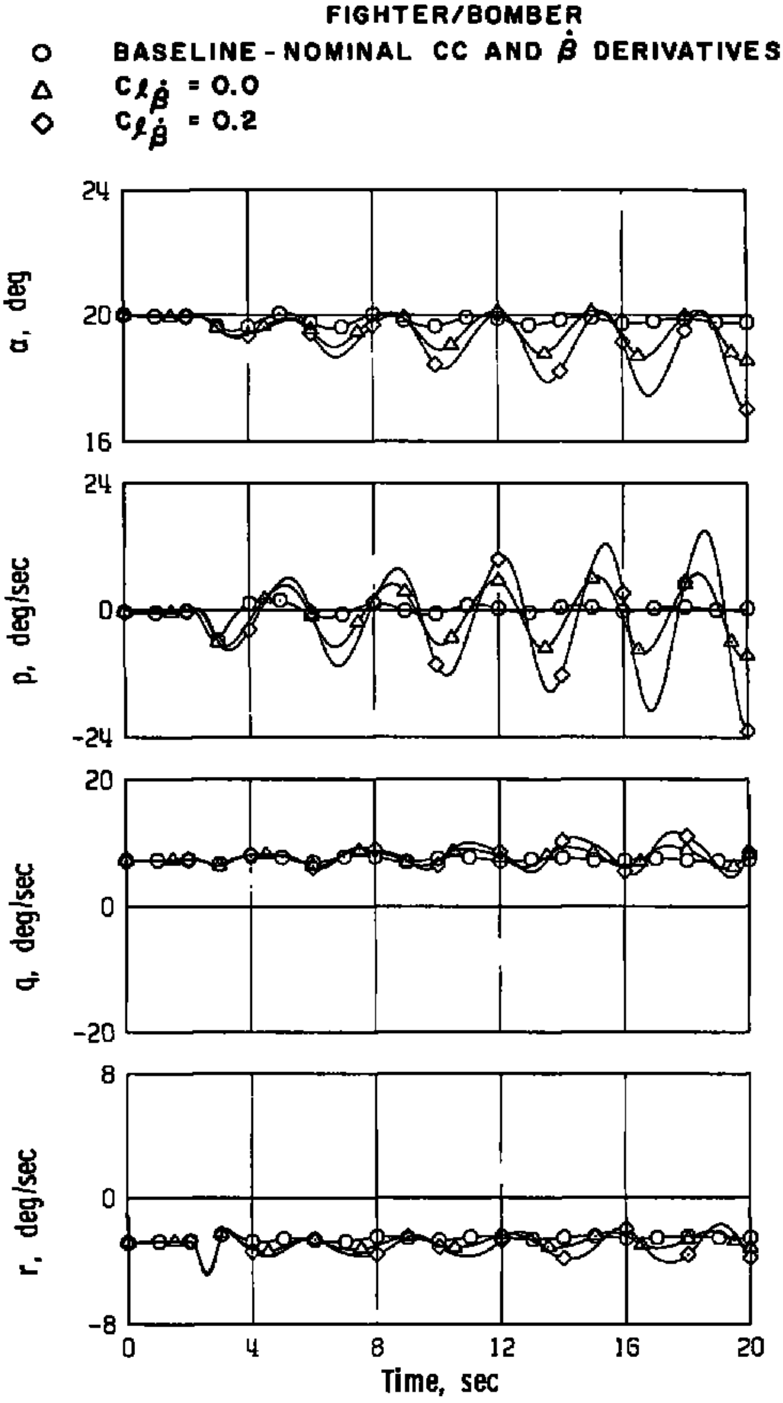

Figure 32. $C_{\ell_{\dot{\beta}}}$ variation, fighter/bomber 3-g turning flight with nominal cross-coupling and $\dot{\beta}$ derivatives, rudder doublet.

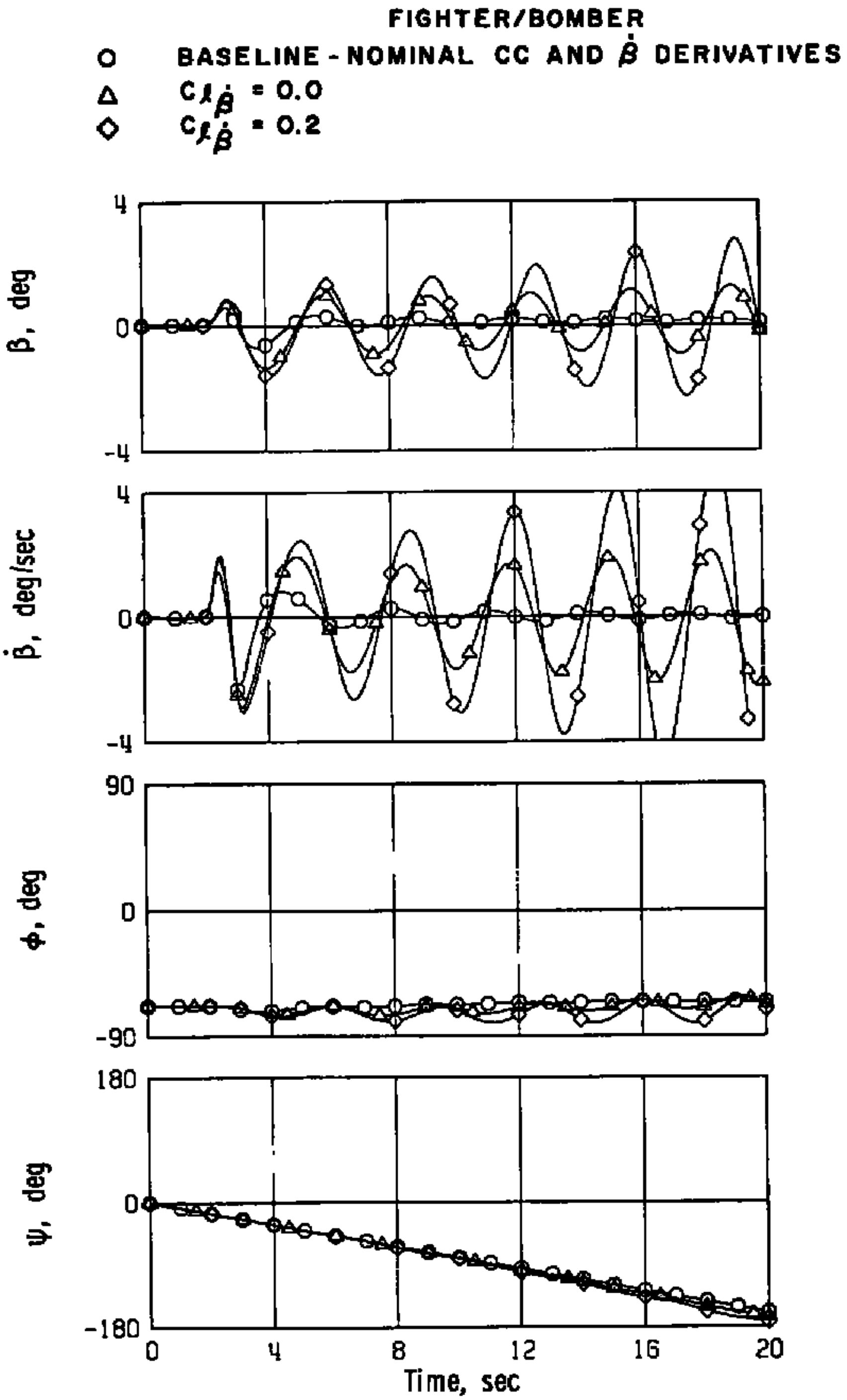

Figure 32. Continued.

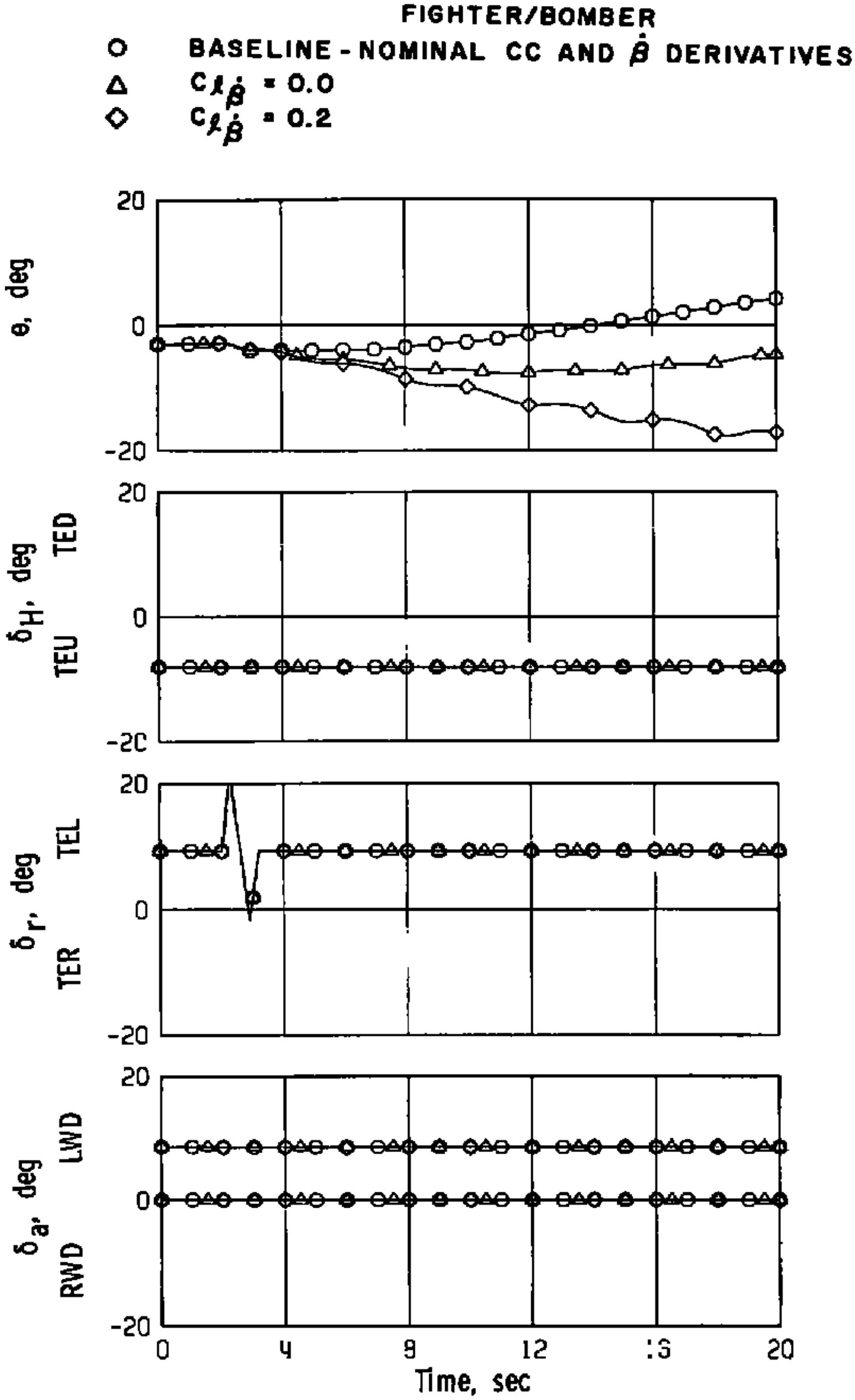

Figure 32. Concluded.

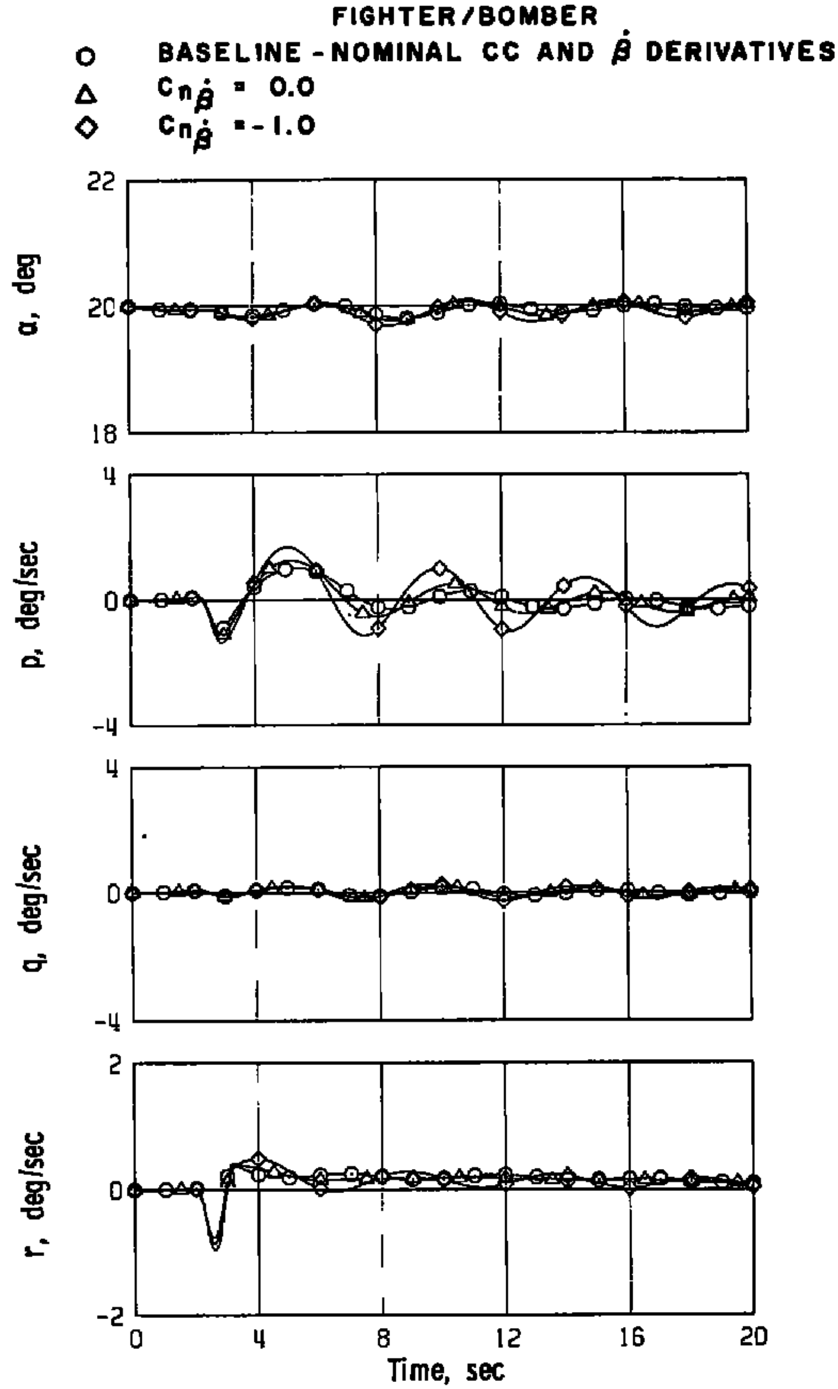

Figure 33. $C_{n_{\dot{\beta}}}$ variation, fighter/bomber level flight with nominal cross-coupling and $\dot{\beta}$ derivatives, rudder doublet.

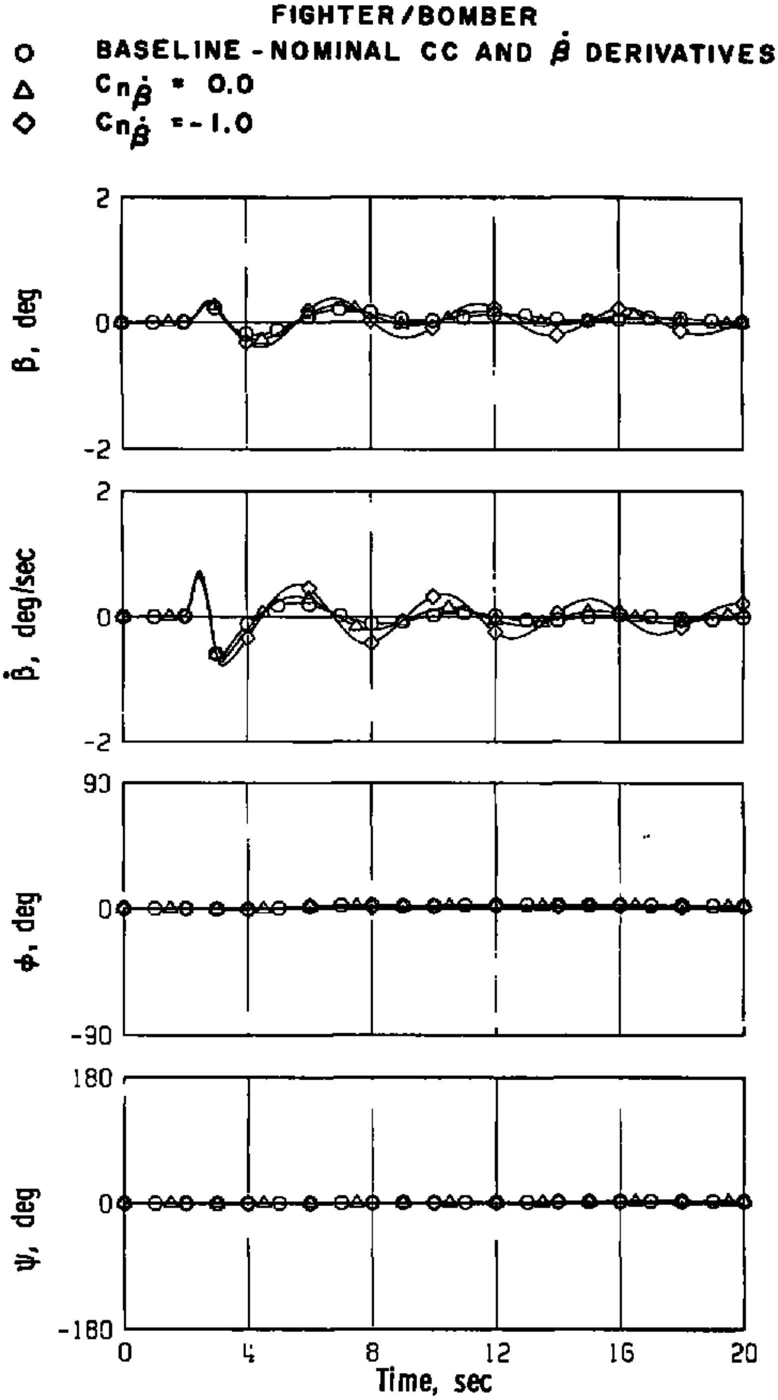

Figure 33. Continued.

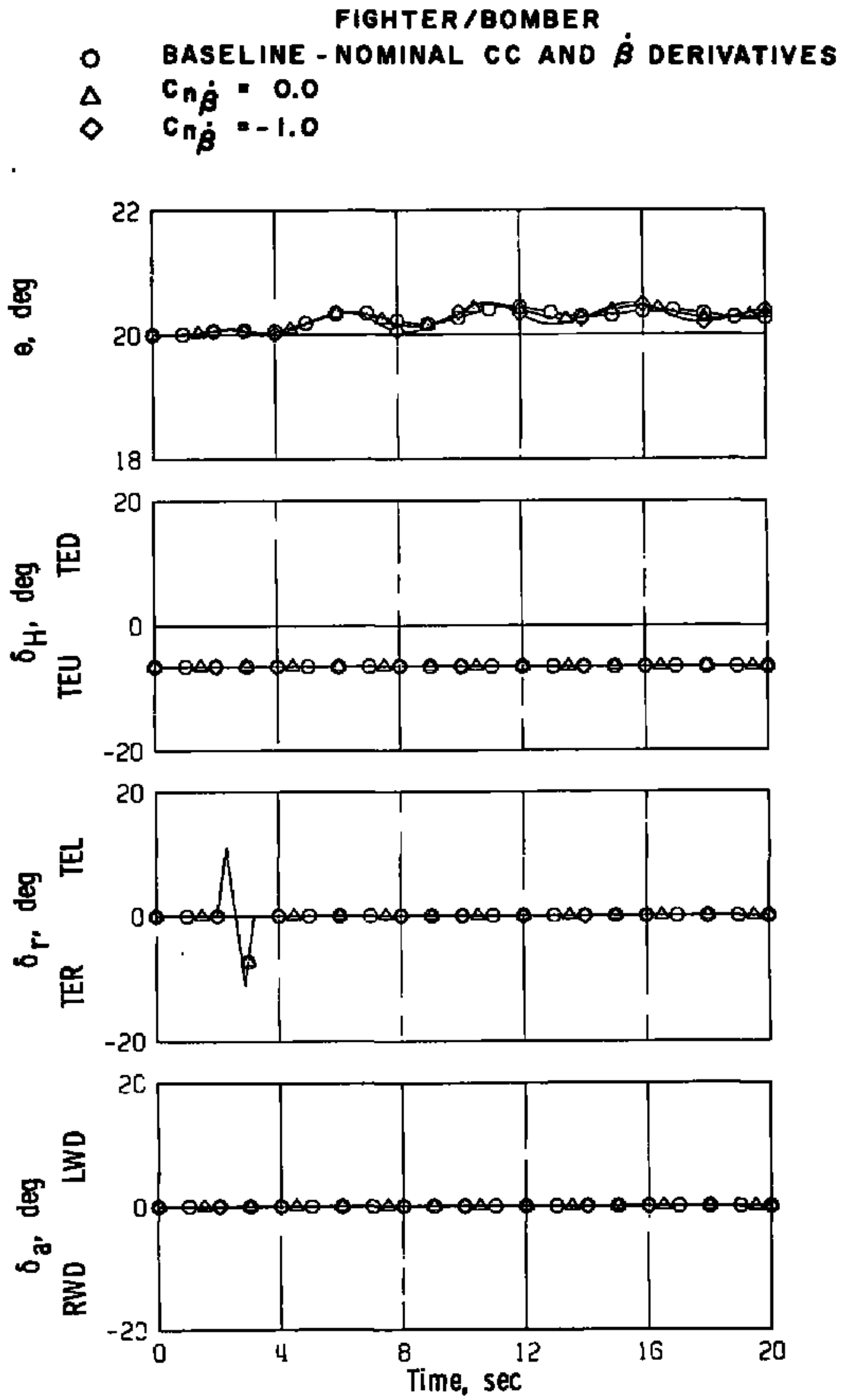

Figure 33. Concluded.

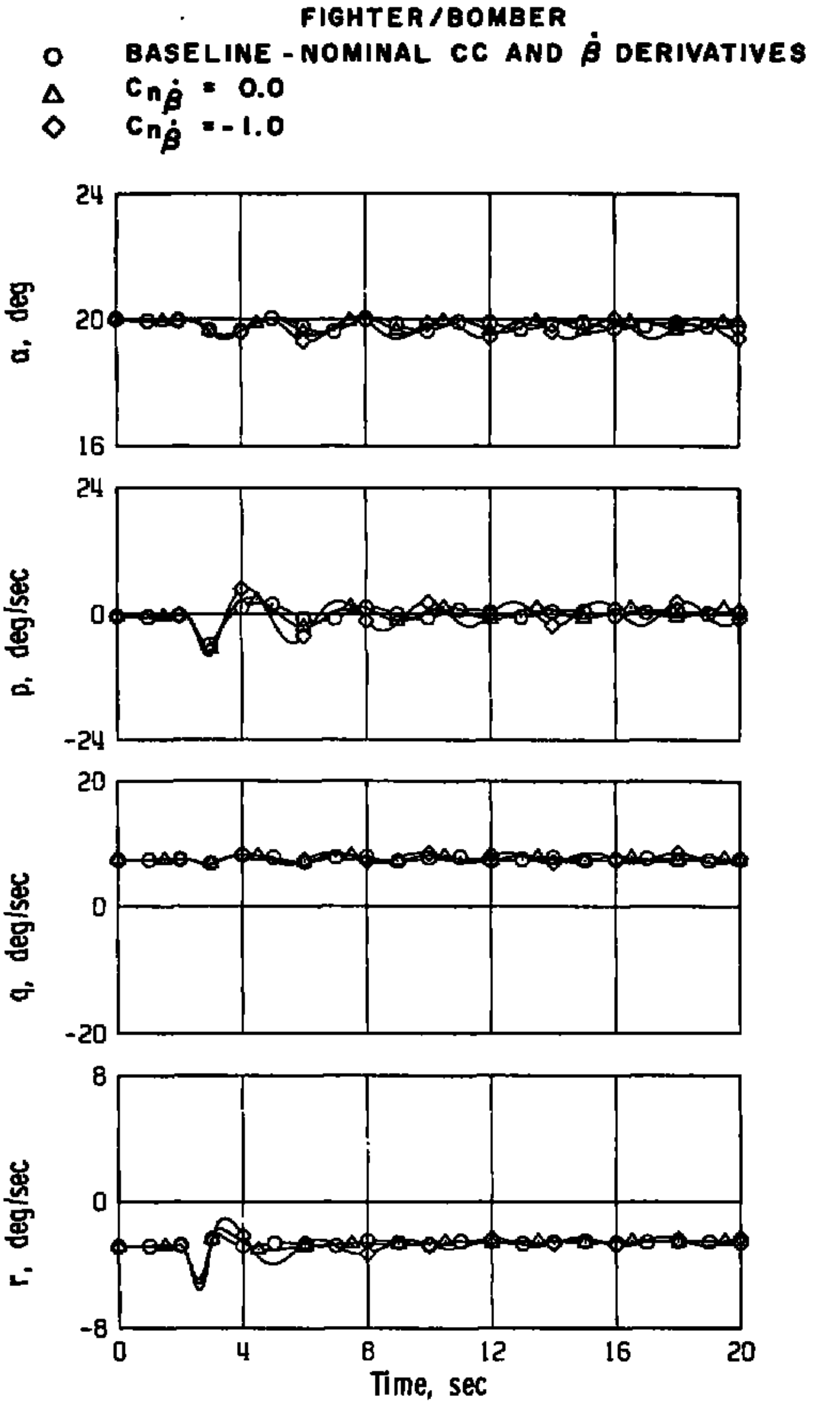

Figure 34. $C_{n_{\dot{\beta}}}$ variation, fighter/bomber 3-g turning flight with nominal cross-coupling and $\dot{\beta}$ derivatives, rudder doublet.

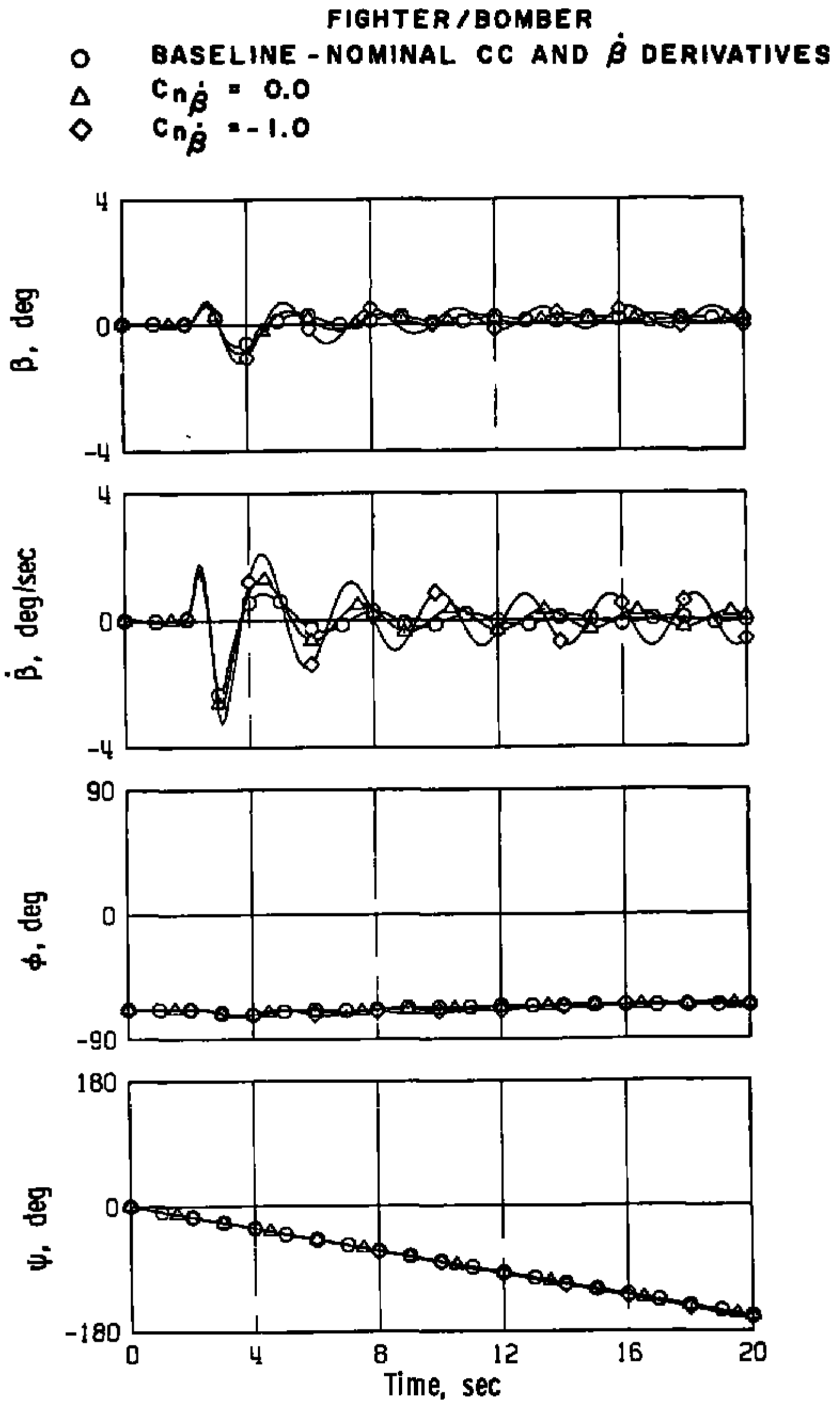

Figure 34. Continued.

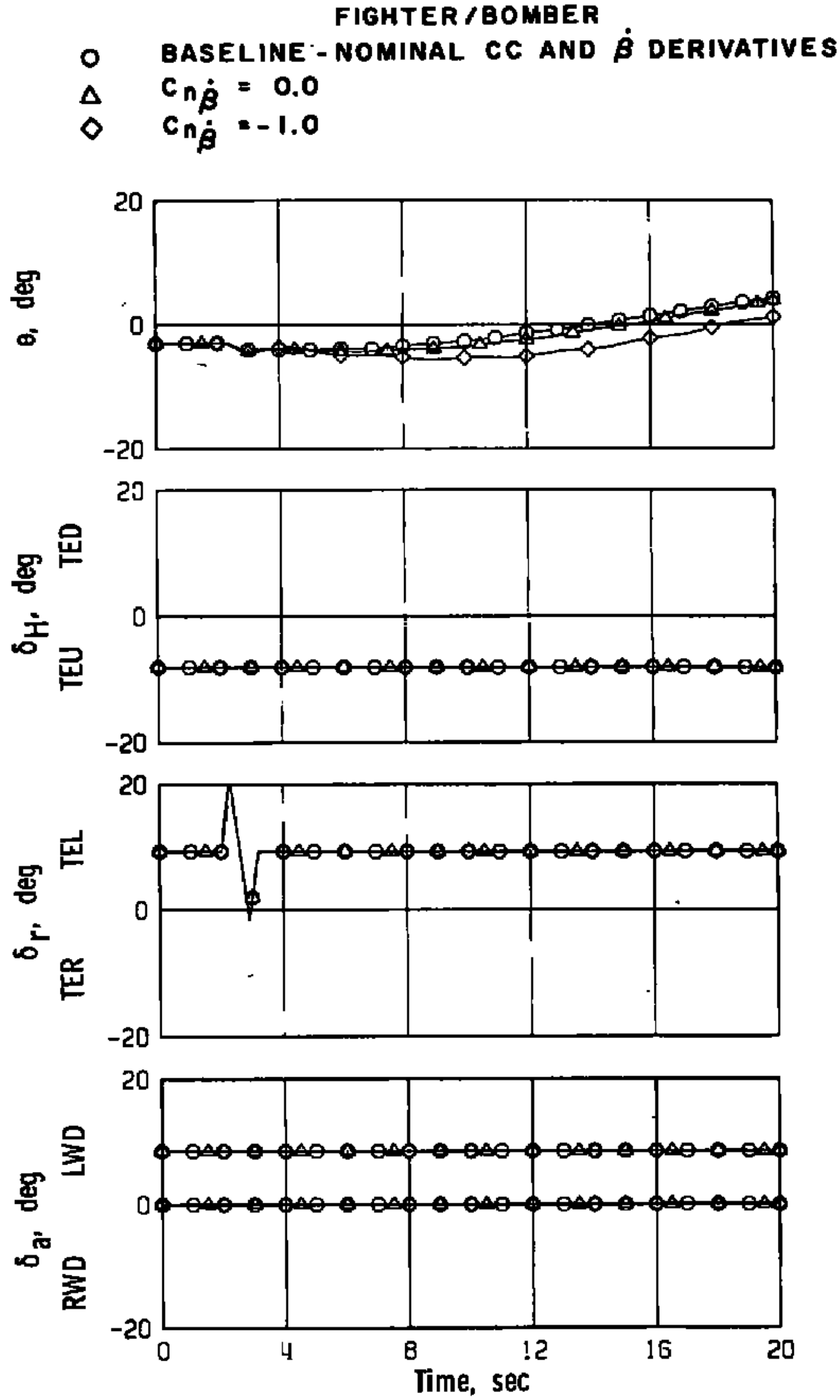

Figure 34. Concluded.

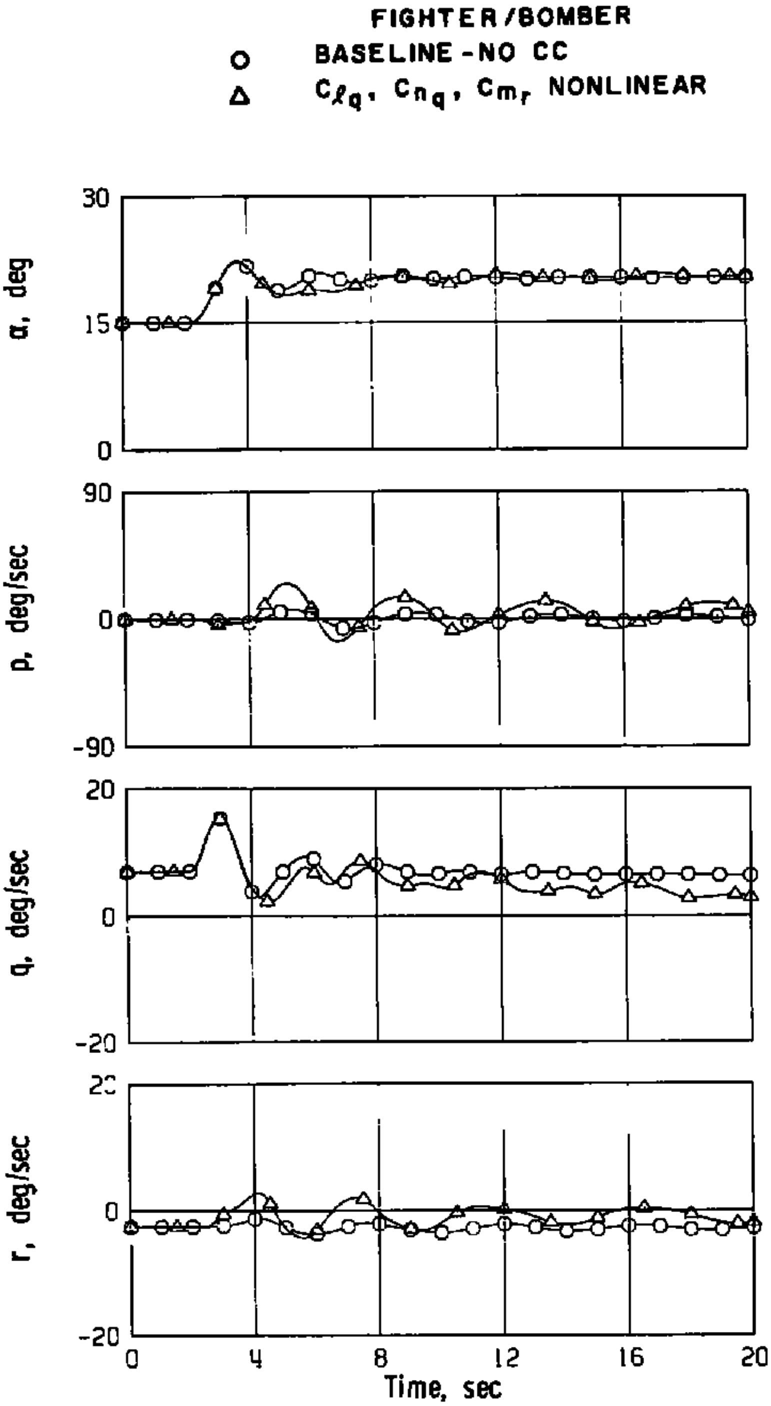

a. Fighter/bomber

Figure 35. C_{ℓ_q}, C_{n_q}, C_{m_r} nonlinear variations, elevator step.

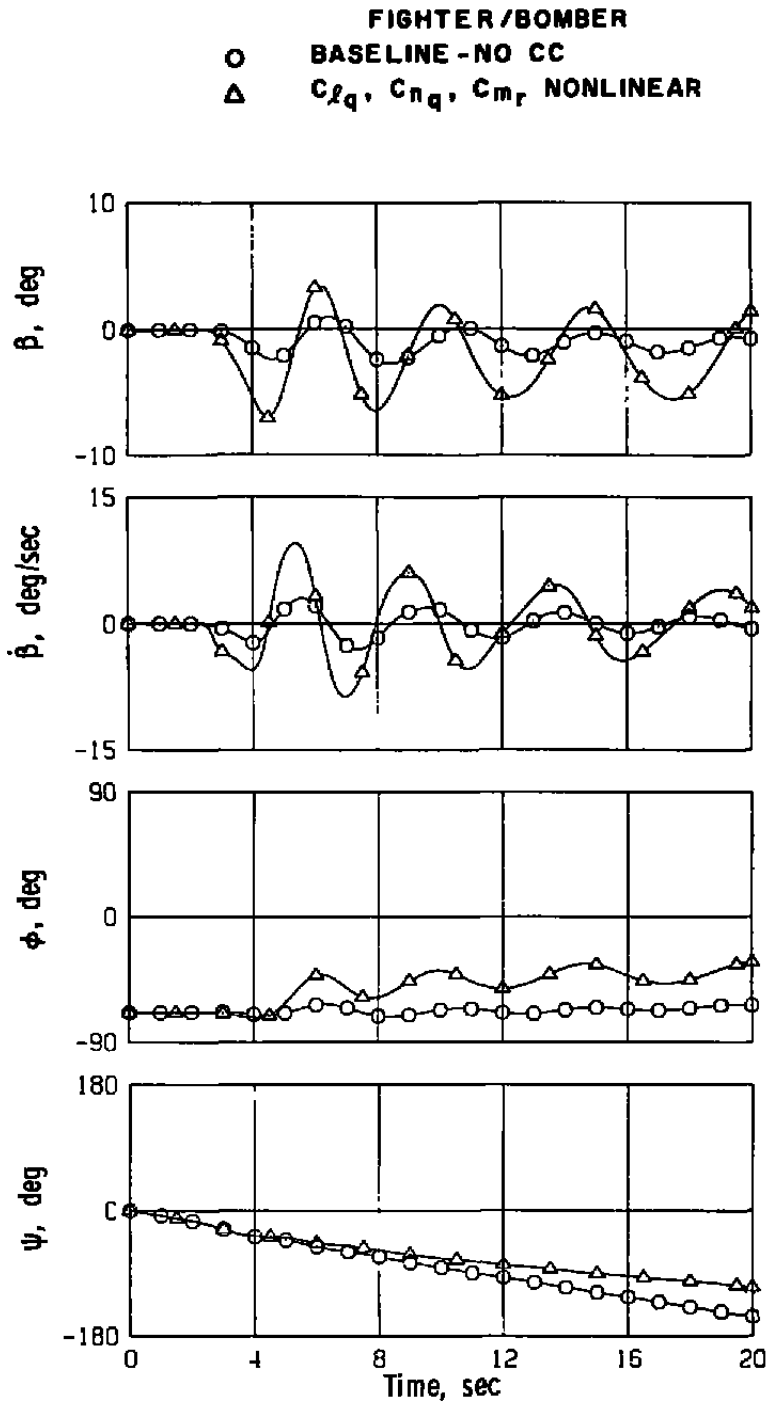

a. Continued
Figure 35. Continued.

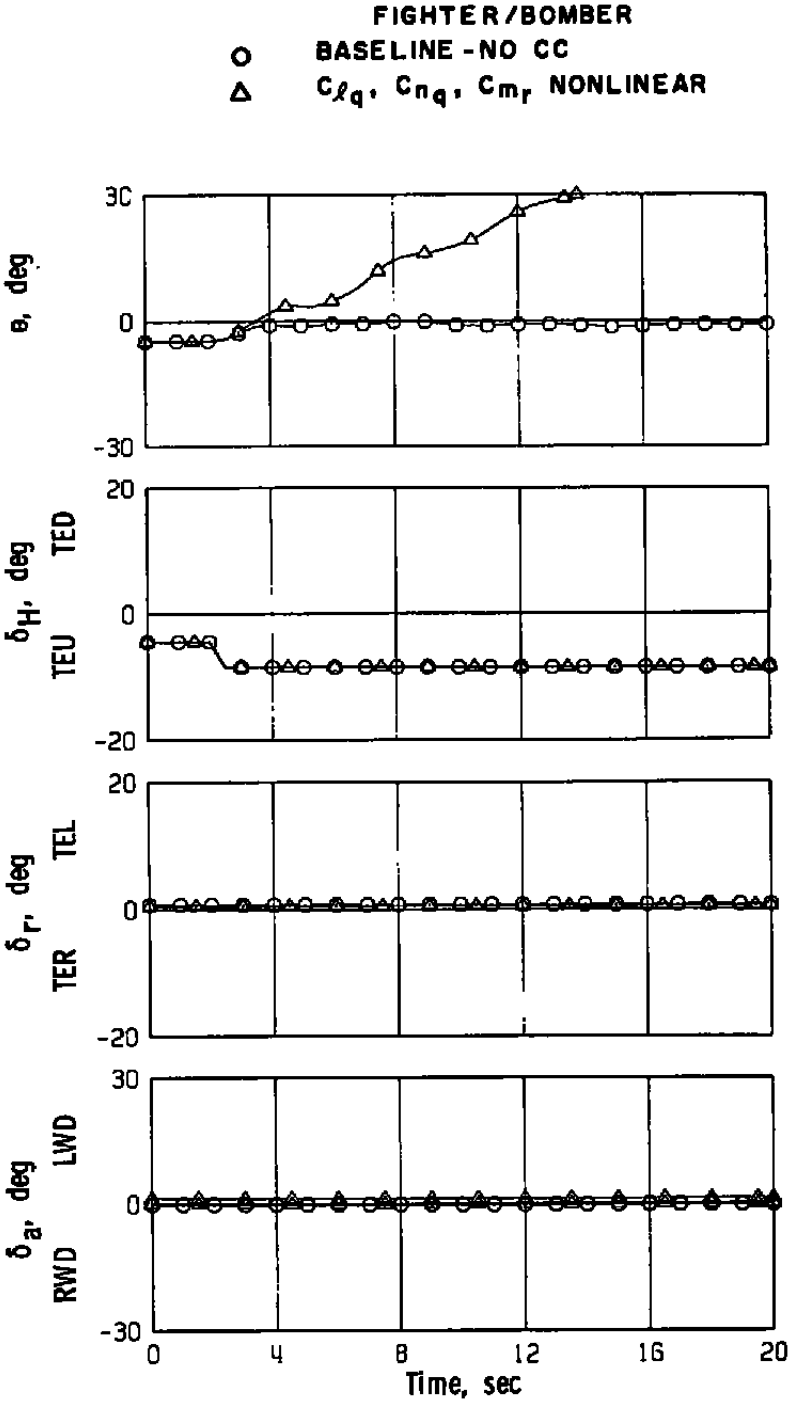

a. Concluded
Figure 35. Continued.

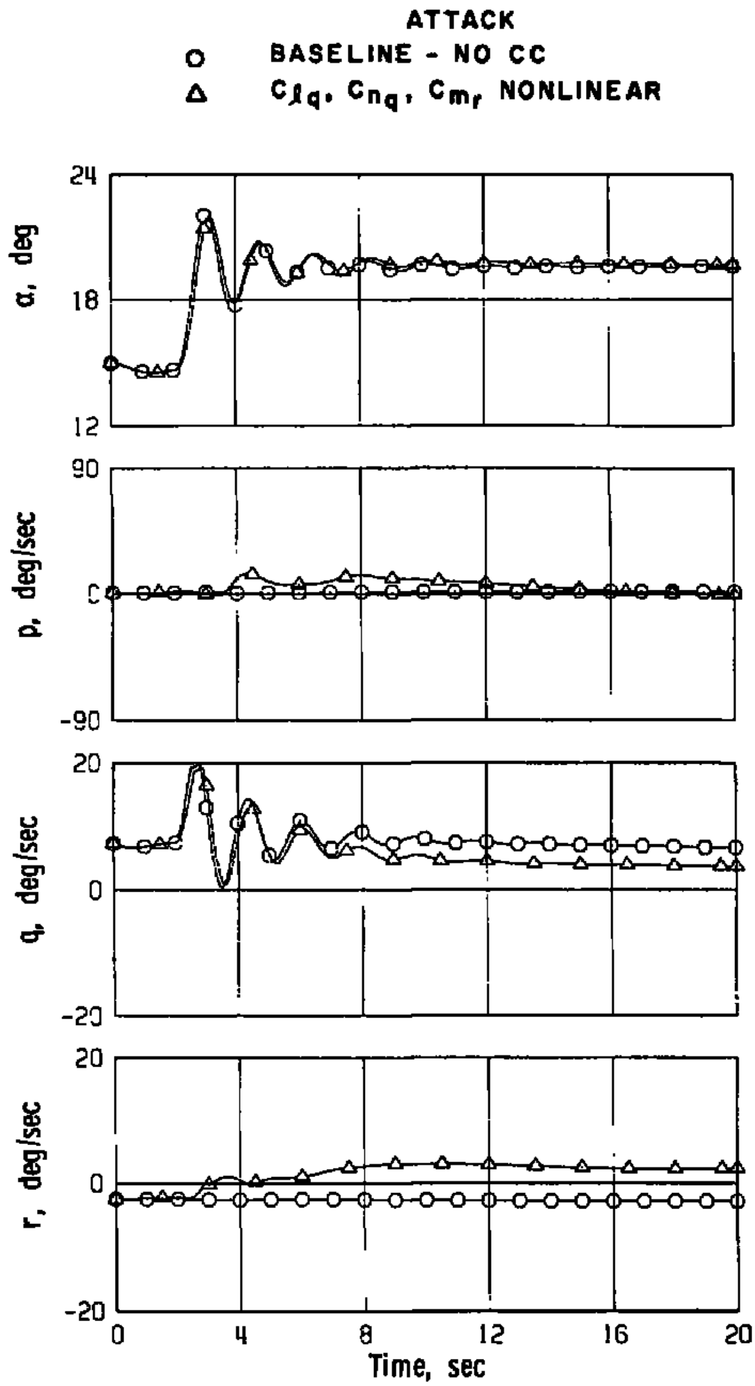

b. Attack aircraft
Figure 35. Continued.

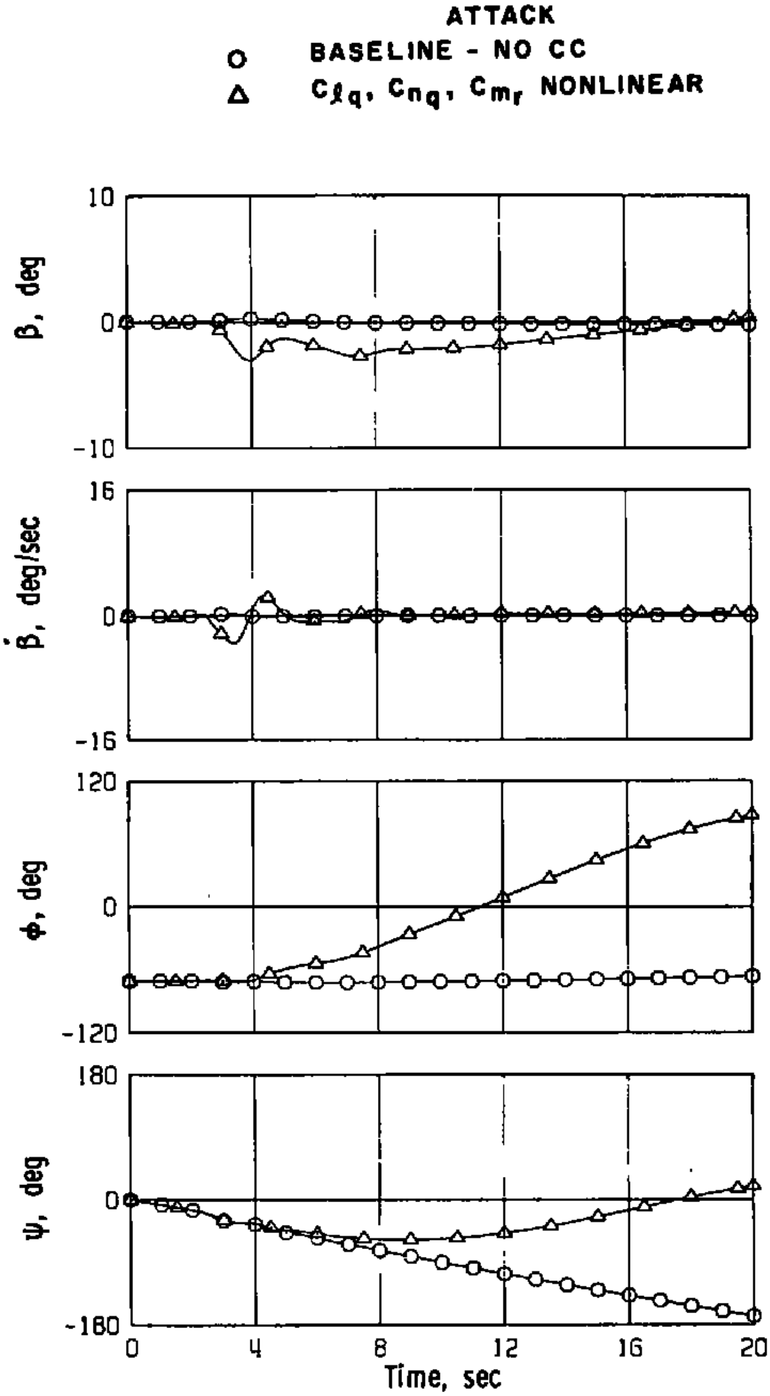

b. Continued
Figure 35. Continued.

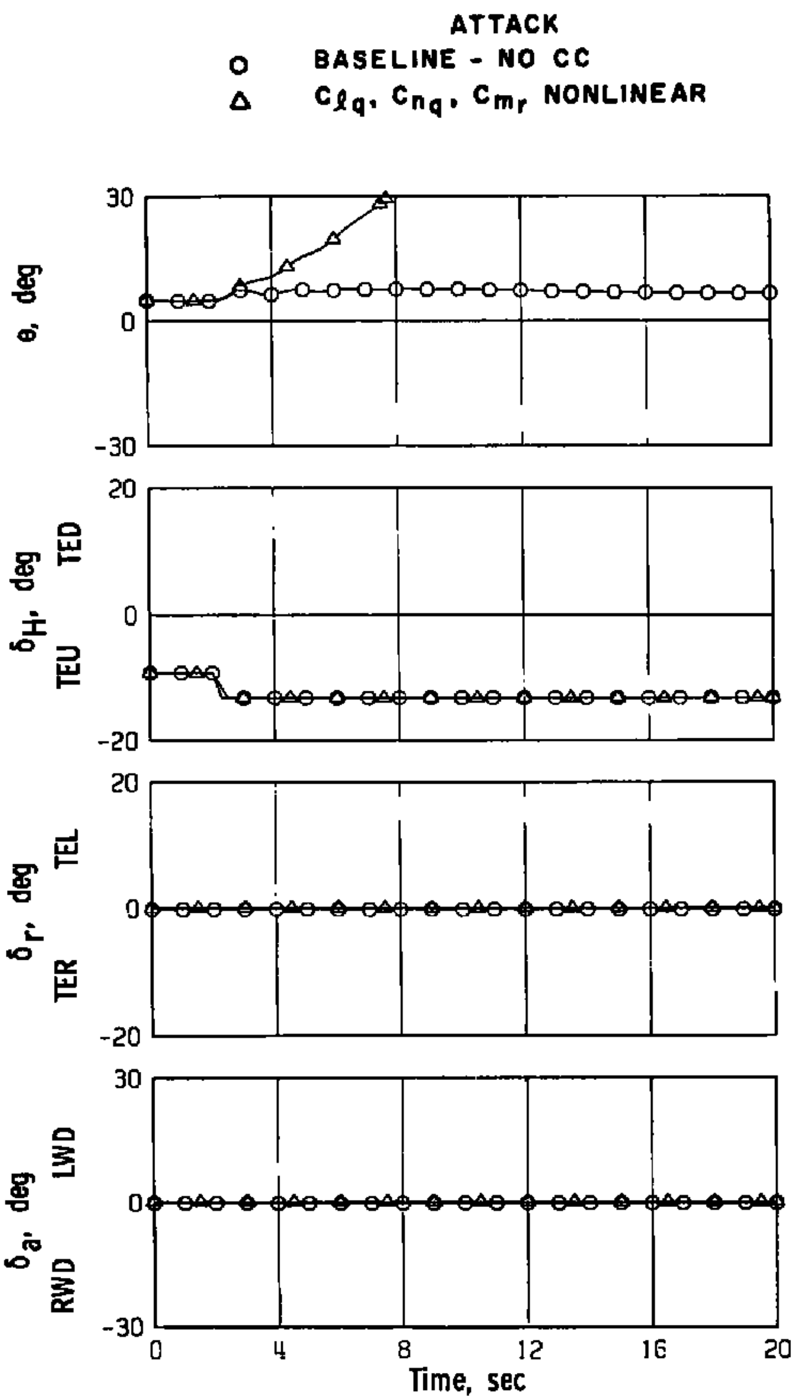

b. Concluded

Figure 35. Concluded.

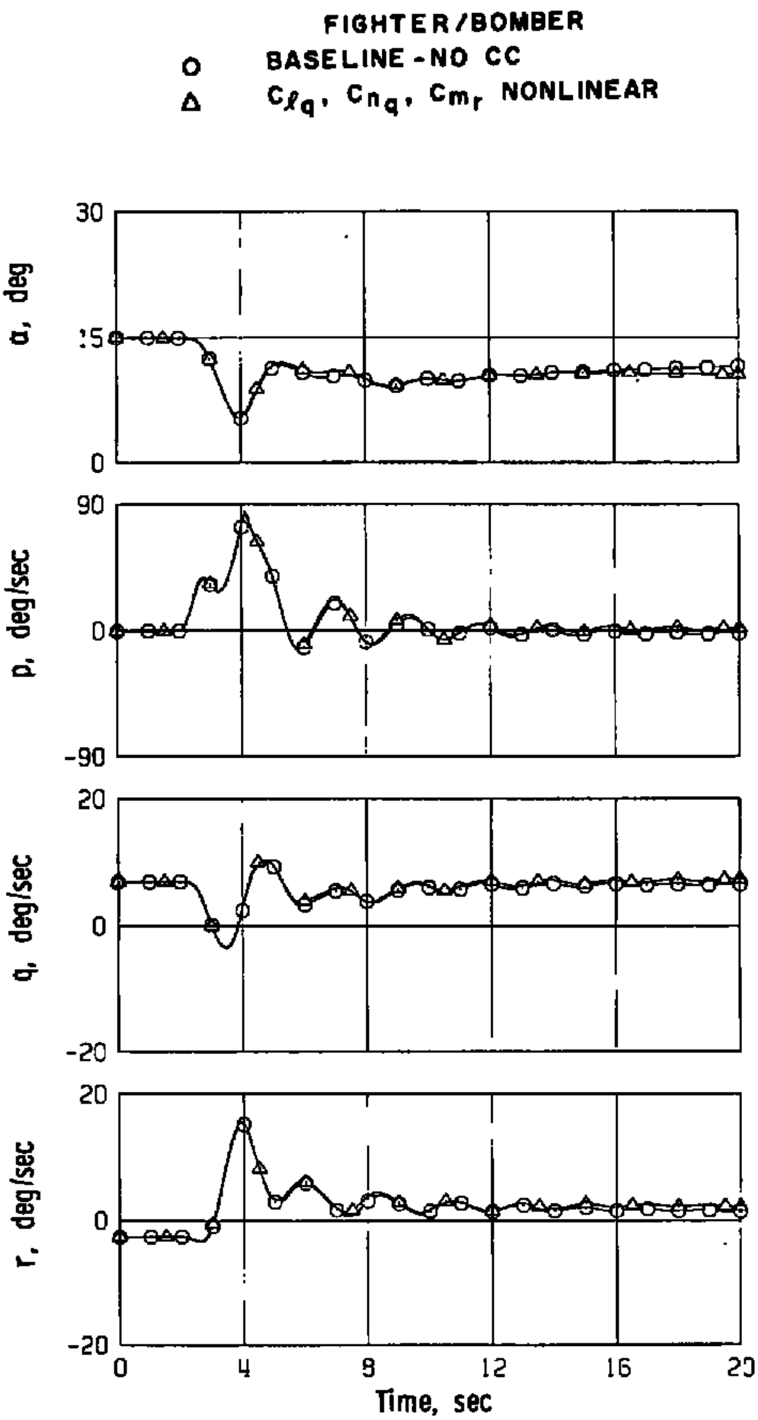

a. Fighter/bomber

Figure 36. C_{ℓ_q}, C_{n_q}, C_{m_r} nonlinear variations, bank-to-bank.

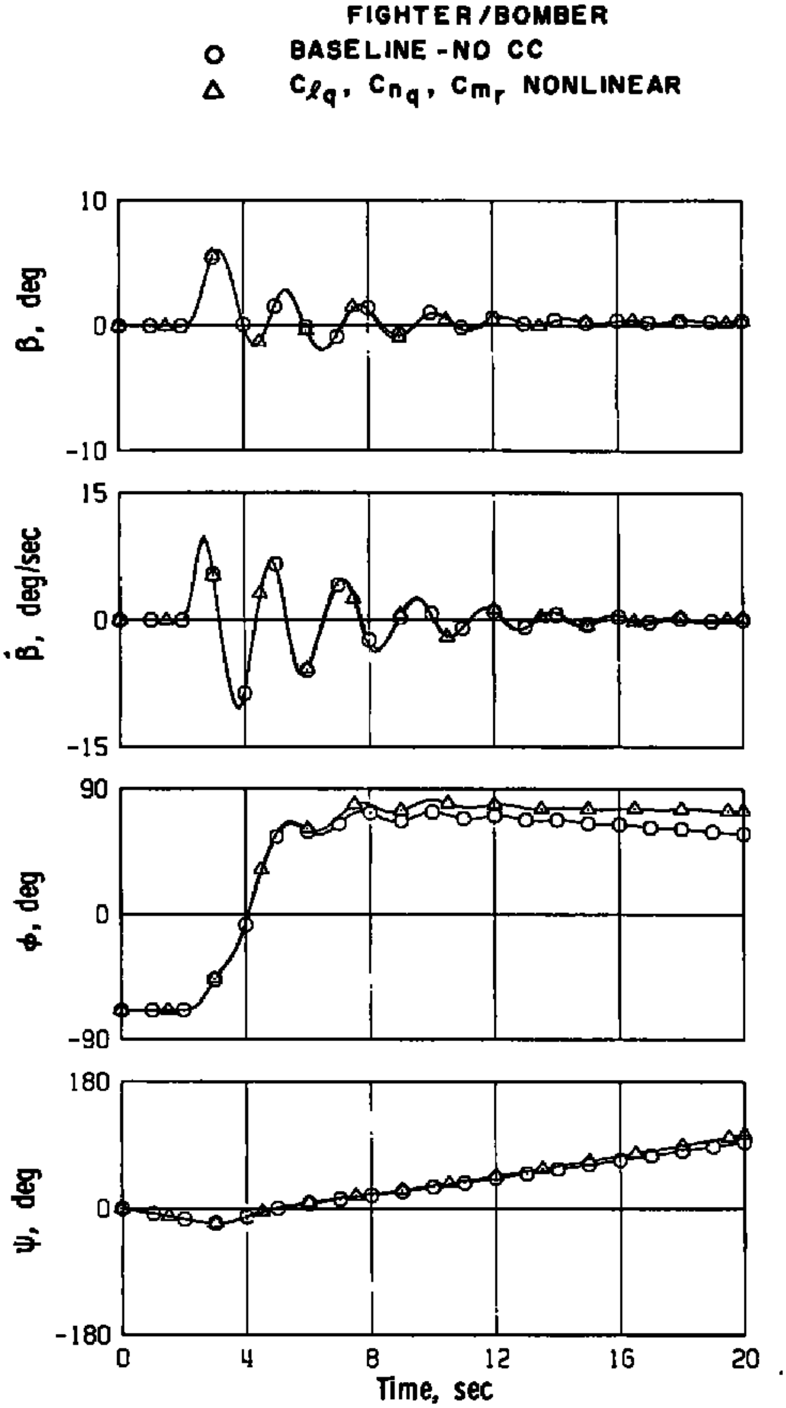

a. Continued
Figure 36. Continued.

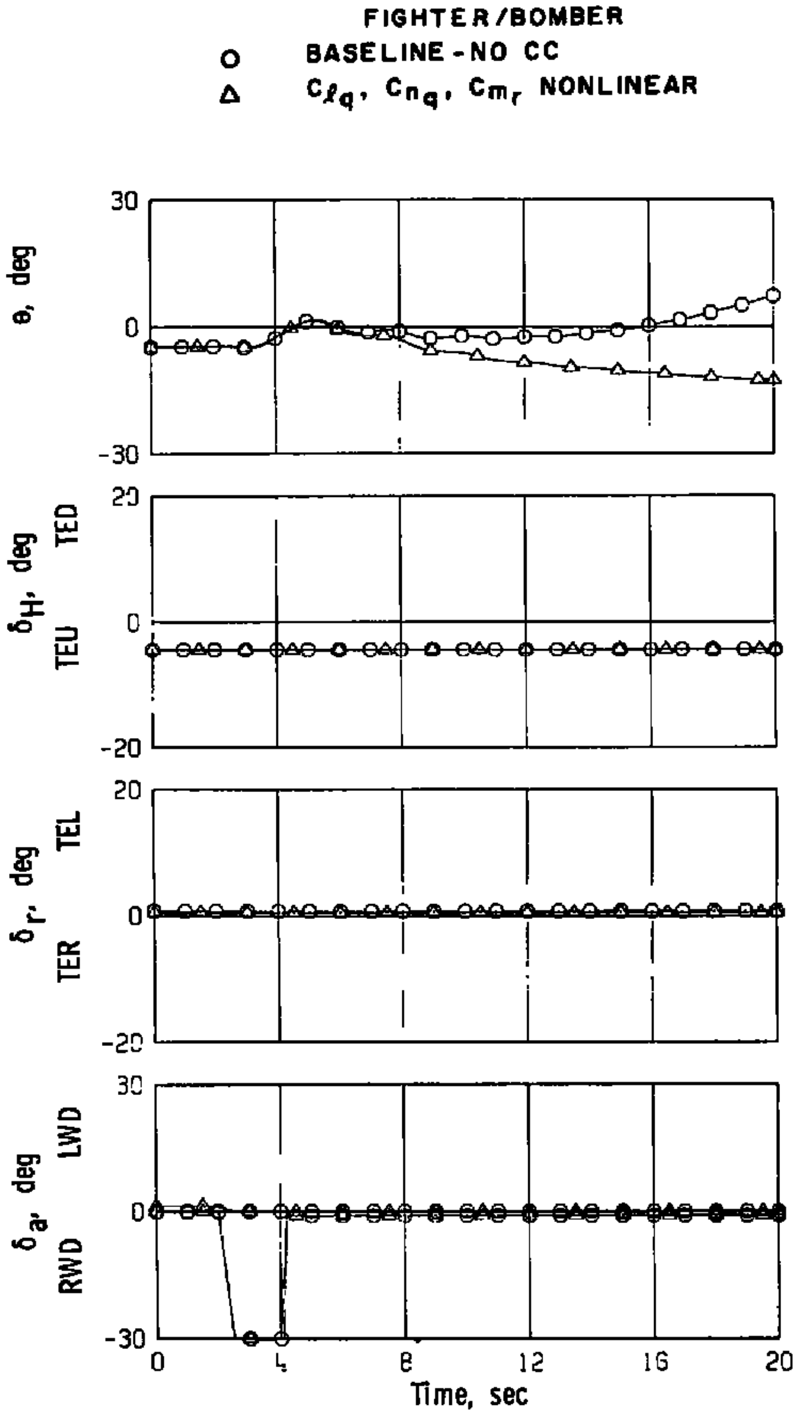

a. Concluded

Figure 36. Continued.

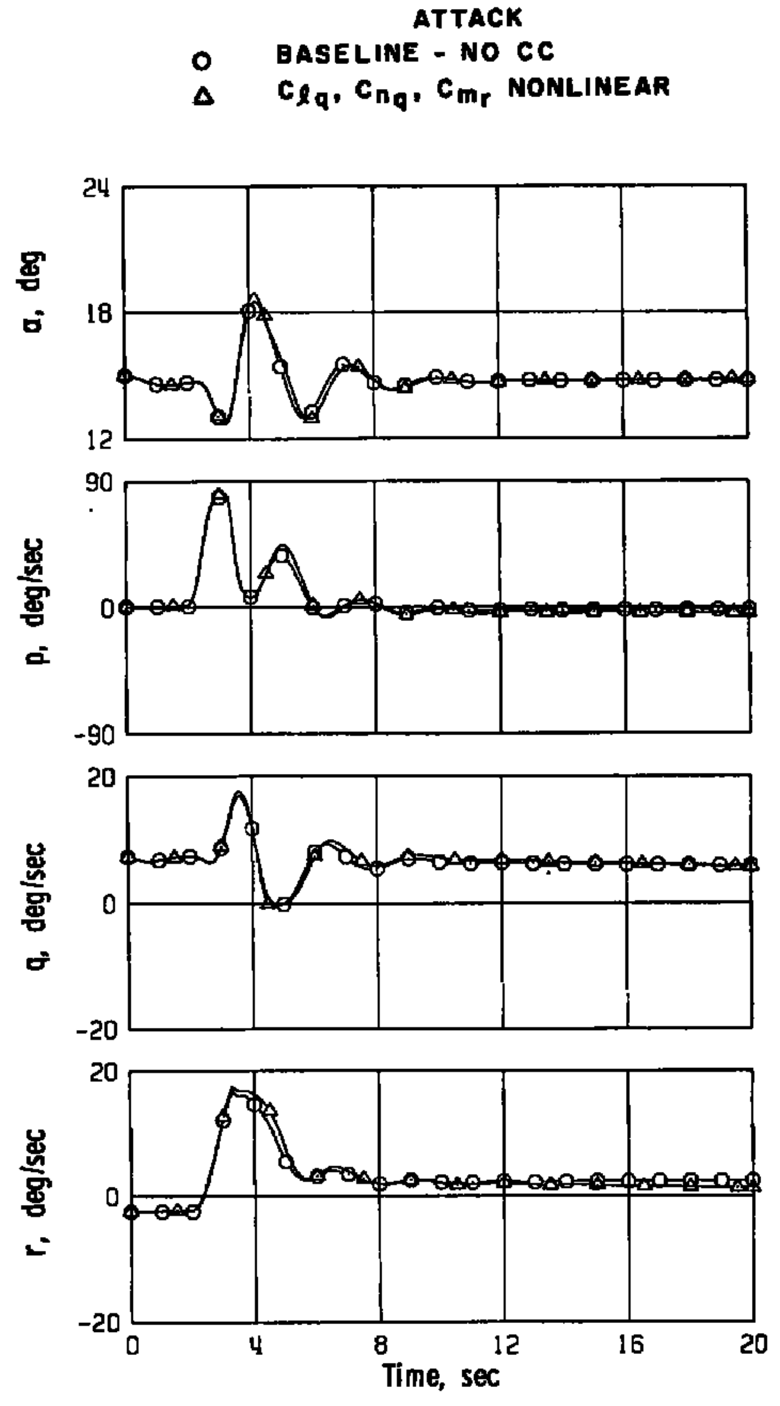

b. Attack aircraft
Figure 36. Continued.

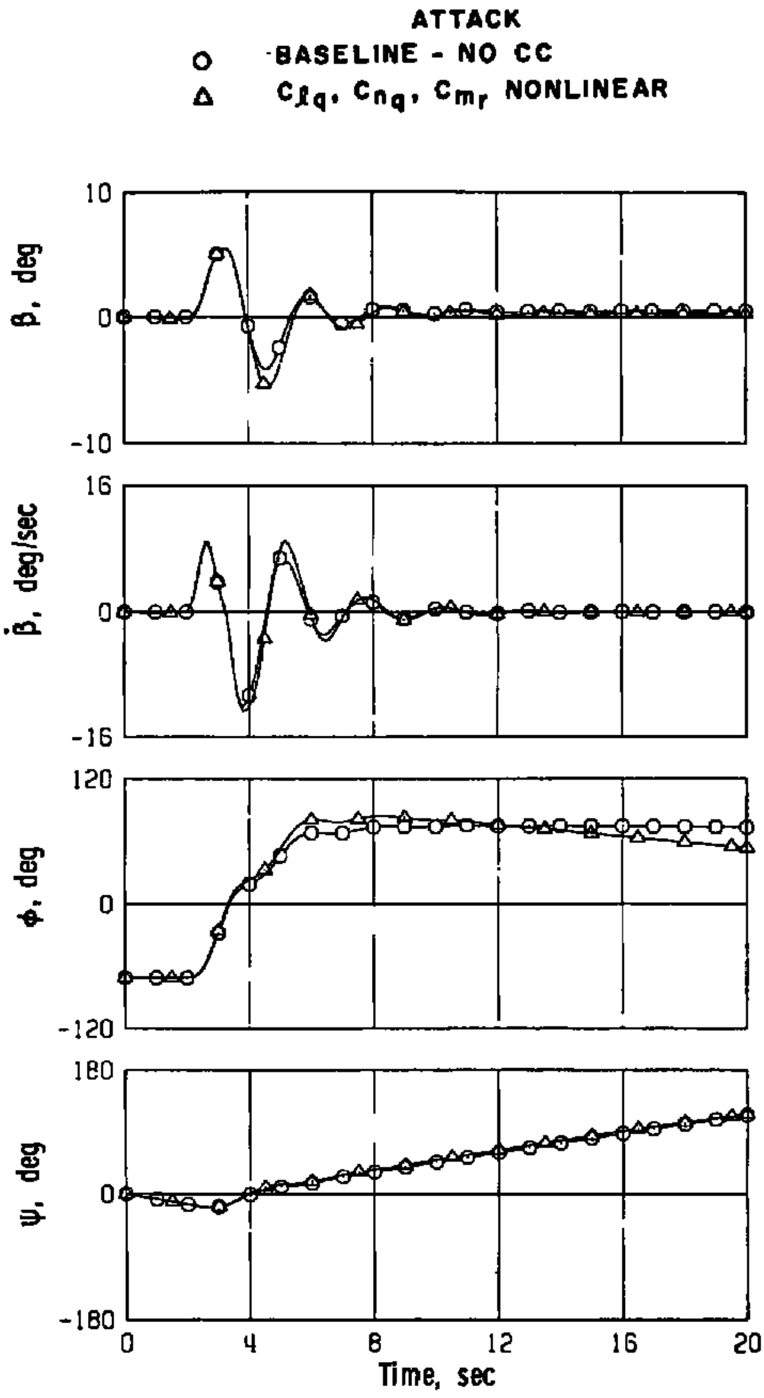

b. Continued
Figure 36. Continued.

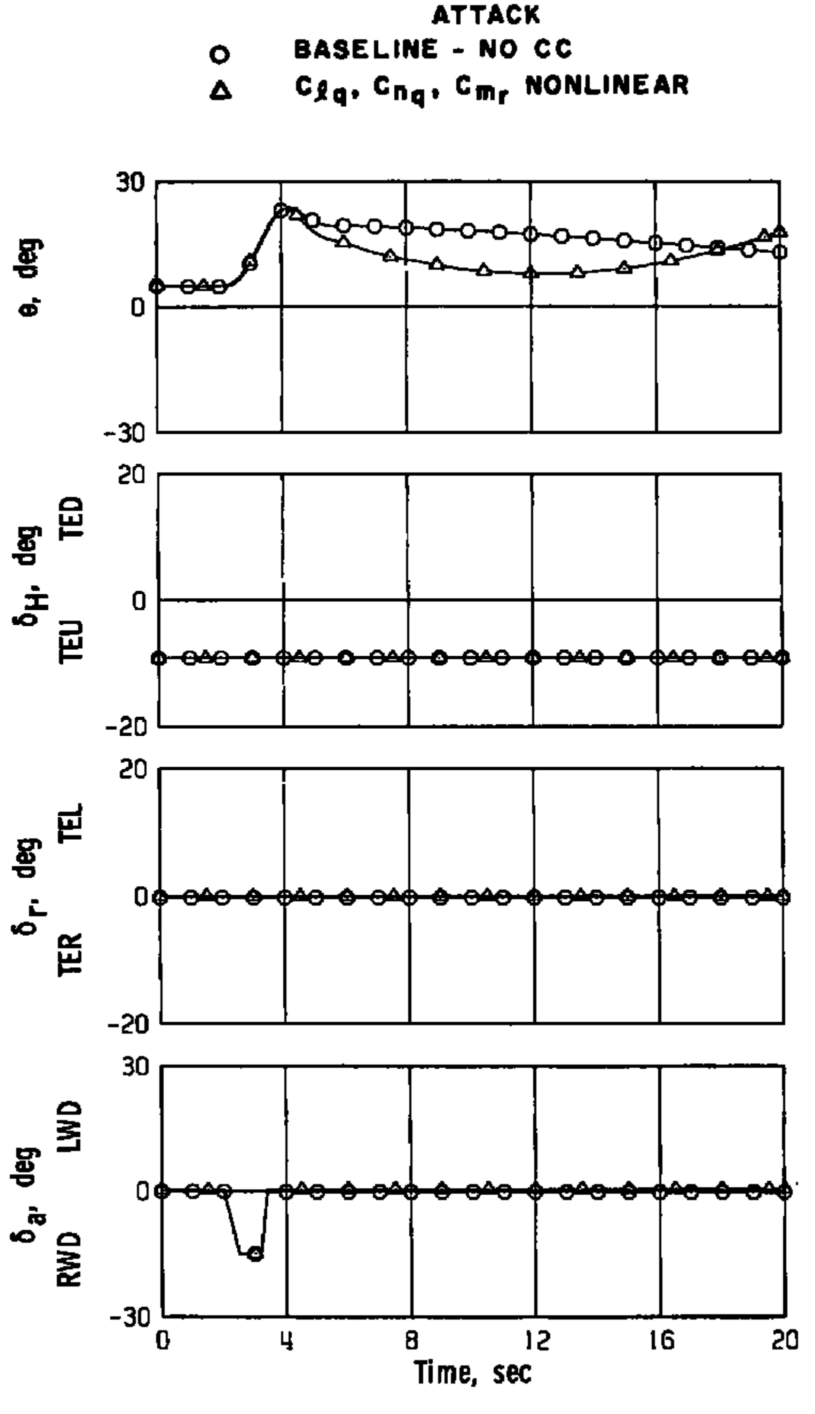

b. Concluded
Figure 36. Concluded.

Table 1. Aircraft Physical and Mass Characteristics

	Attack-Type Aircraft	Fighter/Bomber-Type Aircraft
Mass	719 slugs	1215 slugs
I_X	15,927 slugs-ft^2	29,950 slugs-ft^2
I_Y	64,792 slugs-ft^2	164,300 slugs-ft^2
I_Z	75,976 slugs-ft^2	169,535 slugs-ft^2
I_{XZ}	3885 slugs-ft^2	5241 slug-ft^2
S	375 ft^2	538.3 ft^2
b	38.73 ft	38.4 ft
C	10.84 ft	16.04
cg	30-percent MAC	33.0-percent MAC

Table 2. Initial Trimmed Flight Conditions

	Altitude = 30,000 ft							
	α, deg	ϕ, deg	$\bar{q}$, lb/ft^2	V, ft/sec	$\dot{\psi}$, deg/sec	q, deg/sec	r, deg/sec	Thrust, lb
Fighter/Bomber								
Level (1 g)	20	0	74	395	0	0	0	14,900
Turning (3 g)	20	-68.7	206	675	-7.9	7.3	-2.9	38,800
Turning (3 g)	15	-69.0	232	715	-7.4	6.9	-2.7	26,700
Attack								
Turning (3 g)	20	-71.6	157	588	-8.9	8.4	-2.8	20,300
Turning (3 g)	15	-71.1	204	672	-7.8	7.3	-2.5	12,600

NOTE: The thrust-to-weight ratio for the turning flight conditions at α = 20 deg is 0.99 for the fighter/bomber and 0.88 for the attack aircraft, which is slightly beyond the capability of these aircraft configurations.

Table 3. Range of Derivative Variations

Magnitudes per Radian	Cross-Coupling Derivatives				Acceleration Derivatives	
	C_{ℓ_q}	C_{n_q}	C_{m_r}	C_{m_p}	$C_{n_{\dot{\beta}}}$	$C_{\ell_{\dot{\beta}}}$
Maximum	+2	+2	+1	+1	+1	+0.2
Minimum	-2	-2	-1	-1	-1	-1

Table 4. Cross-Coupling and Acceleration Derivative Nominal Values

C_{ℓ_q} = 2.0 per radian

C_{n_q} = 2.0 per radian

C_{m_r} = 1.0 per radian

C_{m_p} = 0.0 per radian

$C_{n_{\dot{\beta}}}$ = 1.0 per radian

$C_{\ell_{\dot{\beta}}}$ = -1.0 per radian

APPENDIX A
EQUATIONS DEFINING THE TOTAL AERODYNAMIC DATA ALONG AND ABOUT EACH BODY AXIS

A-I FIGHTER/BOMBER

Longitudinal Axis Plane

$$F_X = \bar{q}S\left[C_x(\alpha, \beta, \delta_H) + \left(C_{x_q}(\alpha)\right)\frac{qC}{2V}\right]$$

$$F_Z = \bar{q}S\left[C_z(\alpha, \beta, \delta_H) + \left(C_{z_q}(\alpha)\right)\frac{qC}{2V}\right]$$

$$M_Y = \bar{q}SC\left[C_m(\alpha, \beta, \delta_H) + \left(C_{m_q}(\alpha)\right)\frac{qC}{2V} + C_{m_p}\left(\frac{pb}{2V}\right) + C_{m_r}\left(\frac{rb}{2V}\right)\right]$$

Lateral-Directional Axis Plane

$$F_Y = \bar{q}S\left[C_y(\alpha, \beta) + \Delta C_y(\alpha, \beta, \delta_r) + \left(C_{y_p}(\alpha)\right)\frac{pb}{2V} + \left(C_{y_r}(\alpha, \delta_H)\right)\frac{rb}{2V}\right]$$

$$M_Z = \bar{q}Sb\left\{C_n(\alpha, \beta) + \Delta C_n(\alpha, \beta, \delta_a) + \Delta C_n(\alpha, \beta, \delta_r) + \left[C_{n_p}(\alpha)\right]\frac{pb}{2V} + \left[C_{n_r}(\alpha, \delta_H)\right]\frac{rb}{2V} + C_{n_{\dot{\beta}}}\frac{\dot{\beta}b}{2V} + C_{n_q}\frac{qC}{2V}\right\}$$

$$M_X = \bar{q}Sb\left\{C_\ell(\alpha, \beta) + \Delta C_\ell(\alpha, \beta, \delta_a) + \Delta C_\ell(\alpha, \beta, \delta_r) + \left[C_{\ell_p}(\alpha)\right]\frac{pb}{2V} + \left[C_{\ell_r}(\alpha, \delta_H)\right]\frac{rb}{2V} + C_{\ell_{\dot{\beta}}}\frac{\dot{\beta}b}{2V} + C_{\ell_q}\frac{qC}{2V}\right\}$$

The data matrix was formulated as a function of the following variables and their associated ranges:

α −10 to 110 deg

β −40 to 40 deg

δ_H −21 to 7 deg

δ_a −30 to 30 deg

δ_r −30 to 30 deg

A-II ATTACK AIRCRAFT

$$F_X = \bar{q}\,S\left[C_x(\alpha, \delta_H) + \Delta C_x(\alpha, \delta_s)\right]$$

$$F_Y = \bar{q}\,S\left[C_y(\alpha, \beta, \delta_H) + \Delta C_y(\alpha, \delta_a) + \Delta C_y(\alpha, \delta_s) + \Delta C_y(\alpha, \delta_r) + C_{y_p}(\alpha)\left(\frac{pb}{2V}\right) + C_{y_r}(\alpha)\left(\frac{rb}{2V}\right)\right]$$

$$F_Z = \bar{q}\,C\left[C_z(\alpha, \delta_H) + \Delta C_z(\alpha, \delta_a) - \Delta C_z(\alpha, \delta_s) + C_{z_q}(\alpha)\left(\frac{qC}{2V}\right) + C_{z_{\dot{\alpha}}}(\alpha)\left(\frac{\dot{\alpha}C}{2V}\right)\right]$$

$$M_X = \bar{q}\,Sb\left[C_\ell(\alpha, \beta, \delta_H) + \Delta C_\ell(\alpha, \delta_a) + \Delta C_\ell(\alpha, \delta_s) + \Delta C_\ell(\alpha, \delta_r) + C_{\ell_p}(\alpha)\left(\frac{pb}{2V}\right) + C_{\ell_r}(\alpha)\left(\frac{rb}{2V}\right) + C_{\ell_q}\left(\frac{qC}{2V}\right) + C_{\ell_{\dot{\beta}}}\left(\frac{\dot{\beta}b}{2V}\right)\right]$$

$$M_Y = \bar{q}\,SC\left[C_m(\alpha, \delta_H) + \Delta C_m(\alpha, \delta_a) + \Delta C_m(\alpha, \delta_s) + C_{m_q}(\alpha, \delta_H)\left(\frac{qC}{2V}\right) + C_{m_{\dot{\alpha}}}(\alpha, \delta_H)\left(\frac{\dot{\alpha}C}{2V}\right) + C_{m_p}\left(\frac{pb}{2V}\right) + C_{m_r}\left(\frac{rb}{2V}\right)\right]$$

$$M_Z = \bar{q}\,Sb\left[C_n(\alpha, \beta, \delta_H) + \Delta C_n(\alpha, \delta_a) + \Delta C_n(\alpha, \delta_s) + \Delta C_n(\alpha, \delta_r) + C_{n_p}(\alpha)\left(\frac{pb}{2V}\right) + C_{n_r}(\alpha)\left(\frac{rb}{2V}\right) + C_{n_q}\left(\frac{qC}{2V}\right) + C_{n_{\dot{\beta}}}\left(\frac{\dot{\beta}b}{2V}\right)\right]$$

The data matric was formulated as a function of the following variables and their associated ranges:

α	0 to 90 deg
β	-90 to 90 deg
δ_H	-5 to -25 deg
δ_a	-25 to 25 deg
δ_r	-10 to 10 deg
δ_s	0 to 60 deg

APPENDIX B
SIMPLIFIED LINEARIZED EQUATIONS OF MOTION

Consider the rotational equations of motion $\dot{p}$, $\dot{q}$, and $\dot{r}$ [(Eqs. (4), (5), and (6)] in their linearized form with the assumption that the I_{XZ} terms are zero and that $I_Y = I_Z$, which is approximate for modern fighter aircraft with small wings and high density fuselages. Then

$$M_X = \dot{p}I_X$$

$$M_Y = \dot{q}I_Y + r_o p\left(I_X - I_Z\right)$$

$$M_Z = \dot{r}I_Z + pq_o\left(I_Y - I_X\right)$$

If only the dynamic dimensional derivatives are considered as external forces, the equations with $\dot{\alpha}$ and $\dot{\beta}$ derivatives at zero become

$$\dot{p} - L_p p - L_q q - L_r r = 0$$

$$\dot{q} - M_q q - M_r r - (M_p - A)\,p = 0$$

$$\dot{r} - N_r r - N_q q - (N_p - B)\,p = 0$$

where

$$A = r_o(I_X - I_Z)/I_Y$$

$$B = q_o(I_Y - I_X)/I_Z$$

Now, by assuming an exponential solution ($p = \tilde{p}e^{st}$, $q = \tilde{q}e^{st}$, $r = \tilde{r}e^{st}$) for the linear differential equations, a set of homogeneous algebraic equations may be obtained that have the following characteristic equation:

$$(S - L_p)(S - M_q)(S - N_r) - (S - L_p)N_qM_r - (S - N_r)(M_p - A)L_q$$

$$- (S - M_q)(N_p - B)L_r - (N_p - B)M_rL_q - (M_p - A)N_qL_r = 0$$

Although this equation is a simplified example of a six-degree-of-freedom nonlinear system, it does point out the degree of interaction that occurs between the stability derivatives. As an example to show the necessity for including nonzero nominal values, consider the effect that zero values of the cross-coupling derivatives C_{ℓ_q} (L_q) and C_{n_q} (N_q) would have on the $C_{m_r}(M_r)$ variation. For this linearized case, it becomes obvious from the above equation that the effect of the C_{m_r} derivative on the aircraft motion would be eliminated.

NOMENCLATURE

All aerodynamic data are presented with respect to the body axis shown in Fig. 1.

b	Wing span, ft
C	Wing mean aerodynamic chord, ft
CC	Cross-coupling derivatives
C_ℓ	Rolling-moment coefficient, rolling moment/$\bar{q}$ Sb about airplane cg
C_{ℓ_p}	Derivative of rolling-moment coefficient with respect to roll rate, $\partial C_\ell/\partial(pb/2V)$, per radian
C_{ℓ_q}	Derivative of rolling-moment coefficient with respect to pitch rate, $\partial C_\ell/\partial(qC/2V)$, per radian
C_{ℓ_r}	Derivative of rolling-moment coefficient with respect to yaw rate, $\partial C_\ell/\partial(rb/2V)$, per radian
$C_{\ell_{\dot{\alpha}}}$	Derivative of rolling-moment coefficient with respect to $\dot{\alpha}$, $\partial C_\ell/\partial(\dot{\alpha}C/2V)$, per radian
$C_{\ell_{\dot{\beta}}}$	Derivative of rolling-moment coefficient with respect to $\dot{\beta}$, $\partial C_\ell/\partial(\dot{\beta}b/2V)$, per radian
C_m	Pitching-moment coefficient, pitching moment/$\bar{q}$ SC about airplane cg
C_{m_p}	Derivative of pitching-moment coefficient with respect to roll rate, $\partial C_m/\partial(pb/2V)$, per radian
C_{m_q}	Derivative of pitching-moment coefficient with respect to pitch rate, $\partial C_m/\partial(qC/2V)$, per radian
C_{m_r}	Derivative of pitching-moment coefficient with respect to yaw rate, $\partial C_m/\partial(rb/2V)$, per radian
$C_{m_{\dot{\alpha}}}$	Derivative of pitching-moment coefficient with respect to $\dot{\alpha}$, $\partial C_m/\partial(\dot{\alpha}C/2V)$, per radian

$C_{m_{\dot{\beta}}}$ Derivative of pitching-moment coefficient with respect to $\dot{\beta}$, $\partial C_m/\partial(\dot{\beta}b/2V)$, per radian

C_n Yawing-moment coefficient, yawing moment/$\bar{q}$ Sb about airplane cg

C_{n_p} Derivative of yawing-moment coefficient with respect to roll rate, $\partial C_n/\partial(pb/2V)$, per radian

C_{n_q} Derivative of yawing-moment coefficient with respect to pitch rate, $\partial C_n/\partial(qC/2V)$, per radian

C_{n_r} Derivative of yawing-moment coefficient with respect to yaw rate, $\partial C_n/\partial(rb/2V)$, per radian

$C_{n_{\dot{\alpha}}}$ Derivative of yawing-moment coefficient with respect to $\dot{\alpha}$, $\partial C_n/\partial(\dot{\alpha}C/2V)$, per radian

$C_{n_{\dot{\beta}}}$ Derivative of yawing-moment coefficient with respect to $\dot{\beta}$, $\partial C_n/\partial(\dot{\beta}b/2V)$, per radian

C_x Longitudinal-force coefficient, longitudinal force/$\bar{q}$ S

C_{x_q} Derivative of longitudinal-force coefficient with respect to pitch rate, $\partial C_x/\partial(qC/2V)$, per radian

C_y Side-force coefficient, side force/$\bar{q}$ S

C_{y_p} Derivative of side-force coefficient with respect to roll rate, $\partial C_y/\partial(pb/2V)$, per radian

C_{y_r} Derivative of side-force coefficient with respect to yaw rate, $\partial C_y/\partial(rb/2V)$, per radian

C_z Normal-force coefficient, normal force/$\bar{q}$ S

C_{z_q} Derivative of normal-force coefficient with respect to pitch rate, $\partial C_z/\partial(qC/2V)$, per radian

$C_{z_{\dot{\alpha}}}$ Derivative of normal-force coefficient with respect to $\dot{\alpha}$, $\partial C_z/\partial(\dot{\alpha}C/2V)$, per radian

cg	Center-of-gravity location, percent chord
F_X	Force acting along X-body axis, lb
F_Y	Force acting along Y-body axis, lb
F_Z	Force acting along Z-body axis, lb
g	Acceleration of gravity, ft/sec^2
h	Altitude, ft
I_E	Moment of inertia about X-body axis attributable to engine rotation, slugs-ft^2
I_X, I_Y, I_Z	Moments of inertia about X-, Y-, and Z-body axes, respectively, slugs-ft^2
I_{XZ}	Product of inertia, slugs-ft^2
L	Aerodynamic rolling moment
L_p	Dimensional stability derivative, $(1/I_X)(\partial L/\partial p)$
L_q	Dimensional stability derivative, $(1/I_X)(\partial L/\partial q)$
L_r	Dimensional stability derivative, $(1/I_X)(\partial L/\partial r)$
LWD	Left wing down
M	Aerodynamic pitching moment
MAC	Mean aerodynamic chord
M_p	Dimensional stability derivative, $(1/I_Y)(\partial M/\partial p)$
M_q	Dimensional stability derivative, $(1/I_Y)(\partial M/\partial q)$
M_r	Dimensional stability derivative, $(1/I_Y)(\partial M/\partial r)$
M_X	Moment acting about X-body axis, ft-lb

M_Y	Moment acting about Y-body axis, ft-lb
M_{YT}	Moment acting about Y-body axis caused by engine thrust, ft-lb
M_Z	Moment acting about Z-body axis, ft-lb
m	Mass, slugs
N	Aerodynamic yawing moment
n	Aircraft load factor
p,q,r	Components of $\vec{\Omega}$ about X-, Y-, and Z-body axes, respectively, rad/sec
$\bar{q}$	Dynamic pressure, $\rho V^2/2$, lb/ft^2
RWD	Right wing down
S	Wing reference area, ft^2
TED	Trailing edge down
TEL	Trailing edge left
TER	Trailing edge right
TEU	Trailing edge up
T_X	Component of engine thrust along X-axis, lb
T_Z	Component of engine thrust along Z-body axis, lb
u,v,w	Components of total velocity along X-, Y-, and Z-body axes, respectively, ft/sec
V	Total velocity, ft/sec
X,Y,Z	Body axes

x,y,z	Linear distance along X-, Y-, and Z-body axes, respectively, ft
α	Angle of attack, deg
β	Angle of sideslip, deg
γ	Flight path angle, deg
Δ	Increment for force and moment coefficients
δ_a	Aileron deflection, positive when trailing edge of right aileron is down, deg
δ_H	Elevator deflection, positive when trailing edge is down, deg
δ_r	Rudder deflection, positive when trailing edge is left, deg
δ_s	Spoiler deflection, function of aileron deflection, deg
θ	Angle between X-body axis and horizontal measured in vertical plane, deg
ϱ	Air density, slugs/ft^3
ϕ	Angle between Y-body axis and horizontal measured in vertical plane, deg
ψ	Angle between Y-body axis and vertical measured in horizontal plane, deg
Ω	Resultant angular vector, rad/sec
Ω_E	Engine rotor angular velocity, rad/sec
$\Omega b/2V$	Nondimensional rotation rate

SUPERSCRIPT

•	Derivative with respect to time

SUBSCRIPT

o	Initial condition, time = 0